Available online at www.sciencedirect.com
SCIENCE DIRECT®
Coordination Chemistry Reviews 248 (2004) 955–993
COORDINATION CHEMISTRY REVIEWS
www.elsevier.com/locate/ccr

Review

Coordination chemistry of 1,3,5-triaza-7-phosphaadamantane (PTA) Transition metal complexes and related catalytic, medicinal and photoluminescent applications

Andrew D. Phillips [a], Luca Gonsalvi [a], Antonio Romerosa [b], Francesco Vizza [a], Maurizio Peruzzini [a,*]

[a] *Consiglio Nazionale delle Ricerche, Istituto di Chimica del Composti Organometallici (CNR-ICCOM), Via Madonna del Piano, Area di Ricerca di Firenze, 50019 Sesto Fiorentino, Firenze, Italy*
[b] *Área de Química Inorgánica, Facultad de Ciencias Experimentales, Universidad de Almería, 04071 Almería, Spain*

Received 18 January 2004; accepted 23 March 2004

Available online 27 July 2004

Contents

Abbreviations: Ac, acetyl; acac, acetylacetonate; bmim, 1-butyl-3-methylimidazolium; Bz, benzyl; CI-MS, chemical impact mass spectrometry; COD, 1,5-cyclooctadiene; Cp, cyclopentadienyl; Cp*, pentamethylcyclopentadienyl; CP MAS, cross-polarization magic angle spinning; Cy, *cyclo*-C_6H_{11}; cyep, tris(2-cyanoethyl)phosphine, $P(CH_2CN)_3$; DAPTA, 3,7-diacetyl-1,3,5-triaza-7-phosphaadamantane; dba, dibenzylideneacetone; DMF, dimethylformamide; DMSO, dimethylsulfoxide; DOPC, dioleoylphosphatidylcholine; dppe, diphenylphosphinoethane; DSR, dimethylsulfoxide reductase; ESI, electrospray ionization; ESMS, electrospray mass spectrometry; FAB-MS, fast atomic bombardment mass spectrometry; FTICR-MS, Fourier transform ion cyclotron resonance mass spectrometry; HE, high energy; hmim, 1-hexyl-3-methylimidazolium; HPNMR, high pressure NMR spectroscopy; Hpy, pirydinium; IC_{50}, concentration of sample required to reduce the cell growth by 50% (ng ml^{-1}); lb ratio, linear/branched ratio; LE, low energy; Mes, mesityl; MesH, mesitylene; MLCT, metal-to-ligand charge transfer; NBD, norbornadiene; OAc, acetate; OCT, octahedral; omim, 1-octyl-3-methylimidazolium; OTf, triflate, OSO_2CF_3; PE, photoelectron spectroscopy; PET, positron emission tomography; pip, piperidine, NHC_5H_{10}; PNP, bis(diphenylphosphinoethyl)*n*-propylamine; PTA, 1,3,5-triaza-7-phosphaadamantane; PTA(H), *N*-protonated PTA; PTA(R), *N*-alkylated PTA; (R)PTA, *P*-alkylated PTA; PTA(O), 1,3,5-triaza-7-phosphaadamantane oxide; PTA(S), 1,3,5-triaza-7-phosphaadamantane sulfide; PTA(Se), 1,3,5-triaza-7-phosphaadamantane selenide; py, pyridine; RAPTA, ruthenium/arene/PTA compounds; S, solubility; SP, square planar; TBP, trigonal bipyramidal; THF, tetrahydrofuran; THT, tetrahydrothiophene; TMEDA, tetramethylethylendiamine; TOF, turnover frequency (TON h^{-1}); TON, turnover number (mol product per mol catalyst); tos, toluene-4-sulfonate; TPPMS, sodium triphenylphosphine monosulfonate; TPPTS, trisodium triphenylphosphine trisulfonate; ts, thiosalicylate, $SC_6H_4COO^-$; xs, excess; Y, generic uninegative anion; WGSR, water gas shift reaction

* Corresponding author. Tel.: +39-55-522-5289; fax: +39-55-522-5203.
E-mail address: mperuzzini@iccom.cnr.it (M. Peruzzini).

0010-8545/$ – see front matter
doi:10.1016/j.ccr.2004.03.010

Abstract

The cage-like water-soluble monodentate phosphine 1,3,5-triaza-7-phosphaadamantane (PTA) has received renewed interest in the recent literature due to its properties to solubilize transition metal complexes in aqueous phase. This property has allowed application of Rh, Ru and Pd-PTA complexes in aqueous phase or biphasic homogeneous catalysis, antitumoral tests (Ru- and Pt-PTA) and photoluminescence (Au-PTA). This paper reviews the synthesis and structural properties of PTA and derivatives, their transition metal complexes, catalytic, medicinal and photoluminescence uses.

Keywords: 1,3,5-Triaza-7-phosphaadamantane; Water-soluble ligands; Phosphines; Homogeneous catalysis; Medicinal chemistry; Luminescence

1. Introduction

Organophosphines are among the most common ancillary ligands used in organometallic chemistry, owing to their ability to stabilize low metal oxidation states and to the capacity to influence both steric and electronic properties of the catalytic species. One of the advantages of using phosphines as ligands is that they can be easily modified by changing the organic substituents, thus allowing the fine tuning of the electronic and steric properties of the metal complexes. In homogeneous catalysis, this can be a very useful tool in order to change the activity or selectivity of the catalyst. These advantages can be maintained and solubility in water can be added by modifying the phosphine structure by introducing polar substituents such as hydroxyl or amino functionalities or ionic groups such as sulfonate, carboxylate and ammonium, just to mention some of the more important.

Examples of water-soluble monodentate aryl phosphines are the sulfonated analogues of PPh_3, namely the monosulfonated TPPMS (**1a**) and tris-sulfonated TPPTS (**1b**) (for examples of sulfonated phosphines and applications see among the others [1]). However, also bidentate diphosphines and tridentate tripodal phosphines are represented by their sulfonated derivatives [1b, c; k, l]. A small number of water-soluble cage-like phosphines have been characterized including the well known Verkade-type bases used as ligands in a number of organic reactions [2]. Another cage adamantane-like phosphine, 1,3,5-triaza-7-phosphaadamantane (**2**) (usually abbreviated as PTA)[1] first reported in 1974 by Daigle et al. has seen only sparingly use since its discovery [3]. Originally, the study aimed at synthesizing PTA was intended to create flame-proof polymers. However, with the recent search for water-soluble catalysts [4], PTA and its derivatives have recently received renewed interest and the increasing number of coordination compounds containing this unique ligand and their applications in homogeneous aqueous biphasic catalysis makes the chemistry of PTA timely and worth to be reviewed. In addition to use as ligand for biphasic catalysis, PTA and related species are important hydrophilic coligands in biological active transition metal compounds and are excellent ligands for preparing luminescent gold complexes. It is therefore the intention of this article to provide a comprehensive report highlighting the chemistry of PTA and the application of its derivatives in homogeneous catalysis. Two short sections at the end of this review are dedicated to new applications of PTA complexes such as photoluminescence (Au-PTA) and medicinal chemistry (Ru-PTA).

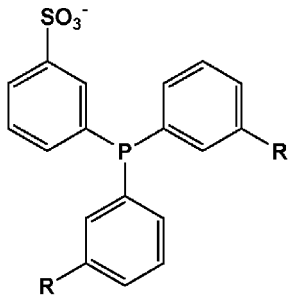

(**1a**, R = H, TPPMS; **1b**, R = SO_3^-, TPPTS)

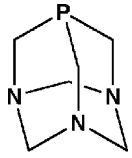

(**2**) PTA

2. Synthesis and derivatization of 1,3,5-triaza-7-phosphaadamantane (PTA)

The synthesis of PTA (**2**) is a straightforward reaction involving the condensation of trishydroxymethylphosphine with formaldehyde and hexamethylenetetraamine in ice-water, the final yield being around 40% (Scheme 1, route (a)) [3]. Alternatively, a solution of ammonia and

[1] The acronym TPA and the name "monophosphaurotropine" have been also used to indicate this ligand. The IUPAC name, 1,3,5-triaza-7-phosphatricyclo[3.3.1.1^{3,7}]decane, has been less commonly used in the scientific literature.

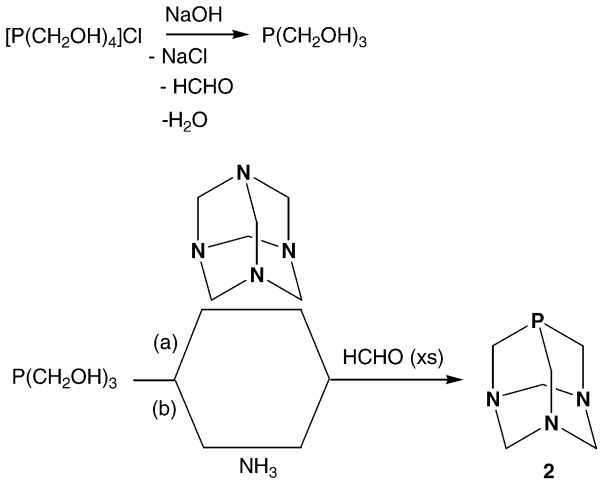

Scheme 1.

formaldehyde can be used in place of hexamethylenetetraamine (Scheme 1, route (b)) [3]. Later research showed that higher yielding preparations (65–80%) are obtained by initially forming trishydroxymethylphosphine $P(CH_2OH)_3$ in situ from reacting the commercially available and less expensive tetrakis(hydroxymethyl)phosphonium chloride $[P(CH_2OH)_4]Cl$ with sodium hydroxide [5]. PTA is generally isolated as an analytically pure compound when recrystallized from hot ethanol or acetone. The synthesis of PTA does not require an inert atmosphere as it is neither air or moisture sensitive. Furthermore, PTA is thermally stable, decomposing at temperatures higher than 260 °C. PTA is soluble in water ($S = 1.5$ M, ca. 235 g/L), MeOH and EtOH, but less soluble in heavier alcohols such as 2-propanol or *n*-butanol and THF at room temperature [5]. The solubility of PTA in acidic media, following the formation of its protonated form, is even larger reaching approximately 350 g/L ($S = 2.2$ M) in 0.1 M HCl. Furthermore, PTA is soluble in DMSO, acetone, chloroform, dichloromethane, but not in hydrocarbons such as toluene, benzene or hexane.

Using $H_2N(CH_2)_nNH_2$ ($n = 0$, 2 and 6) instead of formaldehyde, various PTA-related compounds bearing differently sized spacers (**3**) between the nitrogen groups have been prepared by Majoral and co-workers [6,7]. Modification of the synthetic procedure in Scheme 1 with the addition of sulfamide ($H_2NSO_2NH_2$) in combination with an excess of formaldehyde results in the formation of 2-thia-1,3,5-triaza-7-phosphaadamantane 2,2-dioxide (**4**) [8]. This compound, structurally related to PTA, also behaves as a coordinating phosphine with transition metals [9].

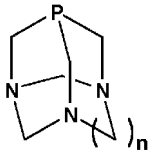

3

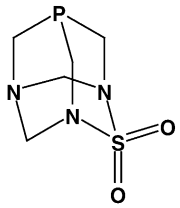

4

Scheme 2 illustrates some reactions of PTA leading to P(III) and P(V) derivatives which maintain the original phosphaadamantane skeleton.

The overall reactivity of PTA is comparable to other alkyl phosphines, with the notable exception that PTA is stable when exposed to oxygen, in contrast to PMe_3 and PEt_3 which are both known to violently ignite in air. Furthermore, PTA appears to have higher resistance to oxidation than other types of water-soluble phosphines including TPPMS and TPPTS. Oxidation of PTA and **3** ($n = 2$ and 6) is accomplished using either hydrogen peroxide, nitric acid [10a] or nitrogen tetraoxide (under reflux conditions) forming the corresponding phosphine oxides [10b]. A report by Espenson demonstrates that PTA is ready oxidized to PTA(O) by H_2O_2 using CH_3ReO_3 as a catalyst. The kinetics of the oxidation was monitored using ^{31}P NMR and UV-Vis spectroscopy and compared with other aryl-phosphines which showed that the rate constant is two orders of magnitude smaller than for PPh_3 [11]. Similarly, the oxide version of **4** is prepared by treatment with *t*-butyl hydroperoxide and the product is re-crystallized from acetone [8,12]. Refluxing **2** with elemental sulfur or selenium results in PTA(S) [3] and PTA(Se) [13], respectively. Both the phosphine oxide (**5**) and sulfide (**6**) are thermally stable, decomposing at high temperatures (>260 °C) [5]. However, overall solubility as compared to the parent PTA is remarkably reduced. The oxide **5** is occasionally observed as a by-product in some preparative and catalytic reactions (vide infra Section 6).

One unique feature of PTA is the ability to be regioselectively protonated at nitrogen rather than at the phosphorus center [14]. In water solutions with a pH lower than 6.5, PTA forms the ammonium-phosphine $[PTA(H)]^+$ (**7**). The basicity of PTA has been measured by Darensbourg et al. with a pK_a of 5.70 [14a,14b] and by Alyea and co-workers with a pK_a of 6.0 [14c]. Experimental data and ab initio calculations show that further *N*-protonation of $[PTA(H)]^+$ is thermodynamically less favorable, as changes in hybridization of nitrogen centers create distortions in the adamantane-like cage structure and decrease overall stability. Oxidation of the phosphorus center results in decreased basicity of the nitrogen neighboring atoms, pK_a of PTA(O) is 2.52 [14a].

PTA can be *N*-alkylated using MeI [10b], EtI [15], $PhCH_2Cl$ [14c,16], or $I(CH_2)_4I$ [17] in acetone or methanol under refluxing conditions. The resulting alkyl salts PTA(R) (R = alkyl) (**7**) are air and water stable, but as expected due to their ionic character, they are less soluble in organic solvents than PTA [5,10b]. However, solubility in water

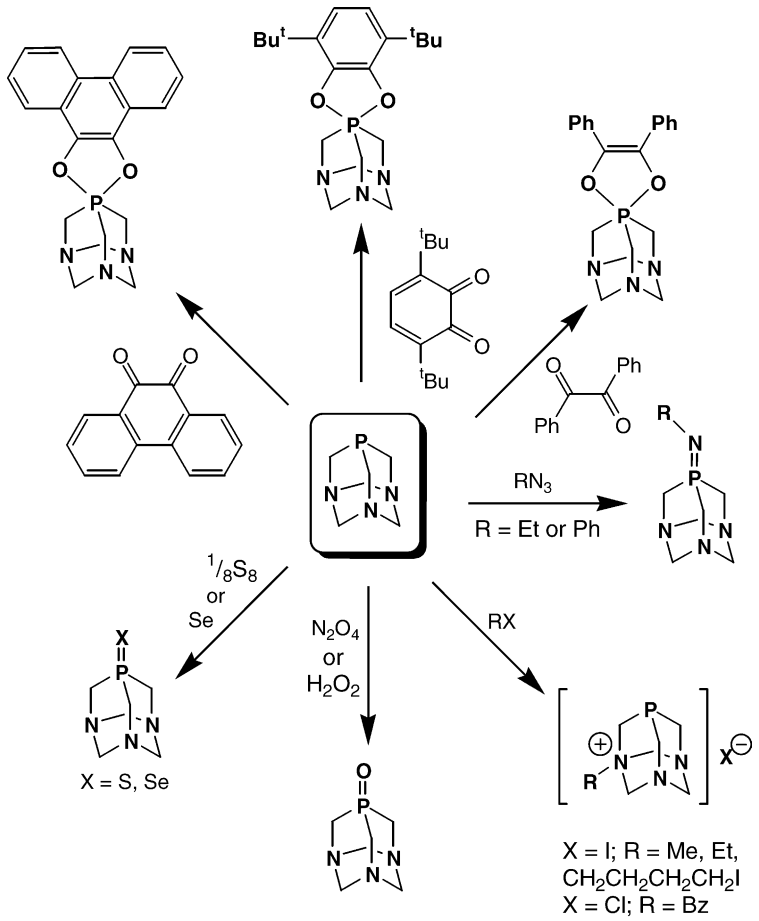

Scheme 2. Some PTA derivatization reactions.

is still maintained except when the anion is PF_6^-. The *N*-methylated species, [PTA(Me)]I is recrystallized from a mixture of methanol and ethylacetate, and readily dissolves in water or DMSO [5]. The *N*-alkylated PTA salts bind to transition metal through the phosphorus donor atom, but only a few complexes have been prepared (vide infra Section 4). The *N*-protonated and *N*-alkylated PTA salts have been shown to be poorer nucleophiles than the parent PTA and this can be in turn a useful strategy for functional group protection of the nitrogen centers.

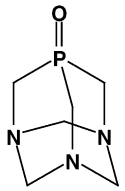

5

R = H, Me, Et, $I(CH_2)_2$, Bz and R = Me, Et, Ph, Bz, Cy.

Reactivity of *N*-alkylated PTA salts **7** differ from that of PTA. For example, oxidation of [PTA(Me)]I with H_2O_2 does not proceed, but [PTA(S)Me]I is readily obtained by refluxing [PTA(Me)]I with elemental sulfur in benzene [10b]. Alternatively, [PTA(S)Me]I can be produced by treating the

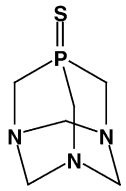

6

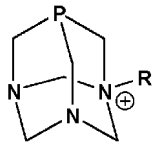

7

phosphine sulfide **6** with methyl iodide [10b]. The PTA sulfide and the corresponding methylated sulfide analogs are reported to have limited solubility in water and chloroform.

P-Alkylation of PTA is not possible directly from PTA. However, refluxing $[RP(CH_2OH)_3]Cl$ (R = Me, Et, Ph, Bz, Cy) in an acetone solution containing ammonium acetate and formaldehyde leads to the appropriate phosphonium salt (**8**) (Scheme 3) [18]. In contrast, the addition of methyl iodide to a solution of **4** forms the phosphonium salt and

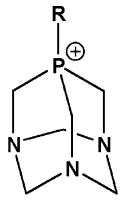

8

not a *N*-alkylated product [8,9]. In the presence of picric acid or hydrochloric acid both PTA and PTA(O) are protonated and subsequent addition of formaldehyde leads to formation of methopicrate or methochloride species as identified through elemental analysis and NMR spectroscopy [19].

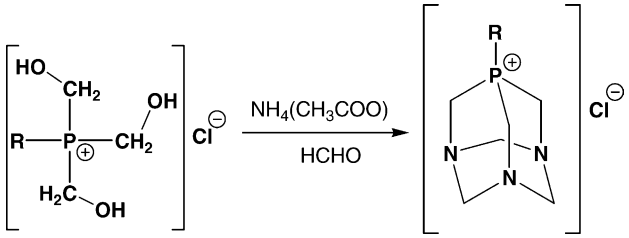

Scheme 3.

In contrast to PTA, **4** is unreactive with formaldehyde in the presence of acid. This marked difference in reactivity between **2** and **4** is not yet properly understood [9,17]. Hydrolysis of **2** carried out in the presence of excess HBr results in multiple cleavage of C–N bonds, forming the highly stable (dec 214 °C) white crystalline solid tris(ammoniomethyl)phospine as a tribromide salt, $[(NH_3CH_2)_3P]Br_3$, with a yield of 74% [20]. Similarly, treatment of PTA(O) with either HBr or HCl, forms white stable solids $[(NH_3CH_2)_3P(O)]X_3$ (X = Cl or Br) in high yield. PTA also reacts with ethyl- or phenyl-azide forming the corresponding phosphoroxoamides which yield spirophosphoranes by further reaction with various 1,2-diols. The latter may also be directly obtained by reacting **2** with different orthoquinones, such as 3,5-ditertbutylorthobenzoquinone and phenanthrenquinone. Dibenzyldione and other α-diketones also give similar P(V)-compounds via nucleophilic attack of the PTA phosphorus atom on the oxygen atom of the ketone (Scheme 2) [7].

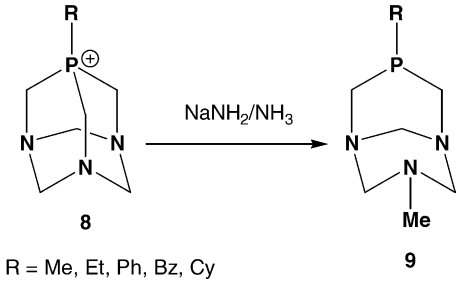

8 9

Scheme 5.

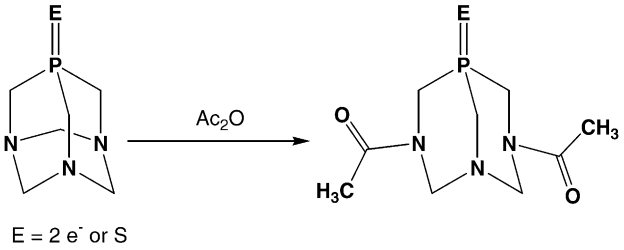

Scheme 6.

The reaction of diethylazodicarboxylate with **2** has been also briefly mentioned [6,7] and results in the formation of a P(V)-spirophosphorane (Scheme 4) which cannot be isolated. However, by further reaction with 1,2-diols a variety of stable dioxospirophosphoranes may be obtained. The reaction with 1,2-benzene-diol is illustrated in Scheme 4.

An open cage version of PTA (**9**) can be synthesized through cleavage of an endo rather than an exo C–P bond of the phosphonium salt (**8**) using sodium amide in liquid ammonia. Product isolation is achieved through sublimation of the crude reaction product (Scheme 5) [18]. The resulting compound behaves as a *P*,*N*-bidentate ligand and complexes of **9** featuring Mo and Au are known [18]. Cleavage of two N–C bonds in PTA can be accomplished by reacting **2** with acetic anhydride. Likewise, both PTA(O) and PTA(S) also undergo identical cage breaking with Ac_2O [10]. The resulting products contain *N*-acetyl amide functionalities as identified by NMR and IR spectroscopy (Scheme 6).

3. Physical properties of PTA and related PTA derivatives

The cone angle of PTA is relatively small for a phosphine (103°). A comparison with other alkyl- and aryl-phosphines

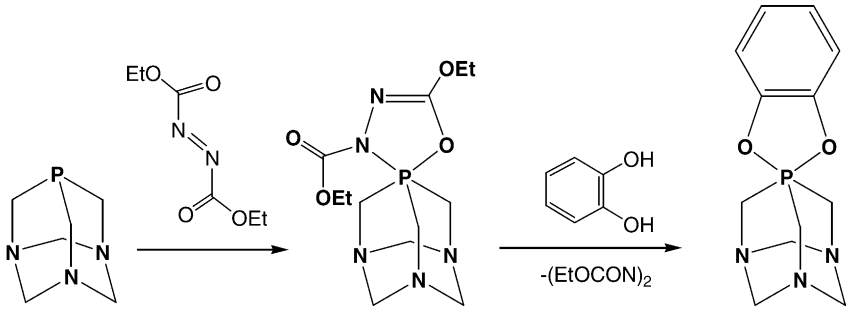

Scheme 4.

is shown below [21].

$$\underset{91^\circ}{PH_3} < \underset{103^\circ}{PH_2Me} = \underset{103^\circ}{PTA} < \underset{110^\circ}{PEt_3} < \underset{127^\circ}{PPhH_2} < \underset{134^\circ}{PMe_3} < \underset{135^\circ}{P(i\text{-}Pr)_3} < \underset{145^\circ}{PPh_3} < \underset{170^\circ}{PCy_3} < \underset{182^\circ}{P(t\text{-}Bu)_3} < \underset{212^\circ}{P(Mes)_3}$$

Hence, the small compact undemanding steric property of PTA combined with the chemical and thermal stability and the high hydrophilicity makes this ligand unique in comparison with less encumbering phosphines such as PMe_3 and allow useful applications such as the synthesis of luminescent gold(I) compounds (vide infra Section 8).

^{31}P NMR spectroscopy is an important tool in studying the coordination properties of PTA and to investigate in situ the mechanisms of catalytic reactions involving PTA complexes. A summary of ^{31}P and ^{1}H NMR data for PTA and related derivates and complexes are provided in Table 1.

A solid-state ^{31}P CP MAS NMR spectrum has been measured and shows a chemical shift of −104.4 ppm, in the range of values observed in solution [18a,22]. The *N*-protonation or *N*-alkylation of PTA decreases molecular symmetry resulting in a highly complex ^{1}H NMR spectra with multiple spin systems, hence literature data for PTA(H) and PTA(R) complexes is often reported as ranges. Furthermore, the ^{31}P chemical shift of $[PTA(H)]^+$ and $[PTA(Me)]^+$ are only slightly different from that of PTA which may cause additional problems in interpreting the spectra of mixed PTA/PTA(R) compounds. However, $\delta(^{31}P)$ of **3** = −115.9 ppm (DMSO-d_6) is slightly shielded compared to PTA [5]. NMR properties of **5** and **6** are typical of phosphine oxides and sulfides as summarized in Table 1.

Raman and infrared spectra have been used to characterize PTA complexes although few data are reported. PTA has poorly diagnostic IR absorption bands at 452 and 405 cm^{-1} and a characteristic Raman absorption at 256 cm^{-1} [5,16a,22]. In comparison, both PTA(O) and [PTA(Me)]I display a similar IR spectrum to **2** [5] and the IR band at 1167 cm^{-1} is characteristic of the P=O bond stretching in PTA(O) [23].

The crystal structure of PTA, PTA(O), PTA(S) and methylated $[PTA(Me)]^+$ analogues have been determined [16a,24]. The compounds crystallize, with the exception of $[PTA(Me)]^+$, in the *R*3*m* space group with the molecules having a three-fold axis of rotation, hence the point group C_{3v}. Both the P–C and N–C bond lengths are typical and show no indication of strain. *N*-Methylation does not affect any of the bond distance associated with the phosphorus center [24]. No crystal structures featuring an uncoordinated *N*-protonated PTA have been reported. The structure of the thioderivative **4** have been determined and, apart from the disruption of the trigonal symmetry of the PTA cage due to the replacement of one NCH_2N group with a NSO_2N unit, the overall structure resembles closely that of PTA, confirming the rigidity of the adamantane skeleton in these molecules [12].

Ab initio calculations by Galasso [25] are consistent with the photoelectron spectrum of both PTA and PTA(O) [13] and suggest that these compounds have a substantial amount of cage strain than other nitrogen substituted adamantane molecules which is consistent with increased difficulty for phosphorus to undergo s-orbital hybridization. This strain has the effect of increasing the energy of phosphorus lone pair by 0.5 eV as compared to PMe_3. Furthermore, photoelectron spectroscopy (PE) measurements show that the HOMO of PTA oxide is significant more stable than that of PTA which agrees with theoretical data indicating a large energy gain (−137.93 kcal/mol) upon oxidation [13]. Thus, the fact that PTA is stable in air whereas PMe_3 is not, suggests that oxidation of PTA is restricted by kinetics and not thermodynamics. Using UV photoelectron spectroscopy, Cowley et al. demonstrated that ionization energy (in eV) of the *e* and a_1 molecular orbitals of PTA(X) sequentially decreases going from E=O (8.19*e*, 10.66a_1) to Se (7.89*e*, 10.18a_1), PTA having an ionization energy (8.05*e*, 11.8a_1) comparable to PTA(S). The observation of a single low-energy signal suggests that the interaction between the phosphorus and nitrogen centers is large enough to make removal of an electron from a N or P/N dominant molecular orbital equal in terms of energy [13].

4. Transition metal complexes involving PTA and related PTA derivatives

The coordination chemistry of PTA is significantly scarce when compared to other tertiary phosphines although its synthesis and characterization has been known for about thirty years. Most developments in PTA coordination chemistry have occurred during the past decade and coincide with the advent of green chemistry and the drive for environmentally friendly catalysis. Furthermore, the luminescent properties of gold–phosphine complexes and the cytotoxicity of a few ruthenium PTA complexes have boosted a new interest in PTA chemistry.

4.1. Chromium, molybdenum and tungsten PTA complexes

Historically, the first PTA–metal complex $Mo(CO)_5(PTA)$ (**10**), was synthesized through ligand exchange by refluxing PTA with $Mo(CO)_6$ in dry diglyme or reacting PTA with the THF adduct of $Mo(CO)_5$. The former procedure is also applicable with $Cr(CO)_6$ and $W(CO)_6$ [26]. Alternatively, mono-substituted PTA molybdenum and tungsten complexes can be synthesized through the addition of Me_3NO to $M(CO)_6$ in acetonitrile followed by reaction with PTA [27]. Scheme 7 highlights these and related synthetic procedures.

The adducts range in color from light yellow for $Cr(CO)_5(PTA)$ (**11**) to deep yellow for $W(CO)_5(PTA)$ (**12**).

Table 1
^{31}P and ^{1}H NMR spectral data of PTA derivatives and complexes

Compound	^{31}P, mult[a] (J_{PP}, J_{MP})[d]	^{1}H, mult[a] (J_{HP}, J_{HH})[d]	Solvent	Color	Reference
PTA (**2**)	−98.3 s −97.4 s −104.4 s	3.90 d (9) 4.43 s	D_2O CD_3OD Solid state	White	[5] [39] [22]
$PTA(SO_2)$ (**4**)	−115.9 s	3.9 d (10) 4.87 br	DMSO	White	[8,9]
PTA(O) (**5**)	−2.49 s	4.28 d (11) 4.0 s	D_2O	White	[3,5]
[PTA(Me)]I (**7**)	−86.1 s −84.3 s	2.71 s 3.78 m, 5.1 s	DMSO-d_6 CD_3CN	White	[5]
$[PTA(Me)]PF_6$ (**7**)	−84.2 s		D_2O	White	[5]
$Mo(CO)_5(PTA)$ (**10**)	−55.9 d (126)[b] −58	4.28 d (2) 4.60 s	CD_3CN DMSO-d_6	Off-white	[27] [26]
$Cr(CO)_5(PTA)$ (**11**)		4.56 s 4.8 d (1.8)	$(CD_3)_2CO$	Light yellow	[26]
$W(CO)_5(PTA)$ (**12**)	−78.4 d	 4.31 s, 4.62 s	CD_3CN $(CD_3)_2CO$	Yellow	[27] [26]
$Mo(CO)_4(PTA)_2$ (**17**)	−54.9 d (126)[b]		CD_3CN		[27]
$Mo(CO)_3(PTA)_3$ (**19**)	−51.47 d (127)[b]	4.6–4.8 m	$CDCl_3$	White	[30]
$W(CO)_5\{PTA(SO_2)\}$ (**20**)	−81.6 d (229)[b]			Yellow	[9]
$CpWH(CO)_2(PTA)$ (**25**)	*cis* −52.3 d (241)[b] *trans* −59.9 d (273)[b]	*cis* 5.30 s *trans* 5.17 s 4.59–3.85 m	CD_2Cl_2	Pale yellow	[33]
$[ReBr_2(CO)_3(PTA)](NEt_4)$ (**26**)	−87.7 s	1.23 tt (7.23) 3.2 q (7.2) 4.53 d (12.9)	CD_3CN	Colorless	[36]
$[ReBr(CO)_3(PTA)_2]$ (**27**)	−91.9 s	4.31 d (14.8), 4.39 d (14.8), 4.64 s	D_2O	White	[36]
$[ReBr(CO)_2\{PTA(H)\}_2]Br_2$ (**28**)	−75.2 s	4.34 d (15.2), 4.41 d (15.2), 4.8 s	D_2O	White	[36]
$[Re(CO)_3(PTA)_3]PF_6$ (**29**)	−95.2 brs	4.29 s, 4.61 d (13.5)	D_2O	White	[36]
$Fe(CO)_4(PTA)$ (**32**)		4.30, 4.62	$(CD_3)_2CO$	Yellow	[36]
[CpFe(CN)$_2$(PTA)] K (**33**)	9.4 s		CD_3OD	Orange	[39]
$CpFe(CN)_2\{PTA(H)\}$ (**34**)	20 s		CD_3OD	Pale yellow	[39]
$RuCl_2(PTA)_4$ (**35**)	−47.6 s	4.40 brs, 4.67 brs	CD_3Cl	Yellow	[40a]
$RuI_4\{PTA(Me)\}_2$ (**39**)	−60.8 s	2.81 s, 4.3 m (16.7), 4.4 m (15.6), 4.7 s, 4.8 m (11.2)	DMSO-d_6		[41]
$[RuI_2\{PTA(Me)\}_2]I_3$ (**40**)	−8.3 t −52.1 d (31.6)	2.89 s, 2.85 s, 4.8 m	DMSO-d_6	Dark orange	[41]
$RuCl_2$(*p*-cymene)(PTA)] (**41**)	−36.6 s	1.22 d (6.93), 2.08 s, 2.78 sept (41.37), 4.53 s, 5.46 q (19.7)	$CDCl_3$	Red	[42a]
$[RuCl$(*p*-cymene)$(PTA)_2]BF_4$ (**42**)	−33.0 s	2.08 s, 4.32 s, 4.53 s	D_2O	Deep red	[42a]
$CpRuCl(PTA)_2$ (**43**)	−25.6 s	4.04 m (14.1), 4.8 m	CD_2Cl_2	Yellow	[44]
$Cp^*RuCl(PTA)_2$ (**44**)	−34.2 s	1.74 t (1.6), 4.1 m (15), 4.54 m	CD_2Cl_2	Yellow	[44]
$Ru_3(CO)_9(PTA)_3$ (**45**)	−44.4 s −44.8 s		$CDCl_3$	Reddish orange	[45]
$RuHCl(PTA)_4$ (**47**)	−5.3 dd (19) −39.8 dd (32) 48.6 dt (22)	8.31 dq (27.5, 86.5, 27.1)	D_2O/HCl		[46]
$Ru(H)_2(PTA)_4$ (**48**)	−21.1 t (23) −28.2 t (23)	−11.4 m (30.5, 27.3)[c]	D_2O		[46]
$[CpRuH(PTA)_2]$ (**51**)	−11.5 s	−14.36 t (36.4)[c] 3.72 s 4.43 brs	DMSO-d_6	Light yellow	[44]
$[Cp^*RuH(PTA)_2]$ (**52**)	−20.8 s	−14.64 t (36.9)[c] 3.73 s 4.43 brs	DMSO-d_6	Light yellow	[44]

Table 1 (*Continued*)

Compound	^{31}P, mult[a] (J_{PP}, J_{MP})[d]	^{1}H, mult[a] (J_{HP}, J_{HH})[d]	Solvent	Color	Reference
$[RhI_4\{PTA(Me)\}_2]I$ (**56**)	−77.4 d (96.8)[b]	2.80 s 4.22 d (8.3) 4.31 d (8.3) 4.77 s 4.16 d (9.7) 4.49 d (9.7) 4.65 d (7.0) 4.74 d (7.0)	CD_3CN	Yellow	[50]
$[Rh(CO)I\{PTA(Me)\}_2]I_2$ (**57**)	−50.5 d (124)[b]	2.76 s, 4.33 d (14) 4.49 d (14), 4.62 s 4.83 d (12) 4.95 d (12)	D_2O	Yellow	[51]
$[Rh(CO)I\{PTA(Me)\}_3]I_3$ (**58**)	−58.4 brs	2.71 s 4.13 d (15.5) 4.22 d (15.5) 4.32 d (12.1) 4.48 d (12.1) 4.57 s 4.81 d (12.2) 4.93 d (12.2)	D_2O	Brownish red	[51]
$[RhCl\{PTA(H)\}(PTA)_2]Cl$ (**59**)	−21 br −23 br	4.2 br s 4.5 br s	D_2O	Yellow	[23]
$[RhCl\{PTA(H)\}_3(PTA)_2]Cl_3$ (**60**)	−21.6 dt (107, 23[b]) −49.2 dt (80, 23[b])		D_2O	Deep red	[23]
Rh(CO)(acac)(PTA) (**61**)	−25.5 d (172.4)	1.97 s, 4.27 s, 6.60 s, 5.60 s.	CD_3OD		[52]
$IrCl(CO)(PTA)_2$ (**64**)	−53.7 s −58.1 s		D_2O DMSO-d_6	Yellow	[54b]
$IrCl(CO)(PTA)_3$ (**65**)	−60.9 t (12) −76.0 d (12)		DMSO-d_6	Pale green	[54a]
$[Ir(CO)(PTA)_4]Cl$ (**66**)	−85.1 s	4.07 br s 4.52 d (14)	D_2O	Yellowish green	[54a]
cis-$[IrCl_2\{PTA(H)\}_2(PTA)_2]Cl_3$ (**67**)	−72.6 t (15)	4.42 brs 4.56 brs	D_2O	White	[54a]
cis-$[IrH_2\{PTA(H)\}_4]Cl_5$ (**68**)	−74.1 t (18) −82.4 t (18)	−13.79 dq (120, 22),[c] 4.19 d (25), 4.65 s, 4.72 s, 4.74 s, 4.78 s	D_2O	White	[54a]
$[Ir(H)Cl(PTA)_4]Cl$ (**70**)	−65.7 dt (19, 17) −83.5 t (19) −91.7 t (19)	−12.00 dq (139, 19)[c]	D_2O		[54a]
$Ni(PTA)_4$ (**72**)	−46.5 s		D_2O	White	[56a]
$NiCl_2(PTA)_2$ (**73**)	−1.2 s	 3.85 d (19) 4.15 q (14)	CD_3OD D_2O	Red	[14b]
$Ni(CN)_2(PTA)_3$ (**74**)	−49.1 s −49.7 s	4.23 brs 4.62 m	CD_3OD DMSO-d_6	Red	[57]
$Ni(CO)(PTA)_3$ (**75**)	−54 s		THF-d_8	Pale Yellow	[14b]
$Ni(CO)_3(PTA)$ (**76**)	−47.2 s		CD_3OD	White	[14b]
$[Ni(NO)(PTA)_3]NO_3$ (**77**)	−48.2 s		D_2O	Purple	[59]
Ni(L, $R_A = R_B = R_D = H$, $R_C = NO_2$)Me(PTA) (**79a**)	−47.10	3.73 s, 4.09 dd (32.69, 12.90)	CD_2Cl_2	Yellow	[61]
Ni(L, $R_A = OMe$, $R_B = R_C = R_D = H$)Me(PTA) (**79b**)	−56.56	4.00 s, 4.08 dd (22.79, 13.20)	C_6D_6	Yellow	[61]
Ni(L, $R_C = CH(CH)_2CH) = R_D$, $R_A = R_B =$ H)Me(PTA) (**79c**)	−60.88	3.83 s, 4.02 dd (34.19, 13.20)	C_6D_6	Yellow	[61]

Table 1 (*Continued*)

Compound	^{31}P, mult[a] (J_{PP}, J_{MP})[d]	^{1}H, mult[a] (J_{HP}, J_{HH})[d]	Solvent	Color	Reference
Ni(L, R_A =R_C =Cl, R_B = R_D = H)Ph(PTA) (**79d**)	−59.36	3.93 s, 4.04 dd (22.79, 13.20)	C_6D_6	Yellow	[61]
Ni(L, R_A = Ph, R_B = R_C = R_D = H)Me(PTA) (**79e**)	−55.34	3.66 s, 3.91 dd (42.29, 13.20)	C_6D_6	Yellow	[61]
Ni(L, R_A = R_B = R_D = H, R_C = NO_2)Me(PTA)	−57.76	3.91 s, 4.313 dd (19.79, 12.90)	CD_2Cl_2	Yellow	[61]
$PdCl_2(PTA)_2$ (**80**)	−18.3 s		DMSO-d_6	Yellowish green	[57]
$[PdCl_3(PTA)]Cl$ (**82**)	−25 br −43.6 br		D_2O		[59]
$Pd(PTA)_4$ (**83**)	−59.2 s −54.2 s	3.79 s, 4.41 d, 4.49 d (13)	D_2O 0.1 M HCl	Gray	[56a] [14b]
$Pd(dba)_2(PTA)_2$ (**84**)	−59.8 s	4.35 m, 4.55 m	$CDCl_3$	Yellowish orange	[56a]
$[Pd\{PTA(H)\}_4]Cl_4$ (**85**)	−54.2 s		D_2O	Pale yellow	[14b]
$Pd(SePh)_2(PTA)_2$ (**86**)	−66.1 s	4.06 br s, 4.25 q	$CDCl_3$		[64]
Pd(L, R_A = R_B = R_D = H, R_C = NO_2)Me(PTA) (**87a**)	−46.18	3.83 s, 3.99 dd (30.59, 13.50)	C_6D_6	Yellow	[61]
Pd(L, R_A = OMe, R_B = R_C = R_D = H)Me(PTA) (**87b**)	−44.74	3.98–4.08 m	C_6D_6	Yellow	[61]
Pd(L, R_C = $CH(CH)_2CH$) = R_D, R_A = R_B = H)Me(PTA) (**87c**)	−47.18	3.85 s, 3.93 dd (29.39, 13.20)	C_6D_6	Yellow	[61]
Pd(L, R_A = R_C = Cl, R_B = R_D = H)Ph(PTA) (**87d**)	−44.54	3.98 s, 3.99 dd (20.39, 12.90)	C_6D_6	Yellow	[61]
Pd(L, R_A = Ph, R_B = R_C = R_D = H)Me(PTA) (**87e**)	−46.16	3.70 s, 3.91 dd (20.09, 13.50)	C_6D_6	Yellow	[61]
trans-$PtI_2(PTA)_2$ (**97**)	−73.1 d (2316)[b]		D_2O	Yellow	[72]
Pt(ts)PTA (**98**)	−49.6 d (2612[b], 25) −63.9 d (2525)[b]		DMSO-d_6/H2O	Pale yellow	[74]
AuCl(PTA) (**99**)	−51.4 s	4.53 s, 4.48 s, 4.35 d (10)	DMSO-d_6	White	[78]
AuBr(PTA) (**100**)	−47.3 s	4.33 d (9), 4.54 m, 4.49 m	DMSO-d_6	White	[78]
AuI(PTA) (**101**)	−47.6 s	4.33 d (9), 4.49 m, 4.54 m	D_2O	White	[78]
AuMe(PTA) (**102**)	−36.6 s	4.31 d (10), 4.53 s, 4.48 s		White	[78]
[AuCl{PTA(Me)}]OTf (**103**)	−33.1 s	2.73 d (2.1), 4.51–5.1 m	DMSO-d_6	White	[78]
[AuCl{PTA(H)}]Cl (**104**)	−38.9 s		D_2O		[79]
$AuCl(PTA)_2$ (**107**)	−36.1 s		CD_3CN	White	[81]
$AuCl(PTA)_3$ (**109**)	−56.3 br		CD_3OD	White	[81]
$[Au(PTA)_4]Cl$ (**112**)	−58 s	3.52 s, 4.88 d	D_2O		[84]
$[Au\{PTA(Me)\}_4](PF_6)_5$ (**113**)	−25.5 s		D_2O	White	[84]
$[Au\{PTA(H)\}_3(PTA)](PF_6)_4$ (**114**)	−60.3 br		D_2O	White	[84]
AuPh(PTA) (**119**)		4.2 s, 4.5 d	CD_3CN	White	[85]
Au(SPh)(PTA) (**120**)	−49.8 s	4.2 s, 4.5 d	$CDCl_3$	White	[86]
Au{S(*o*-PhOMe)}(PTA)	−45.6 s	3.85 s, 4.3 s, 4.5 d	$CDCl_3$	White	[86]
Au{S(*m*-PhOMe)(PTA)	−49.9 s	3.75 s, 4.3 s, 4.5 d	$CDCl_3$	White	[86]
Au{S(*o*-PhCl)}(PTA)	−45.3 s	4.3 s, 4.5 d	$CDCl_3$	White	[86]
Au{S(*m*-PhCl)}(PTA)	−50.1 s	4.3 s, 4.5 d	$CDCl_3$	White	[86]
Au{S(*p*-PhCl)}(PTA)	−50.2 s	4.3 s, 4.5 d	$CDCl_3$	White	[86]
Au{S(3,5-$PhCl_2$)}(PTA)	−50.7 s	4.3 s, 4.5 d	$CDCl_3$	White	[86]
$HgCl_2(PTA)$ (**121**)	−38.3 d (6559)[b]		Solid state		[22]
$HgBr_2(PTA)$	−44.1 d (6184)[b]		Solid state		[22]

Table 1 (*Continued*)

Compound	^{31}P, mult[a] (J_{PP}, J_{MP})[d]	^{1}H, mult[a] (J_{HP}, J_{HH})[d]	Solvent	Color	Reference
$HgI_2(PTA)$	−61.4 d (4037)[b]		Solid state		[22]
$Hg(SCN)_2(PTA)$	−32.6 d (4589)[b] −38.2 d (6510)[b]		Solid state		[22]
$Hg(CN)_2(PTA)$	−50.4 d (4589)[b] −59.4 d (4581)[b]		Solid state		[22]
$Hg(NO_3)_2(PTA)_2$ (**122**)	−29.9 d (5111)[b]		Solid state		[22]
$HgCl_2(PTA)_4$ (**123**)	−63.4 d (1937)[b]		Solid state		[22]
$HgBr_2(PTA)_4$	−62.8 d (1953)[b]		Solid state		[22]
$Hg(NO_3)_2(PTA)_4$	−58.0 d (1876)[b]		Solid state		[22]

[a] mult = multiplicity; s, singlet; d, doublet; dq, doublet of quartets; t, triplet; dt, doublet of triplets; tt, triplet of triplets; br, broad; brs, broad singlet; q, quartet; sept, septuplet; m, multiplet.
[b] J_{PM}.
[c] Hydride resonance.
[d] Coupling constants are in Hz. L = salicylaldiminato.

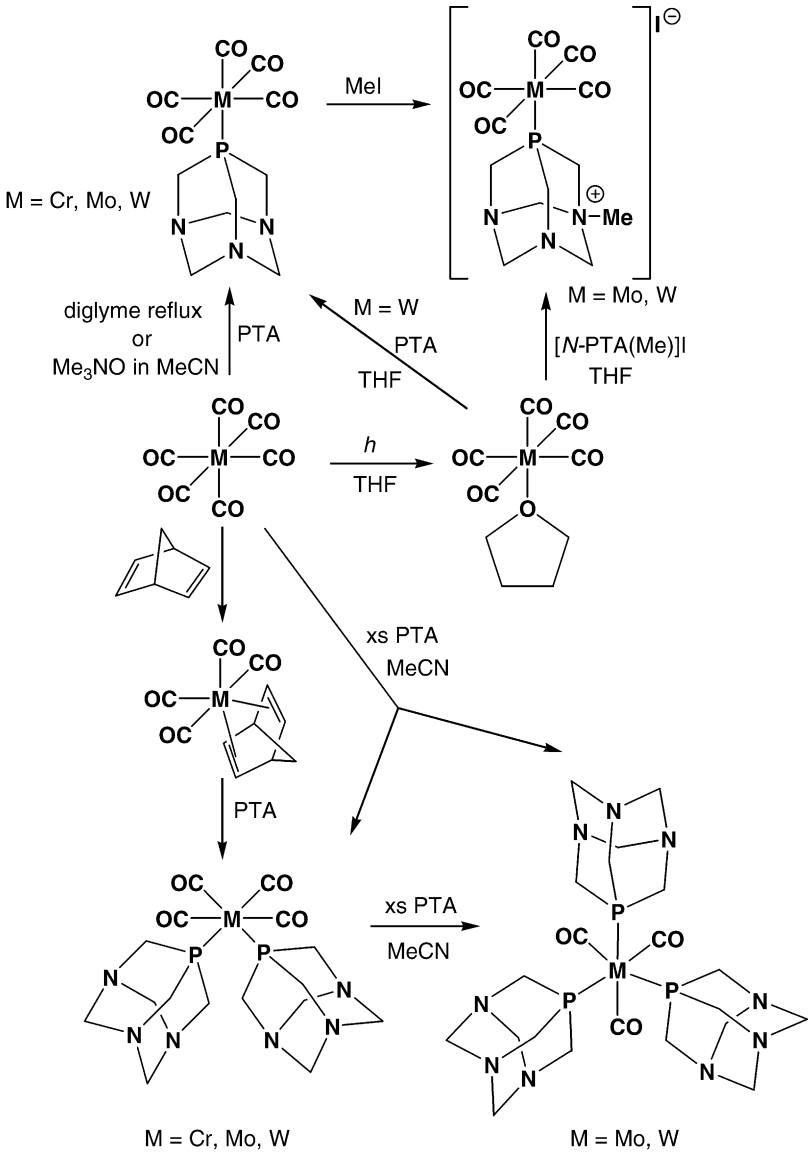

Scheme 7.

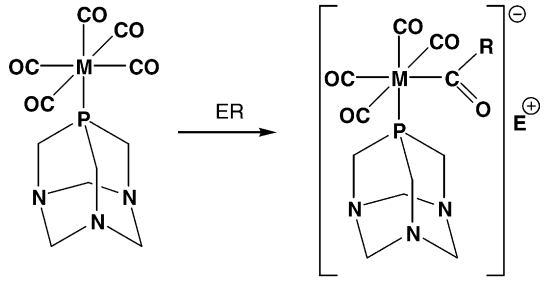

M = Cr, Mo; ER = $PhCH_2MgCl$, PhLi **13**

Scheme 8.

All compounds were characterized by NMR and IR spectroscopy, the latter method identifying single phosphine substitution from the CO absorption pattern. Furthermore, axial and equatorial Cotton-Kraihanzel force constants [26] are unaffected by the nature of the metal center. The nucleophilicity of PTA was established by examining the location of the CO stretching frequencies in $Mo(CO)_5(PTA)$, which showed that PTA is roughly equal to PMe_3 [27]. ^{31}P CP MAS NMR data show for **10** a chemical shift of −55.9 ppm in the solid-state and compares well with that found in solution (DMSO-d_6, −58 ppm).

Complex **12** has small $^1J(^{183}W\text{-}^{31}P)$ coupling constants suggesting a donor strength close to that of $P(^nBu)_3$. The $M(CO)_5(PTA)$ complexes (M = Cr, Mo) were shown to react with both Grignard and organolithium reagents, where one carbonyl group undergoes nucleophilic attack by the carbanion to yield ionic acyl derivatives $[M(CO)_4\{C(O)R\}(PTA)]E$ (E = Li, R = Ph; E = MgCl; R = Bz) (**13**) (Scheme 8) [26]. Kinetic studies of the reaction between $Cr(CO)_5(PTA)$ and $PhCH_2MgCl$ show that the rate of nucleophilic addition to CO is equal to that observed for $Cr(CO)_5(PMe_3)$. Attempts to alkylate electrophilically the carbonyl group of **13** either with $CH_3SO_3CF_3$ or Meerwin's salt, $[Et_3O]BF_4$, resulted in mixtures including complexes featuring *N*-alkylated PTA (Scheme 8).

An interesting property of PTA is the ability to be alkylated while coordinated as demonstrated by the reaction of $W(CO)_5(PTA)$ with CH_3I [26]. Alternatively, the reaction of [*N*-PTA(Me)]I with $W(CO)_5(THF)$ affords the same product, $[W(CO)_5(N\text{-}PTA(Me)]I$ (**14**) (Scheme 7). However, the resulting salt is thermally less stable than the non-alkylated complex. Similarly, the alkylation reaction can be performed with $Mo(CO)_5(PTA)$ [27]. ^{31}P CP MAS NMR data for $[M(CO)_5\{N\text{-}PTA(Me)\}]I$ [M = Mo (**15**), W (**14**)] differ significantly from those of non-alkylated analogs. In addition, ^{95}Mo NMR, a useful technique for determining the number of substituted PTA ligands in molybdenum complexes, shows a significant difference in chemical shift between $Mo(CO)_5(PTA)$ and $Mo(CO)_5[N\text{-}PTA(Me)]I$ [27]. Solid-state ^{95}Mo NMR data show similar changes, hence suggesting that the alkylation of the PTA ligand decreases π-accepting ability. Moreover, comparisons with other phosphines and phosphorus-coordinating ligands suggest PTA has coordinating properties closer to those of $P(OMe)_3$ rather than PMe_3 with PTA having a weaker nephelauxetic effect. Structural investigation on **10** using X-ray diffraction techniques confirmed P-coordination of the PTA and indicate good σ- and π-bonding abilities for the cage molecule as the Mo–P bond length is relatively small at 2.48 Å [28].

Higher substituted PTA complexes involving Cr, Mo and W have been prepared by nucleophilic displacement of piperidine, from *cis*-$M(CO)_4(pip)_2$ in dichloromethane [29] or substitution of norbornadiene from $M(CO)_4(NBD)$ [29] forming compounds of the type $M(CO)_4(PTA)_2$ (M = Cr (**16**), Mo (**17**), W (**18**)]. Similarly, trisubstituted complexes are synthesized by refluxing excess of PTA with $M(CO)_6$ (M = Mo or W) in MeCN. However, in the latter reaction, the product is contaminated with bis-substituted species [27]. Clean isolation of $Mo(CO)_3(PTA)_3$ (**19**) is accomplished by reacting PTA and $Mo(CO)_3(Mes)$ (Mes = mesitylene) in methanol/dichloromethane [30]. The PTA substitution pattern for the bis and tris complexes was determined through IR spectroscopy. Synthesis of $M(CO)_4(PTA)_2$ (M = Mo, W) resulted in *cis*-substitution. In the original report, the occurrence of an extremely slow isomerization to the *trans*-product was suggested [29], whereas a later report failed to observe any isomerization [30]. In comparison, in reactions involving other phosphines, both *cis*- and *trans*-isomers were observed and the related triphenylphosphine complexes were found to readily isomerize. The mechanism is thought to involve dissociation of the phosphine followed by re-association [27]. The fact that the *cis*-$M(CO)_4(PTA)_2$ complexes do not isomerize reflects the small steric requirement of PTA favoring the thermodinamically stable *cis*-compound over the *trans*-isomer. ^{95}Mo NMR spectra of **19**, show coupling of the molybdenum with three equivalent P-atoms, allowing Alyea et al. to assign a fac geometry to the trisubstituted derivative **19** [27].

The related thiadioxide derivative $PTA(SO_2)$ (**4**) was also shown to coordinate with tungsten, forming the yellow complex $W(CO)_5\{PTA(SO_2)\}$ (**20**) [9]. Comparison of CO stretching frequencies with Cotton-Kraihanzel analysis for **20** and **12** reveals that the coordinated ligands show identical electronic properties.

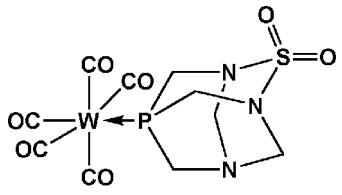

20

Structures from single crystal X-ray diffraction studies have been obtained for $Mo(CO)_5(PTA)$ [28] and $Mo(CO)_3(PTA)_3$ [30]. In both structures, the Mo–P distances are identical (2.48 Å versus $2.489(9)_{ave}$ Å, respectively). As anticipated from ^{95}Mo NMR spectroscopy, the trisubstituted molybdenum derivative exhibits a facial OCT geometry.

The ligand displacement property of PTA was kinetically compared with other types of phosphines in the substitution of piperidine from the complex *cis*-$Cr(CO)_4\{P(O^iPr)_3\}$(pip) [31]. The PTA complexes, $Cr(CO)_4$(PTA)(pip) (**21**) and $Cr(CO)_4\{P(O^iPr)_3\}$(PTA) (**22**), were isolated and characterized by IR spectroscopy and elemental analysis. The A′, A″ and A″ + E_{trans} CO stretch frequencies for **22** are identical to those of $Cr(CO)_4\{P(^nBu)_3\}\{P(O^iPr)_3\}$ [31].

PTA has found use in the stabilization of 19-electron Mo species including **23** and **24** which are important intermediates resulting from photochemical induced disproportionation of metal carbonyl dimers [32]. The irradiation of $[(CpCH_2CH_2NH_3)_2Mo_2(CO)_6]^{2+}$ in water containing PTA results in a mixture of bis-, mono- and unsubstituted products. Similarly, $(CpCOO)_2W_2(CO)_2$ with PTA in H_2O dissociates to 19-electron species $(CpCOO)W(CO)_3$PTA. Mo(II) complexes $[(CpCH_2CH_2NH_3^+)Mo(CO)_3(PTA)]$ (**23**) and $[(CpCH_2CH_2NH_3^+)Mo(CO)(PTA)_2]$ (**24**) are obtained by photolysis of the corresponding carbonyl dimers in water. They were used as stoichiometric reducing agents for methyl viologen (MV^{2+}), ferricyanide and cytochrome c in the presence of sulfur at pH 7 in water [32].

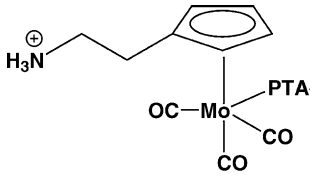

23

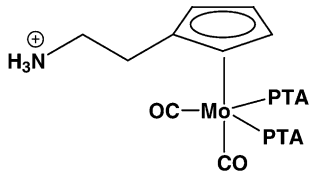

24

A remarkable tungsten hydride species, $CpWH(CO)_2$(PTA) (**25**) was synthesized by Bullock and co-workers by reacting $CpWH(CO)_3$ with PTA in toluene [33]. The high yielding reaction results in a 64 to 36 ratio of *cis*- and *trans*-isomers as determined by NMR spectroscopy. However, only the *trans*-$CpWH(CO)_2$(PTA) complex crystallized from a CH_2Cl_2/THF/MeCN solvent mixture, yielding crystals suitable for an X-ray diffraction study. The product, however, is insoluble in water [33].

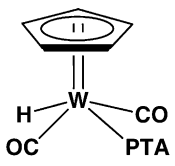

25

PTA was used as catalytic reducing agent in water for $Mo^{VI}O_2$ species including Mo-containing enzymes, especially Rhodobacter sphaeroides dimethylsulfoxide reductase (DSR). Using labelled ^{18}O-DMSO, the reduction of DMSO with DSR and PTA in water was followed using CI-MS showing transfer of oxygen and the final formation of PTA(^{18}O) (100% atom transfer) [34].

4.2. Rhenium PTA complexes

Although no manganese or technetium complex containing PTA has been so far described, its coordination chemistry with the higher group **7** element, rhenium, has received significant attention. The chemistry of rhenium has indeed special interest also because of its proximity in the periodic table to ^{99m}Tc which is important for radio-pharmaceutical applications [35]. Use of water-soluble phosphines such as PTA are more favorable for in vivo applications. Schibli et al. demonstrated that is possible to replace stepwise the halide ligands of *fac*-$(NEt_4)_2[ReBr_3(CO)_3]$ with PTA [36]. Reaction of *fac*-$(NEt_4)_2[ReBr_3(CO)_3]$ with one or two equivalents of PTA in MeOH and extracting with THF yields the white products $(NEt_4)[ReBr_2(CO)_3(PTA)]$ (**26**) and $ReBr(CO)_3(PTA)_2$ (**27**), respectively. Protonation of the PTA ligand in these complexes was accomplished by either adding HBr to **27**, forming $[ReBr(CO)_2\{PTA(H)\}_2]Br_2$ (**28**), or reacting *fac*-$(NEt_4)_2[ReBr_3(CO)_3]$ with two equivalents of $AgPF_6$ followed by addition of a solution of PTA and acidification with HBr. The trisubstituted product $[Re(CO)_3(PTA)_3]Y$ (Y = PF_6 or NO_3) (**29**) was synthesized by reacting the $[ReBr_3(CO)_3]^{2-}$ anion in THF with three equivalents of silver salt followed by three equivalents of PTA. All products were obtained in high yield and were authenticated by X-ray crystallography which confirmed an OCT coordination of the metal atom and a *fac* arrangement of the PTA ligands [36].

Complex **26** has high solubility in both organic solvents and water. Similarly, $ReBr(CO)_3(PTA)_2$ is soluble in organic solvents, but fairly water insoluble, whereas the *N*-PTA protonated derivative **28** is only soluble in water. Furthermore, the double positive charge of **28** causes a weakening of the Re-carbonyl π-back-bonding as inferred from the blue-shifting of the stretching frequencies of the CO bands. The solubility in water of the $[Re(CO)_3(PTA)_3]Y$ adduct depends on the nature of the anion. Only when the counter-anion is nitrate, the complex is water soluble. The rhenium-PTA complexes **26**–**29** exhibit an ambivalent solubility behavior in organic and aqueous media which may be adjusted through the protophilic properties of the PTA ligand, which, therefore, has the advantage of facile phase transfer by simple protonation. As an example, it was demonstrated by ^{31}P NMR experiments that it is possible to control efficiently the speciation of this system and its phase distribution. Thus, $ReBr(CO)_3(PTA)_2$ can be re-

moved completely from the organic phase of a H_2O/THF 1:1 mixture and transferred to the aqueous phase as $[ReBr(CO)_3\{PTA(H)\}_2]^{2+}$ by simply alternating the pH. At slightly alkaline pH 8.0 only $ReBr(CO)_3(PTA)_2$ in THF is observed, whereas at pH = 2.0, $[ReBr(CO)_3\{PTA(H)\}_2]^{2+}$ is present in water. This has strong implications for the safe and efficient separation and recycling of catalysts under biphasic conditions as it will be evident in Section 6 of this review. Compounds (**26**–**29**) were analyzed for kinetic ligand stability, an important parameter for the assessment of chemicals to be used as radio-pharmaceutical drugs [36]. The investigations with time-dependent ^{31}P NMR reveal that replacement of one or two bromide anions with solvent (DMSO or MeOH) is rapid, followed by slow replacement with PTA. However, in the case of DMSO, further substitution by PTA of $[Re(DMSO)_2(CO)_3(PTA)]^+$ was not observed and is attributed to stronger coordination strength of this solvent. The final observed species $[ReBr(CO)_3(PTA)_2]^+$ is formed by the displacement of solvent ligand by bromide which is more favorable due to increased electron-deficiency of the Re(I) center.

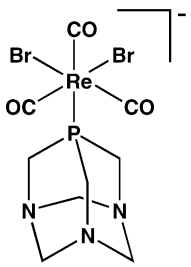

26

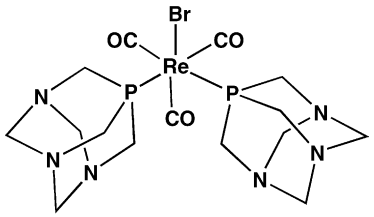

27

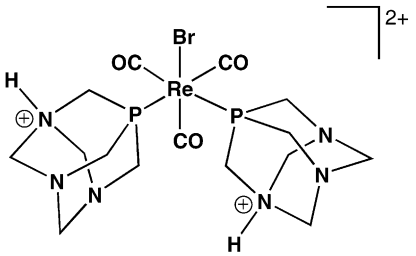

28

The high nucleophilic properties of PTA were demonstrated by Espenson and co-workers when the oxorhenium complex $[Re(O)(\eta^2\text{-}SCH_2CH_2S)(\eta^2\text{-}SCH_2CH_2SMe)]$

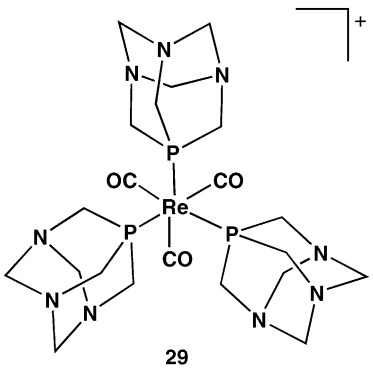

29

was reacted with PTA in toluene effecting the displacement of the thioether arm of the *S*-methylthioether-thiolate ligand. The reaction afforded the dark red compound $[Re(O)(\eta^2\text{-}SCH_2CH_2S)(\eta^1\text{-}SCH_2CH_2SMe)(PTA)]$ (**30**), featuring a dangling dithiolate ligand and a coordinated PTA ligand, see Scheme 9 [37].

The hexanuclear Re cluster $[Re_6Se_8(PTA)_6]I_2$ (**31**) has been prepared by Holm's group in quantitative yield by refluxing for 12 h an aqueous solution of $Cs_4[Re_6Se_8I_6]$ with excess PTA, the resulting compound is patented as an aqueous X-ray contrasting agent [38].

4.3. Iron and ruthenium PTA complexes

Only three iron-containing PTA complexes have been reported, the simple adduct $Fe(CO)_4(PTA)$ (**32**) [26] and the two ionic cyclopentadienyl derivatives, $K[CpFe(CN)_2(PTA)]$ (**33**) [39], and $CpFe(CN)_2\{PTA(H)\}$ (**34**) [39]. The first complex was synthesized in a similar way to $M(CO)_5(PTA)$ (M = Cr, Mo and W) by replacing one carbonyl ligand in $Fe(CO)_5$ with the phosphine. A TBP structure with the CO in axial position was assigned to **32** on the basis of the ν(CO) IR spectrum typical of axially substituted TBP iron carbonyl complexes [26]. Photolysis of a methanol solution of $K[CpFe(CN)_2(CO)]$ in the presence of PTA was the method used by Darensbourg to prepare the orange compound $K[CpFe(CN)_2(PTA)]$ (Scheme 10).

Reaction of **33** with hydrochloric acid results in the protonated **34**, isolated as contaminated with coproduced KCl. Instead, $CpFe(CN)_2\{PTA(H)\}$ is cleanly synthesized by pass-

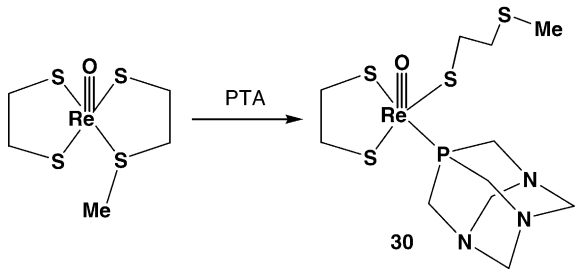

Scheme 9.

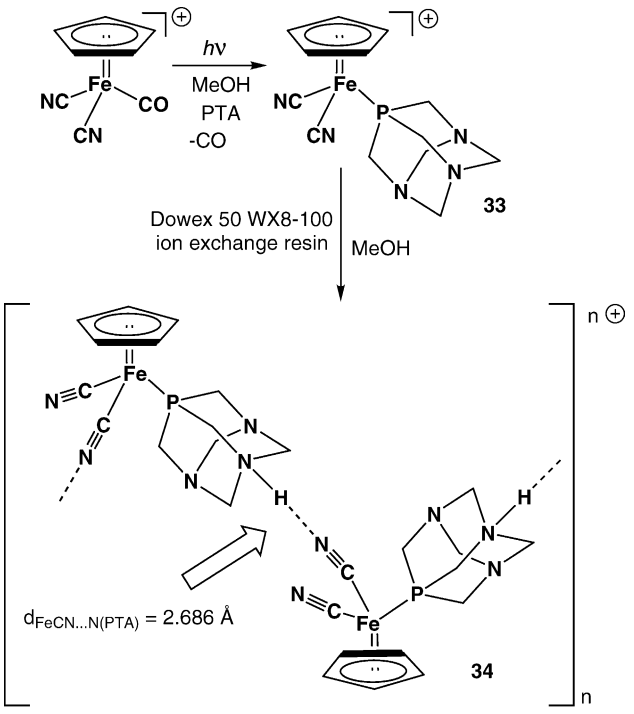

Scheme 10.

ing **33** through a ion exchange column containing a strongly acidic resin [39]. The ^{31}P NMR data show that the chemical shift of **33** (ca. 9.8 ppm) is significantly different from that of free PTA. Protonation of **34** causes a further downfield shift of the ^{31}P chemical shift giving rise to a singlet at, ca. 20 ppm. In an effort to synthesize a mixed metallocyano compound, complex **34** was reacted with $Zn(N(SiMe_3)_2)_2$, however, the resulting product prove to be insoluble in all common solvents and was not further characterized.

The solid-state structure of both **33** and **34** was determined by X-ray diffraction analysis. The $[CpFe(CN)_2PTA]^-$ anion of **33** exhibits a three-legged piano stool structure with a Fe–P distance of 2.145(3) Å. The structure shows extensive contacts and ion pairing interactions between potassium and cyanide [$d_{(K^+\cdots NC^-)ave} = 2.785(7)$ Å]. The crystal structure of **34** is similar to that of **33** apart that the two Fe–C_{CN} distances differ to each other (Fig. 1). Thus, one of the two

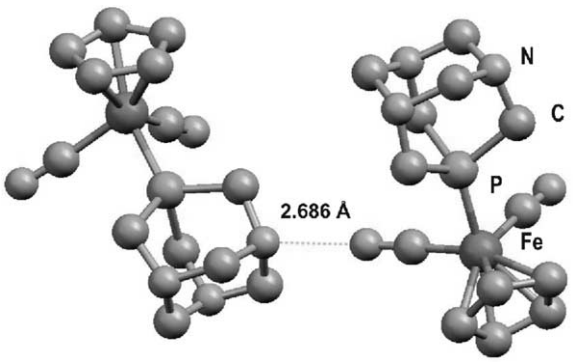

Fig. 1. Crystal structure of $CpFe(CN)_2\{PTA(H)\}$. Adapted from [39].

Fe–C bonds (1.839(12) Å) is ca. 0.1 Å shorter than the other one (1.940(12) Å). The shortness of one Fe–C_{CN} bond reflects the presence of an intermolecular hydrogen-bonding chain motif which traverses the lattice structure involving the protonated nitrogen atom of the PTA ligand of a second molecule of **34** [$d_{CN\cdots H-N} = 2.686$ Å]. The latter separation is considerably shorter than the sum of the van der Waals radii of two nitrogen atoms.

Many reports concerning Ru complexes of PTA appeared in recent years. Due to the catalytic ability and potential medicinal properties of ruthenium complexes, these derivatives have been a key point in the development of PTA coordination chemistry. Initial work has concentrated on the halogenated complexes; *cis*-$RuCl_2(PTA)_4$ (**35**) and *fac*-$RuCl_2(CO)(PTA)_3$ (**36**). Two synthetic pathways are known for preparing **35**, the simplest involves the reaction of excess PTA with $RuCl_3$ in refluxing ethanol [40a] or reacting aqueous solutions of PTA with toluene solution of $RuCl_2(PPh_3)_3$ [40b]. Complex **35** is not soluble in non-polar organic solvents, but soluble in alkaline or neutral aqueous solution. Solubility is limited in ethanol and 2-methoxyethanol. The reaction of *cis*-$RuCl_2(PTA)_4$ with CO results in loss of a single PTA forming the yellow solid $RuCl_2(CO)(PTA)_3$ (**36**) as identified by IR spectroscopy (ν(CO) = 1987 cm^{-1}) [40a]. If *cis*-$RuCl_2(PTA)_4$ is reacted with an aqueous HCl solution, the OCT bis-protonated species $[RuCl_2(PTA)_2\{PTA(H)\}_2]Cl_2$ (**37**) is obtained along with a small of amount of Ru(III) complex $[RuCl_4\{PTA(H)\}_2]Cl$ (**38**). Pruchnik and co-workers have recently synthesized iodo-methylated complexes by reacting a combination of $RuCl_3$ and KI with an appropriate amount of [PTA(Me)]I, all reactions preformed in water at either 40 or 80 °C [41]. The air and moisture stable salts *trans*-$RuI_4\{PTA(Me)\}_2\cdot 2H_2O$ (**34**/**39**) is a brownish yellow solid whereas *mer*-$[RuI_2(H_2O)\{PTA(Me)\}_3]I_3$ (**40**) is dark red. All species are soluble in polar solvents (DMSO, MeCN, DMF) including alcohols and water. The ^{31}P NMR spectrum of **40** reveals two peaks at −8.3 (triplet) and −60.8 (doublet) ppm which indicate a meridional arrangement of the PTA ligands, the spectra of **39** shows a single doublet located at −60.8 ppm which suggests that the PTA ligands are *trans* to one another. The crystal structure of both compounds confirms the geometry indicated by ^{31}P NMR [41]. The catalytic performance of both **39** and **40** in the hydroformylation of 1-hexene and in the hydrogenaton of cinnamaldehyde have been shortly evaluated (vide infra Section 6).

Another class of catalytically active compounds are $[RuCl_2(p\text{-cymene})(PTA)]$ (**41**) and $[RuCl(p\text{-cymene})(PTA)_2]BF_4$ (**42**) which were shown by Dyson and co-workers to catalyze the hydrogenation of various substituted arenes (see Section 6) [42]. Complex **41** was prepared by refluxing for 5 h a methanol solution of the dimer $[Ru(p\text{-cymene})Cl_2]_2$ with PTA, whereas **42** is prepared by adding one equivalent of PTA to **41** in CH_2Cl_2 followed by the addition of $AgBF_4$ [42a]. Both compounds were synthe-

sized in high yield. From these two complexes **41** and **42**, a whole new class of compounds, named RAPTA (ruthenium/arene/PTA), have been patented for potential use in cancer therapy and include bromo, iodo and thiocyanate with mono- and bis-PTA substituted derivatives [43]. Complex **41** was found to be soluble in polar organic solvents including dichloromethane, chloroform and acetone. Using UV-Vis spectroscopy, a pK_a value of 6.5 was measured for **41** [42a]. The X-ray structure of the mono-PTA complex **41** was also reported.

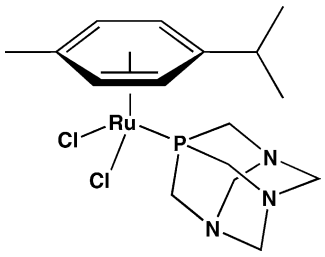

41

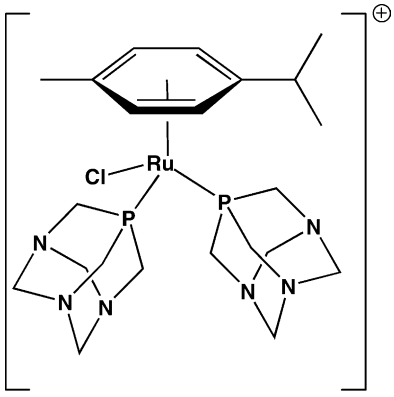

42

Recently two cyclopentadienyl Ru complexes featuring PTA, namely CpRuCl(PTA)$_2$ (**43**) and Cp*RuCl(PTA)$_2$ (**44**) were synthesized and characterized [44]. These compounds demonstrated both catalytic and biological activity. Complex **43** was prepared by phosphine exchange of CpRuCl(PPh$_3$)$_2$ with PTA in refluxing toluene, while species **44** can be synthesized either in analogous method to **43** or by reacting the chloro-bridged dimer [Cp*RuCl (μ-Cl)]$_2$ with PTA in the presence of zinc as reducing agent. Both complexes, yellow in color, are soluble in chlorinated organic solvents and in water [$S_{(25\,^\circ C)} = 40\,mg\,cm^{-3}$ (**43**) and $25\,mg\,cm^{-3}$ (**44**)]. Furthermore, **43** and **44** are stable in boiling water (16 h) and do not incorporate deuterium upon heating with D_2O. An X-ray crystal structure of **44** was also obtained. The crystal structure of the Dyson's complex **41** is quite similar to that of **44** both exhibiting typical three-legged piano stool geometries with comparable Ru-P$_{PTA}$ (2.297 Å for **41**; 2.28 Å for **44**) and Ru–Cl (2.415 Å for **41**; 2.46 Å for **44**) distances.

The water-soluble ruthenium cluster Ru$_3$(CO)$_9$(PTA)$_3$ (**45**) was synthesized by adding PTA in CH_2Cl_2 to solution of Ru$_3$(CO)$_{12}$/CH_2Cl_2 and refluxing for 1 h [45].

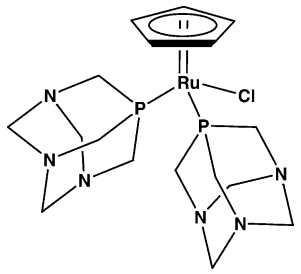

43

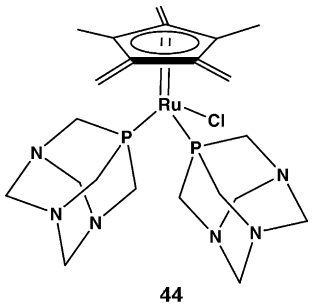

44

Alternatively, **45** can be obtained by heating to 65 °C a solution of Ru$_3$(CO)$_{12}$ and PTA in MeOH. A similar complex [Ru$_3$(CO)$_9${PTA(Me)}$_3$]I$_3$ (**46**) is prepared using the former method with [PTA(Me)]I in place of PTA and refluxing for 2 h. The crystal structure of **45** consists of a triangle of ruthenium atoms with each metal bearing one PTA molecule in an equatorial position. Unlike other PTA complexes, **45** is soluble in polar non-aqueous solvents like CH_2Cl_2, but insoluble in hydrocarbons or methanol. However, **45** can be extracted from organic solvent by treatment with acid. The resulting triprotonated species [Ru$_3$(CO)$_9${PTA(H)}$_3$]$^{3+}$ and **46** have much greater solubility in water than **45**. The process was found to be reversible by neutralizing [Ru$_3$(CO)$_9${PTA(H)}$_3$]$^{3+}$ with K_2CO_3. ^{31}P NMR spectrum of **45** shows two sets of almost equivalent PTA ligands which change slightly (−44.4 and −44.8 ppm) when the complex is dissolved in D_2O at pH = 3.5. The UV-Vis spectrum of Ru$_3$(CO)$_9$(PTA)$_3$ demonstrates more pronounced changes under different solvent conditions. For example, **45** has an intense band at 446 nm with a 348 nm shoulder which shifts to 434 and 334 in 0.3 M HCl, consistent with the 426 and 310 nm bands observed for **46**. This absorption has been assigned as the $\sigma \rightarrow \sigma^*$ transition which is higher in energy than the band at 507 nm observed for Ru$_3$(CO)$_9$(PPh$_3$)$_3$. This observation suggests that PTA is a stronger donor ligand than PPh$_3$ [45].

A small number of Ru-hydride compounds featuring PTA, which have important consequences for catalytic hydrogenation mechanisms, have been characterized. The reaction of RuCl$_2$(PTA)$_4$ with 60 bar of H_2 yields two products which are dependent on pH. At low pH (2.0), the mono-hydride is observed, RuHCl(PTA)$_4$ (**47**), while at high pH (12.0), the classical dihydride RuH$_2$(PTA)$_4$ (**48**) is present [46]. Complexes **47** and **48** form slowly under these conditions due to pre-equilibrium reactions. Both compounds were identified through their characteristic hydride signals, exhibit-

ing an AA′MM′XX′ spin system in **48** [46]. The small steric profile of PTA allows for the formation of the unusual species $[RuH(PTA)_5]^+$ (**49**) which was synthesized by reacting $[Ru(H_2O)_6](tos)_2$ (tos = toluene-4-sulfonate) with excess PTA under an atmosphere of pressurized H_2. Although **49** was not isolated, its identity was proven by ^1H and ^{31}P NMR spectroscopy which show the hydride signal split into a doublet of quintets ($\delta_{Ru-H} = -11.62$ ppm). Furthermore, from the same precursor, $[Ru(H_2O)_6](tos)_2$, the addition of PTA and refluxing results in the species $[Ru(H_2O)_2(PTA)_3](tos)_2$ (**50**), obtained in 80% yield. The same is also obtained from the displacement of THF by PTA from $[Ru(H_2O)_2(THF)_2](tos)_2$ [47].

The hydrides $CpRuH(PTA)_2$ (**51**), $Cp^*RuH(PTA)_2$ (**52**) and $[Cp^*RuH_2(PTA)_2]Cl$ (**53**) have been directly observed as relevant intermediates by HPNMR spectroscopy during the in situ study of the catalytic hydrogenation of benzylidene acetone by the chloride precursors **43** and **44** (vide infra Section 6) [44]. Their syntheses have been accomplished using sodium formate as the hydride source [48]. and a theoretical analysis addressing the role of the Cp versus Cp* in **51** versus **52** in determining the heterolysis versus the homolysis of the H–H bond is currently in progress [49].

4.4. Rhodium and iridium–PTA complexes

Rhodium-PTA systems have received much attention due their potential catalytic activity. The trisubstituted PTA complex $RhCl(PTA)_3$ (**54**) is conveniently synthesized by reacting $RhCl_3$ with an excess of PTA in refluxing ethanol [40a]. If **54** is reacted with dilute HCl, the bis-substituted product $[RhCl(PTA)_2]\cdot 2HCl$ (**55**) is produced, for which a X-ray crystal structure was obtained. In addition, the rhodium(III) iodo species $[RhI_4\{PTA(Me)\}_2]I$ (**56**) is obtained by mixing $RhCl_3$ with KI in water with subsequent addition of [PTA(Me)]I [51]. Complex **56** is a dark red solid which is soluble in DMSO, MeCN, DMF and water, but only sparingly soluble in methanol and other alcohols. The Rh–P coupling constant in **56** is small ($^1J_{Rh-P} = 96.8$ Hz) which confirms hexacoordination of Rh. This compound is active both as a hydroformylation and hydrogenation catalyst [41,50].

The Rh-PTA carbonyl complexes $[RhI(CO)\{PTA(Me)\}_2]I_2$ (**57**) and $[RhI(CO)\{PTA(Me)\}_3]I_3$ (**58**) were synthesized, under inert atmosphere, by reacting the dimer $[Rh_2Cl_2(CO)_4]$ with [PTA(Me)]I in the presence of NaI. The reaction with four equivalents of [PTA(Me)]I affords **57**, whereas species **58** is formed using six equivalents of [PTA(Me)]I [51]. Both compounds are very sensitive to oxidation in solution, even trace amounts of O_2 in MeCN and water result in the formation of [PTA(O)Me]I and CO. However, **57** and **58** are stable in the solid-state and highly soluble in water, but only sparingly soluble in methanol. The ^{31}P NMR spectrum of **57** shows a doublet at –50.2 ppm, while **58** shows a broad singlet which narrows at higher temperature, but no resolution of $^1J_{Rh-P}$ was obtained. Thus, it was suggested that $[RhI(CO)\{PTA(Me)\}_3]I_3$ has fluxional behavior in solution. IR studies of the two compounds reveal high carbonyl stretching frequencies (ν(CO) = 1999 and 2001 cm^{-1}), thus indicating [PTA(Me)]I has strong π-acceptor abilities [51].

Differently *N*-alkylated versions of PTA, called *tpa* by the authors [51], namely 1-alkyl-1-azonia-3,5-diaza-7-phosphaadamantane iodides ($Rtpa^+I^-$), with R = methyl ($mtpa^+I^-$), ethyl ($etpa^+I^-$) and *n*-propyl, ($ptpa^+I^-$), and $mtpa^+Cl^-$ were synthesized and reacted with $[Rh_2Cl_2(CO)_4]$ giving the rhodium(I) complexes $[RhCl(CO)(tpa)_2]$, $[RhI(CO)(Rtpa^+I^-)_2]$, $[RhCl\text{-}(CO)(mtpa^+Cl^-)_3]$ and $[RhI(CO)(Rtpa^+I^-)_3]$. The properties and reactivities of the complexes were investigated using ^1H and ^{31}P NMR and IR spectroscopies. The complexes were tested as catalysts for the water–gas shift reaction, the hydrogenation of C=C and C=O bonds, the hydroformylation of alkenes and the isomerization of unsaturated compounds [51b].

Mixed rhodium complexes featuring both PTA and $PTA(H)^+$ have also been synthesized. The yellow colored product $[RhCl\{PTA(H)\}(PTA)_2]Cl$ (**59**) was prepared by refluxing for 2 h an ethanol solution of $RhCl_3$ and 6 equivalents of PTA, whereas $[RhCl\{PTA(H)\}_3(PTA)]Cl_3$ (**60**) was formed by reacting $RhCl(PTA)_3$ with two equivalents of PTA in water [23]. PTA(O) is always formed as a by-product in both reactions. Dissolving **59** in H_2O led to the immediate formation of PTA(O) as evidenced by UV-Vis and ^{31}P NMR spectroscopy, where use of $H_2{}^{18}O$ gave the incorporation of ^{18}O by PTA [23]. Higher pH (>7.0) also promotes more rapid oxidation of the Rh centers. Furthermore, it was found that water is source of the protons that protonate the ligands in **59** and **60**. It was postulated that the reaction of $[RhCl(PTA)_2\{PTA(H)\}]Cl$ with H_2O begins with an oxidative addition of water followed by releasing of PTA(O) and reductive elimination of HCl, Scheme 11, although the authors were unable to detect any hydride containing species. Compound **59** is an active catalyst for hydroformylation whereas **60** is unreactive [23].

A Rh(I) acetylacetonato complex featuring PTA was synthesized by reacting Rh(acac)$(CO)_2$ (acac = acetylacetonate) with one equivalent of PTA in ethanol, refluxing for 3 h [52]. The yellow compound Rh(acac)(CO)(PTA) (**61**) is soluble in H_2O, methanol and dichloromethane, but less soluble in $CHCl_3$ and higher alcohols and insoluble in non-polar solvents. Spectroscopic comparison (IR, ^1H and ^{31}P NMR) of **61** with other Rh(acac)(CO)L complexes with different types of phosphines (L) show that PTA is a strong σ-donor but a much weaker π-acceptor. It was also shown that the proton chemical shift of the methyl groups of the acac are influenced by the steric profile of coordinating phosphine. The ^1H chemical shift of the methyl groups in Rh(acac)$(CO)_2$ and Rh(acac)(CO)(PTA) [δ_{Me} = 1.97] were found to be identical which indicates that PTA is a sterically poor-demanding phosphine. Two rhodium hydride compounds featuring alkylated PTA

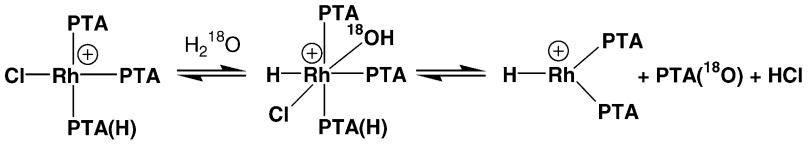

Scheme 11.

ligands were synthesized and characterized. The yellow colored [RhH{PTA(Me)}$_4$]I$_4$ (**62**) and [RhH{PTA(Et)}$_4$]I$_4$ (**63**) were prepared by addition of one equivalent of either [PTA(R)]I to [Rh(CO){PTA(R)}$_3$]I$_3$ (R = Me or Et) and subsequent treatment with the $NaBH_4$ [53]. The compounds were characterized by ^{1}H and ^{31}P NMR spectroscopy. In solid form, the two hydrides are stable to air and moisture, but oxidize easily in solution. However, the complexes are stable for several months dissolved in deoxygenated water.

Iridium complexes of PTA are much less represented than the rhodium analogs which reflects the generally assumed poor catalytic activity of iridium derivatives in comparison to rhodium species and the minor interest in studying the coordination chemistry of this metal. An important compound is the water-soluble PTA version of Vaska's complex *trans*-[IrCl(CO)(PTA)$_2$] (**64**) (Scheme 12) [54]. The compound is prepared through standard methodology, stirring a hexane/CH_2Cl_2 solution of PTA and [Ir(COD)Cl]$_2$ under an atmosphere of carbon monoxide [54a]. Compound **64** is isolated as a yellow colored compound. The regioselective synthesis of the *trans* product was confirmed by ^{13}CO labeling where **64** has a doublet in the ^{31}P NMR spectra with a $^2J_{CP}$ of 11 Hz. A related compound IrCl(CO)(PTA)$_3$ (**65**) was synthesized by either refluxing *trans*-[IrCl(CO)(PPh$_3$)$_2$] with three equivalents of PTA in absolute ethanol or by combining 3 equivalents of PTA with [Ir(COD)Cl]$_2$ under CO. The reaction is completed by slowly purging with N_2. A higher yield (77% from 54%) is obtained doubling the amount of PTA. The *trans*-[IrCl(CO)(PTA)$_2$] compound is insoluble in common organic solvents and only sparingly soluble in DMSO. Axial rather than equatorial coordination of CO in the TBP coordination polyhedron around iridium in **65** was inferred by an analysis of the IR spectrum (ν(CO) = 1950 cm^{-1}) [54a]. Interestingly, the reaction between [Ir(COD)Cl]$_2$ and two equivalents of PTA leads to

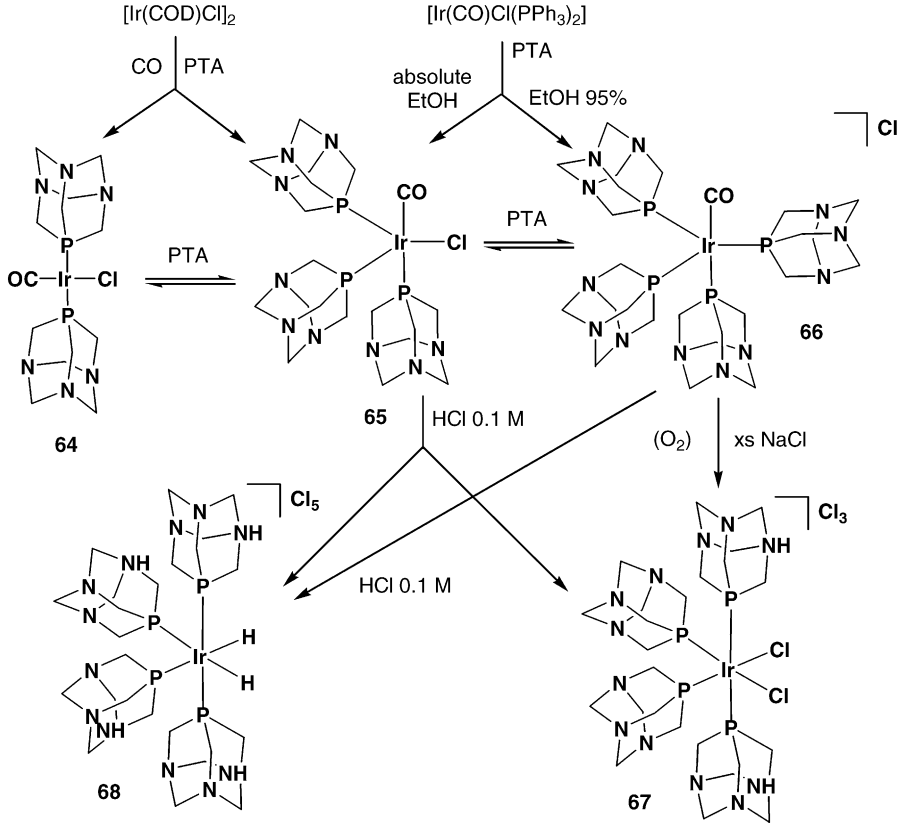

Scheme 12.

a mixture of **64** and **65** as confirmed by IR spectroscopy. ^{31}P NMR of the reaction mixture shows the presence of only **64** (−58.1 ppm), whereas IrCl(CO)(PTA)$_3$ separates out being virtually insoluble. It is suggested that both **64** and **65** are in equilibrium with free PTA (Scheme 12). The tris-PTA derivative **65** reacts with water converting into the tetrakis cationic adduct [Ir(CO)(PTA)$_4$]Cl (**66**). The latter is also formed by heating *trans*-[IrCl(CO)(PPh$_3$)$_2$] with PTA in H_2O at 60 °C for 4 h or by refluxing Vaska's compound with excess PTA in 95% EtOH. Alternatively **66** is produced through 60 °C heating of IrCl(CO)(PTA)$_3$ with excess PTA in ethanol. In contrast to **65**, [Ir(CO)(PTA)$_4$]Cl has superb solubility in H_2O (6×10^{-2} M), but not in organic solvents. The structure of **66** has been determined by X-ray diffraction which confirmed the putative TBP geometry with an axial carbonyl ligand. The formation of the higher substituted PTA complexes (**65** and **66**) is favored over the bis-PTA complex **64** and this remarkable behavior is attributed to the smaller cone angle of PTA in comparison to most tertiary phosphines [54a]. Addition of excess NaCl to **66** in MeOH under an atmosphere of O_2 does not restore **65**, but unexpectedly produces the decarbonylated iridium(III) octahedral dichloride [IrCl$_2${PTA(H)}$_2$(PTA)$_2$]Cl$_3$ (**67**) with two *N*-protonated PTA ligands (Scheme 12) [54a]. From the ^{31}P NMR spectrum of **67**, an OCT geometry with two *cis*-chloride ligands was concluded based on the presence of two triplets with small coupling constants (J_{PP} = 15 Hz). A similar structure has been assigned to the ruthenium complex [RuCl$_2${PTA(H)}$_2$(PTA)$_2$]Cl$_2$ (**37**) [40].

All three iridium complexes (**64**–**66**) can be protonated in aqueous solutions with 0.1 M HCl. Reaction of IrCl(CO)(PTA)$_3$ with 0.1 M HCl results in formation of a mixture of the dichloride **67** and of the dihydride [IrH$_2${PTA(H)}$_4$]Cl$_5$ (**68**) complexes. The two compounds readily crystallized and were physically separated in the solid-state due to different crystal habits. Complex **68** was authenticated by X-ray diffraction analysis and exhibits an OCT geometry with two *cis*-disposed H ligands.[2] The solid-state structure is likely maintained in solution where the ^{31}P NMR spectrum displays two triplets with J_{PP} = 18 Hz. Acidification of [Ir(CO)(PTA)$_4$]Cl with 0.1 M HCl solution also affords the dihydride **68**. A mechanism accounting for the formation of **67** and **68** from the protonation of **65** has been proposed by Krogstad et al. [54a]. This entails CO dissociation from the relatively labile axial coordination position and replacement by free PTA which is presented in solution from the dissociative equilibrium interconverting **65** and **64**. Oxidative addition of HCl to a transient 16-electron [Ir(PTA)$_4$]$^+$ cation (**69**) leads to the hydride intermediate [Ir(H)Cl(PTA)$_4$]$^+$ (**70**) from which the two isolable OCT compounds **67** and **68** originates via disproportionation and ligand exchange. The single hydride species **70** has not been isolated, but has been observed by IR, ^{31}P and ^{1}H NMR (see Table 1). Similarly to other Ir(III) dihydrides, **68** was shown to be inert when treated with 0.1 M DCl in D_2O, as the hydride ligand was not replaced by deuterium, but the dideuteride analogue (**68**-d$_2$) can be easily made by reacting [Ir(PTA)$_4$(CO)]Cl with 0.1 M DCl in D_2O [54].

The water-soluble iridium carbonyl cluster Ir$_4$(CO)$_7$-(PTA)$_5$ (**71**) was synthesized by refluxing Ir$_4$(CO)$_{12}$ with an excess of PTA in toluene [45]. The isolated red–orange solid, which was characterized by X-ray diffraction analysis, is soluble in water at pH 7 or below and in a variety of organic solvents including dichloromethane.

4.5. Nickel, palladium and platinum-PTA complexes

Traditional phosphine complexes of this group, particularly those of palladium, have played an extremely important role in the development of homogeneous catalysis. Thus, it is not surprising that also transition metal complexes of the nickel triad elements with water-soluble phosphines have attracted a considerable interest in recent years. In fact, numerous complexes with sulfonated ligands have been reported (see for example [55]). Ni, Pd, Pt compounds featuring PTA are rapidly increasing in recent years. The tetra-substituted nickel(0) complex Ni(PTA)$_4$ (**72**) was independently prepared both by Cermak et al. by reacting four equivalents of PTA with Ni(COD)$_2$ in toluene/methanol solutions (Scheme 13) [56], and by Darensbourg et al. by allowing $NiCl_2$ and PTA to react in water [14b]. In this latter reaction, the two electron reduction of nickel(II) is accomplished by excess PTA which results in the generation of PTA(O). Two equivalents of HCl are also released during the reaction which encompasses the formation of the red *cis*-NiCl$_2$(PTA)$_2$ (**73**) as an instable intermediate product [14b]. Scheme 13 illustrates these transformations. *cis*-NiCl$_2$(PTA)$_2$ (**73**) was obtained through the addition of appropriate amount of PTA with $NiCl_2$ in anhydrous methanol [14b,57]. Similarly Ni(CN)$_2$(PTA)$_3$ (**74**) was made by reacting NaCN and $NiCl_2$ in H_2O followed by addition of excess PTA [57]. The molecular structure of **74** has been obtained by X-ray diffraction and revealed that the complex adopts a TBP geometry with the two cyanide ligands sitting on the apical vertices of the polyhedron [57].

The broad ^{31}P signal observed for Ni(CN)$_2$(PTA)$_3$ at room temperature has been attributed to a fluxional behavior involving exchange of both PTA and DMSO in the intermediate OCT species Ni(CN)$_2$(PTA)$_3$(DMSO) (**75**) obtained via coordination of one DMSO solvent molecule to the Ni center [57]. The nickel complexes are insoluble in organic solvents, but soluble in DMSO and water. The solubility of **73** in H_2O and 0.1 M HCl were measured as 200 and 400 g/L. During the reaction forming **72** a number of color changes were observed which were investigated by Darensbourg et al. [14b]. The blue colored solution

[2] Complex **68** readily desolvates and eliminates HCl if exposed to air. Thus, samples of formula [IrH$_2${PTA(H)}$_{4-x}$(PTA)$_x$]Cl$_{5-x}$ (x = 0–2) with different content of protonated PTA ligands and chloride counteranions have been isolated and characterized.

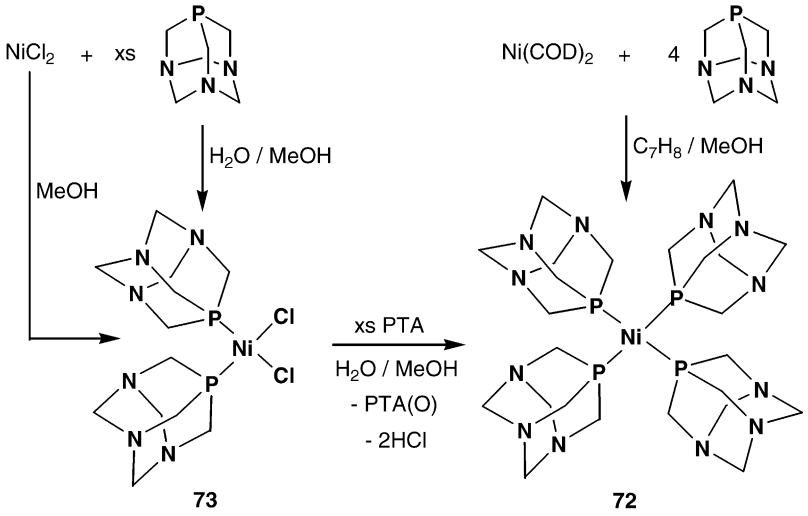

Scheme 13.

initially observed during the reaction between $NiCl_2$ and PTA in H_2O/MeOH was attributed to the formation of the OCT species $[Ni(H_2O)_n(PTA)_{6-n}]^{2+}$ with *N*-coordinated PTA ligands. However, coordination of PTA through the amine center has not yet been documented. Preliminary crystallographic data on a crystal obtained from the reaction between $CpRuCl(PTA)_2$ and AgOTf in DMSO indicate however that formation of a polynuclear complex featuring both P- and N-coordination of the PTA cage could be achieved [58].

The tetra-substituted Ni(0) complex can be fully protonated with 0.1 M HCl yielding complexes featuring up to four PTA(H) ligands [56a,59]. The X-ray structure of the tetrachloride salt $[Ni\{PTA(H)\}_4]Cl_4{\cdot}H_2O$ has been determined as a slightly distorted tetrahedron [59]. The tetrakis-PTA-nickel complex **73** is air-sensitive, and was found not able to catalyze olefin polymerization [56a].

Nickel carbonyl complexes are conveniently synthesized from reacting $Ni(PTA)_4$ with carbon monoxide in various solvents, the nature of the solvent determines the amount of CO substitution [14b]. Kinetic studies using solution IR spectroscopy show replacement of PTA by fast, first-order rate ($k_{obs} = 7.92 \times 10^{-4}\ s^{-1}$, 20 °C), forming $Ni(CO)(PTA)_3$ (**75**). However, a second replacement is slow taking 12 h in MeOH at 50 °C. Third replacement is even slower requiring one week to complete. In contrast, the formation of $Ni(CO)_3(PTA)$ (**76**) from $Ni(CO)_4$ and one equivalent of PTA is very fast. In addition, the presence of excess PTA significantly decreases the rate of PTA substitution. All the observations suggest that substitution proceeds through a dissociative pathway and that PTA is strongly bound to the nickel center. The water solubility of the $Ni(PTA)_{4-n}(CO)_n$ ($n = 1$–4) decreases with increasing CO substitution where $Ni(PTA)(CO)_3$ is completely insoluble in water. Successive formation of the $Ni(PTA)_{4-n}(CO)_n$ series is extremely useful for determining steric and electronic properties following the rules defined by Tolman [60]. From IR studies, an analysis of the antisymmetric and symmetric CO stretching vibrations suggest that the cone angle for the phosphaadamantane cage ranges from 103.2° (CH_2Cl_2) to 107.6° (MeOH). The electron donor properties of PTA were determined by calculating the electronic parameter derived from the A_1 ν(CO) band, which shows that PTA is a weaker electron donor than PMe_3 [59]. The nitrosyl compound $[Ni(NO)(PTA)_3]NO_3$ (**77**) was prepared by adding $Ni(NO_3)_2{\cdot}6H_2O$ to a solution of excess PTA with $NaNO_2$ in hot ethanol [59]. The purple colored solid was isolated after 3 h of refluxing. Counter ion exchange with $NaBPh_4$ afforded the tetraphenylborate salt $[Ni(NO)(PTA)_3]BPh_4$ (**78**) whose tetrahedral structure was determined by X-ray methods. Compound **77** is soluble in water ($S = 26$ g/L) and DMSO ($S = 57$ g/L), but less soluble in MeCN (3.0 g/L) and MeOH (7.5 g/L) and insoluble in THF and acetone. Fading of the dark purple color of **77** occurs when a D_2O solution is treated with 0.1 M HNO_3. PTA(O), $[PTA(H)]^+$ and unidentified species were detected by ^{31}P NMR spectroscopy.

Recently Darensbourg and co-workers prepared a series of Ni-PTA complexes featuring various substituted salicylaldiminato ligands (**79**). The compounds were prepared in variable yields depending on the nature of the salicylaldiminato ligand, either by ligand exchange of PPh_3 with PTA in homogeneous toluene/methanol solution (Scheme 14) or by direct synthesis from $(TMEDA)Ni(CH_3)_2$ and PTA in the presence of the appropriate substituted salicylaldimine at −30 °C [62]. The ligand exchange method does not proceed under biphasic aqueous conditions. Attempts to use **79a** as catalyst for ethene polymerization in 1/1 biphasic water/toluene at room temperature failed likely as a consequence of the strong binding of PTA to the nickel center. Increasing the temperature to 80 °C caused extensive decomposition with formation of PTA(O) in the aqueous phase and separation of a Ni(0) species [61].

Studies on palladium-PTA complexes, like those of other highly catalytically active metals, i.e. ruthenium

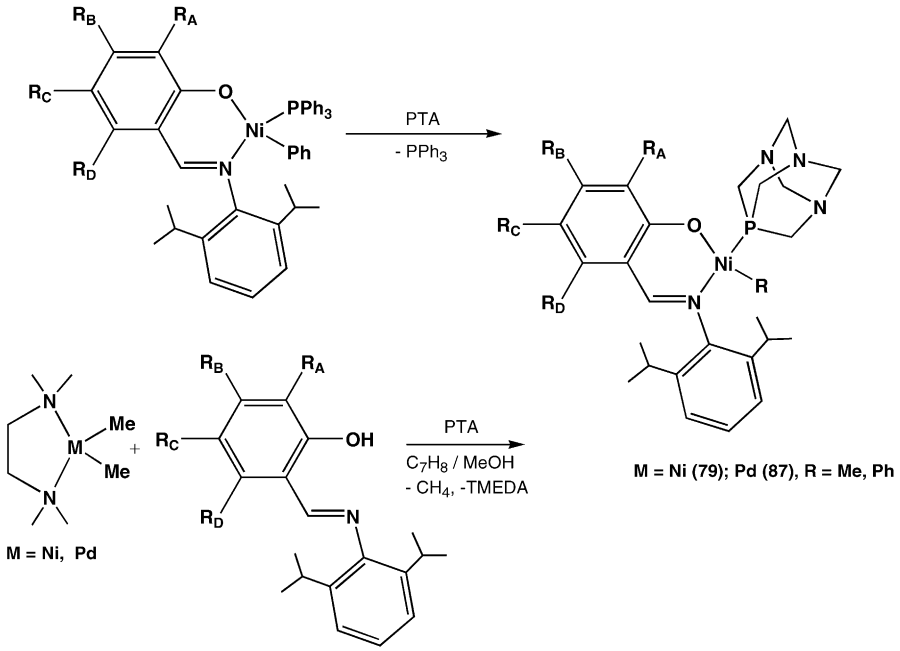

79/87a $R_C = NO_2$, $R_A = R_B = R_D = H$; **79/87b** $R_A = OMe$, $R_C = R_B = R_D = H$; **79/87c** R_C, $R_D = CH(CH_2)CH$, $R_A = R_B = H$; **79/87d** $R_A = R_C = Cl$, $R_B = R_D = H$; **79/87e** $R_A = Ph$, $R_C = R_B = R_D = H$; **79/87f** $R_A = 9$-anthra, $R_C = R_B = R_D = H$

Scheme 14.

and rhodium, have received some attention due to the potential as water-soluble catalysts [4]. No mono substituted PTA complexes of Pd are known, but bis-, tris-, and tetrakis-substituted species have been characterized.

Scheme 15 illustrates some of the synthetic procedures used to prepare the most intriguing palladium derivatives featuring PTA. The synthesis of *cis*-$PdCl_2(PTA)_2$ (**80**) is accomplished by reacting $PdCl_2$ with excess PTA in H_2O

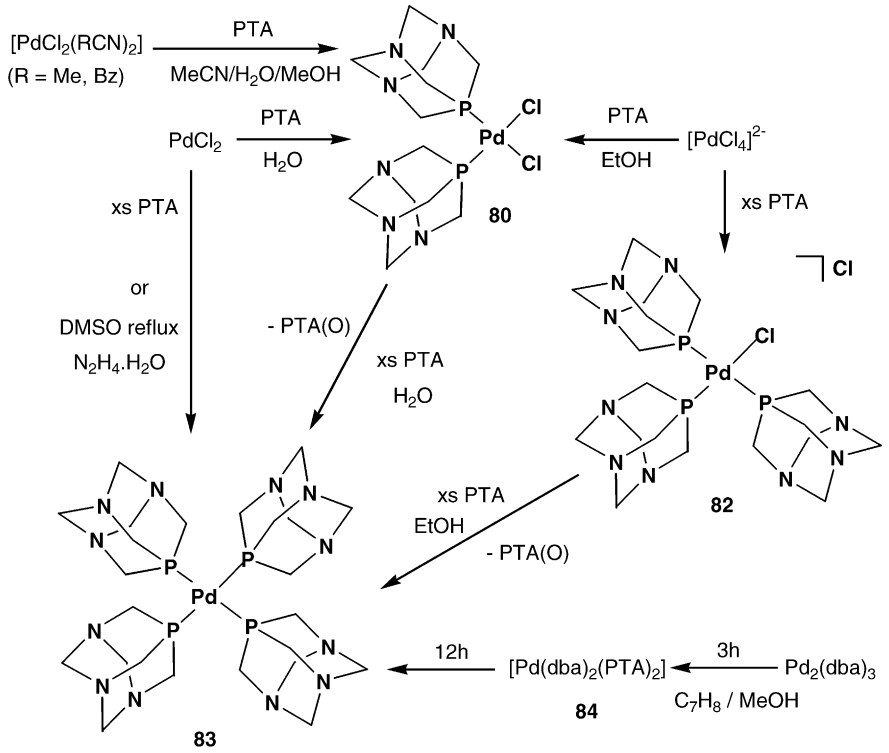

Scheme 15.

[57]. Alternative syntheses include ligand exchange of MeCN or PhCN with PTA from both $PdCl_2(MeCN)_2$ and $PdCl_2(PhCN)_2$, respectively [57],or metathesis reaction of $(NH_4)_2PdCl_4$ with a double amount of PTA in refluxing EtOH [60]. The *cis*-arrangement of the two PTA ligands in **80** has been independently determined by X-ray diffraction analysis on two polymorphs of the square-planar (SP) complex [59,62]. In one polymorph crystal Alyea et al. observed an intermolecular hydrogen bonding with a solvated water molecule linking a pair of *cis*-$PdCl_2(PTA)_2$ units via O–H···N hydrogen bonds. Most intriguing, it was found that pairs of molecules of **80** are linked to each other by intermolecular Pd···H–C contacts which are shorter than the sum of the van der Waals radii for the two elements [$d_{Pd\cdots H-C}$ = 2.86–3.00 Å]. This represents a rare example of M···H–C interaction that was interpreted as a three-center-four-electrons hydrogen bond (3c–4e) rather than in terms of classic agostic interaction (3c–2e) [62].

The bromide analogue of **80**, i.e. $PdBr_2(PTA)_2$ (**81**) has been obtained by reaction of LiBr with $[Pd(PTA)_3Cl]Cl$ (**82**) (vide infra) in water [63]. The X-ray analysis confirmed the SP geometry and highlighted, at variance with **80**, a *trans*-arrangement of the two PTA ligands. The tris-PTA derivative $[PdCl(PTA)_3]Cl$ (**82**) is prepared by adding $(NH_4)_2PdCl_4$ to five equivalents of PTA and refluxing for 3 h [59]. However, the reaction also contains some $PdCl_2(PTA)_2$ and free PTA. The addition of more PTA resulted in the formation of $Pd(PTA)_4$ (**83**) and PTA(O). Air and moisture sensitive yellow crystals of **82** were slowly grown after two months storage in a 0.1 M HCl/MeOH solution at 5 °C [14b]. The coordination geometry around palladium was approximately SP and the complex was isomorphous to the platinum analogue (vide infra).

The homoleptic tetrakis-PTA substituted complex $Pd(PTA)_4$ (**83**) is formed by mixing $PdCl_2$ with five equivalents of PTA in H_2O solvent [14b]. Alternatively, the compound is formed by reacting $PdCl_2$ with four equivalents of PTA in refluxing DMSO with the addition of hydrazine monohydrate, a strong reducing agent [59]. A further alternative synthesis can be accomplished through the addition of $Pd_2(dba)_3$ (dba = dibenzylideneacetone) to a solution of PTA in methanol [56a].

At variance with the reaction of $Ni(COD)_2$ and PTA affording **73**, the latter reaction is not straightforward, as an intermediate product can be first isolated before slowly converting to **83**. The intermediate compounds, which are insoluble in common organic solvents, except $CHCl_3$ in which the product slowly decomposes, was assigned the composition $Pd(dba)_2(PTA)_2$ (**84**) on the basis of NMR analysis [56a]. $[Pd\{PTA(H)\}_4]Cl_4$ (**85**), the fully protonated version of $Pd(PTA)_4$, was obtained by dissolving **83** in 0.1 M HCl, and its crystal structure has been determined [59]. The solubility of **83** in water is exceptionally high (240 g/L), but, opposite to the nickel cognate species **73**, is decreased in 0.1 M HCl. The tetrakis-PTA palladium complex is stable in solution towards dissociation of the phosphine, the stability of $Pd(PTA)_4$ has been attributed to a small steric profile and high basicity [59]. Slow decomposition of **83** in water to metallic palladium and the free phosphine has been however described by Cermak [56a]. In contrast to **83**, which has a sharp singlet in the ^{31}P NMR spectrum, $[PdCl(PTA)_3]Cl$ shows broad peaks in its phosphorus NMR spectrum consistent with ligand dissociation and exchange of the coordinated ligand with free PTA. $Pd(PTA)_4$ has been tested for catalytic oligomerization of buta-1,3-diene (vide infra) [56a,56b].

A series of phenylselenolato palladium(II) complexes featuring a variety of different phosphine was synthesized [64]. The preparation of $Pd(SePh)_2(PTA)_2$ (**86**) was performed by reacting $PdCl_2(PTA)_2$ with NaSePh in dichloromethane/methanol solution. As with other complexes of the series **86** decomposes in $CHCl_3$ and more slowly in CH_2Cl_2. Analogously to the nickel-salicylaldiminato complexes **79**, mentioned above, a series of palladium salicyladiminato-PTA complexes (**87**) were prepared by Darensbourg and co-workers by reacting PTA and the appropriate salicylaldimine ligand with $(TMEDA)Pd(CH_3)_2$ in MeOH at −30 °C (Scheme 14) [61].

Finally, an unique PTA complex worth to be mentioned in this section, namely $[Mo_3(Pd(PTA)_4(H_2O)_9]^{4+}$ (**88**), has been reported by Sykes et al. The molybdenum–palladium cluster is prepared through Pd–S cleavage of a dimeric cuboidal Mo_3PdS_4 cluster, the PTA having the ability to dissociate dimers $[\{Mo_3PdS_4(H_2O)_9\}_2]^{8+}$ by coordinating to the Pd centers [65]. PTA was found to be particularly useful because of its water-soluble properties, the rate of dissociation/coordination was faster than that of TPPTS ($2.78 \times 10^6\,M^{-1}\,s^{-1}$ versus $9.6 \times 10^5\,M^{-1}\,s^{-1}$) which provide a similar reaction with the Mo_3PdS_4 cube. Although, not containing palladium, but nickel, the cluster $[Mo_3S_4Ni(PTA)]^{4+}$ (**89**) is strictly related to **88**. The Mo_3NiS_4 moiety is indeed prepared by PTA addition to $[Mo_3S_4Ni(H_2O)_{10}]^{4+}$ and features a tetrahedral Ni center [66]. This study was important since kinetic data for substitutions featuring a tetrahedral Ni environment are rare. The rate of the substitution reaction was monitored by UV-Vis spectroscopy and it was observed that the rate was pH dependent which is directly related to protonation of PTA. The kinetic data reveal an inhibition of the substitution reaction upon acidification, suggesting that PTA is a stronger nucleophile than $[PTA(H)]^+$ which the authors suggest is a result of increased electrostatics. Compared with TPPTS, substitution with PTA was faster.

In contrast to nickel and palladium, platinum PTA complexes have been much more widely studied, especially $Pt(PTA)_4$ (**90**) (Scheme 16). The synthesis of **90** is carried out in H_2O with the addition of $PtCl_2$ to PTA [14b]. The product is obtained after 2 days stirring as off-white microcrystals. However, **90** is accompanied by the formation of a second Pt(0) complex identified as the fully protonated species $[Pt\{PTA(H)\}_4]Cl_4$ (**91**). The straightforward synthesis of **91** can be accomplished by repeating the synthesis mentioned above using 0.1 M HCl or simply dissolv-

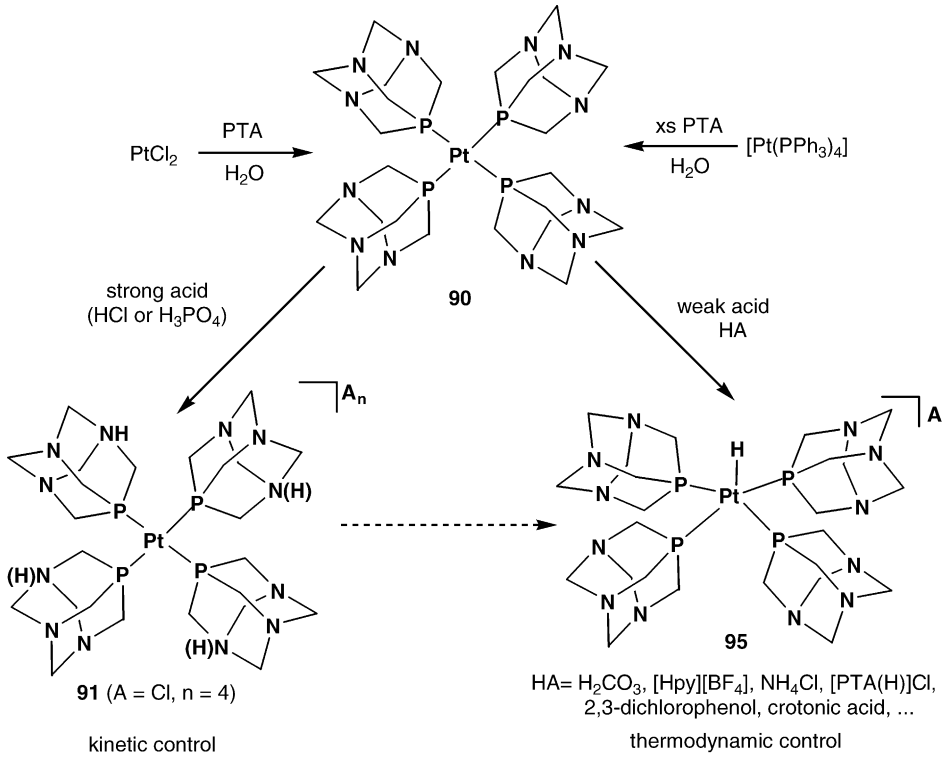

Scheme 16.

ing a sample of tetrakis-PTA complex in acidic media (HCl 0.1 M). The crystal structure of $[Pt\{PTAH\}_4]Cl_4$ has been determined. The slightly distorted tetrahedron does not significantly differ from that of the Ni and Pd related complexes [59]. An alternative method to prepare **90** involves reacting $Pt(PPh_3)_4$ with PTA in a ligand exchange reaction. If the reaction is not carried out in the presence of an excess of PTA, mixed PPh_3/PTA species $Pt(PPh_3)_{4-n}(PTA)_n$ ($n = 1$–3) can be formed. These mixed complexes are all water insoluble whereas the solubility of **90** is 295 g/L in water and, practically identical, 290 g/L, in 0.1 M HCl [59]. The complex *cis*-$[PtCl_2(PTA)_2]$ (**92**) is prepared by reacting either K_2PtCl_4 or $PtCl_2(SMe_2)_2$ with two equivalents of PTA in hot aqueous media or, in case of K_2PtCl_4, hot 95% EtOH [60]. The Zeise's salt, $[PtCl_3(C_2H_4)]Cl$, which is known to force *trans*-disposition in Pt(II)-diphosphine complexes, failed to produce the *trans*-isomer, yielding only the *cis*-adduct **92**. Alternatively, **92** can be straightforwardly formed through ligand exchange of PhCN with PTA from $PtCl_2(PhCN)_2$ in MeOH [57]. Crystals of **92** suitable for an X-ray analysis were obtained by Roodt and co-workers by slow evaporating an aqueous solution [67]. The crystals obtained featured two independent molecules held together by a bridging H_2O molecule, forming a dimeric unit, $[\{PtCl_2(PTA)_2\}_2(\mu\text{-}H_2O)]$, with strong intermolecular hydrogen bonds [$d_{(N\cdots H-O)_{ave}} = 2.914$ Å]. The structure of the dimeric aggregate is shown in Fig. 2. In each unit two platinum atoms are surrounded by two PTA ligands and by two chlorides and attain a regular SP geometry.

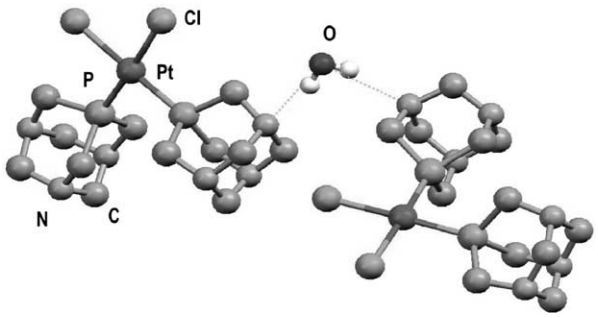

Fig. 2. Crystal structure of $[\{PtCl_2(PTA)_2\}_2(\mu\text{-}H_2O)]$. Adapted from [67].

Double protonation of **92** forming $[PtCl_2\{PTA(H)\}_2]Cl_2$ (**93**) is obtained through crystallization of **92** in 0.1 M HCl solution. The crystal structure of **93** was reported as a slightly distorted SP with two *cis* protonated PTA ligands and two *cis* chlorides. An extensive pattern of hydrogen bonds support the solid-state structure of **93** involving Cl^- and $PTA(H)^+$ ligands as well as solvated water molecules [59].

The white tris-substituted PTA species $[PtCl(PTA)_3]Cl$ (**94**) was prepared by either refluxing an aqueous solution of $PtCl_2$ and PTA or ligand exchange of PhCN with PTA from $Pt(PhCN)_2Cl_2$ [68,69] The tetraphenylborate salt was isolated upon addition of $NaBPh_4$ to a dichloromethane solution of $PtCl_2(PhCN)_2$ in the presence of PTA in MeOH [58]. Electrospray ionization studies (ESI) of **94** in MeOH indicated that a series of platinum ions were present in solution including monometallic species such as $[PtCl(PTA)_3]^+$

and $[PtCl_2(PTA)_2]^+$ and a variety of polymetallic ions. Reaction of the monopositive ion $[PtCl(PTA)_3]^+$ with H_2S in the gas-phase resulted in chloride replacement and formation of the hydrosulfido complex cation $[Pt(SH)(PTA)_3]^+$ [68]. The structure of **94** was determined by X-ray crystallography and the cation, isomorphous with the palladium analogue **82**, exhibits the expected SP geometry [69].

The behavior $Pt(PTA)_4$ with respect to acidic media of different acid strength has been carefully and elegantly studied by Darensbourg et al. (Scheme 16) [14b]. Strong acids such as 0.1 M HCl or H_3PO_4 yield regioselective protonation at the nitrogen centers forming the already mentioned tetrachloride salt **91**. In contrast, if a series of weaker acids like H_2O/CO_2, [PTA(H)]Cl, $HpyBF_4$ ($pK_a > 5.25$) is reacted with $Pt(PTA)_4$, protonation occurs selectively at the platinum center forming $[PtH(PTA)_4]Y$ (**95**) (Y = monodentate anion). Using ammonium chloride, 2,3-dichlorophenol or crotonic acid gave mixtures of $[PtH(PTA)_4]Y$ and $Pt(PTA)_4$ in different ratios. The identity of **95** as a genuine Pt–H in solution was demonstrated by ^1H NMR spectroscopy which shows a quintet (δ −14.3) in the hydride region due to coupling of the platinum bonded hydride to four equivalent ^{31}P nuclei ($^2J_{HP} = 28$ Hz). This signal is flanked by ^{195}Pt satellites showing the same multiplicity ($^1J_{HPt} = 567$ Hz). In keeping with the proton NMR spectrum, the $^{195}Pt\{^1H\}$ NMR spectrum display a binomial quintet at −6289 ppm, in the range proper of Pt(0) derivatives ($^1J_{PtP} = 2362$ Hz). Turning off the broad-band proton decoupler split each line of the Pt-spectrum into a doublet with separation of 567 Hz. The hydride **95** is not static on the NMR time-scale. At low temperature ^{31}P NMR spectra (−80 °C) show that the four PTA ligands are equivalent pointing to rapid intramolecular exchange. In contrast, at higher temperature, intermolecular ligand exchanges occurs between free and coordinated PTA. These results are intriguing because suggest that protonation at the N-atom of the phosphaadamantane cage in the platinum(0) derivative **90** is kinetically controlled, whereas the metal atom, being more basic than the coordinated PTA nitrogen atoms, is the thermodynamic site for protonation of the $Pt(PTA)_4$ complex [14b] (kinetic versus thermodynamic acidity of transition metal complexes has been reviewed, see [70]).

Dark red crystals of the pentacoordinate dioidide $PtI_2(PTA)_3$ (**96**) were obtained by Otto and Roodt by reacting $[Pt(PTA)_3Cl]Cl$ (**94**) with sodium iodide in aqueous methanol [71]. The course of the reaction was monitored by both ^{31}P NMR and UV-Vis which show that stepwise addition of iodide to **96** first results in the formation of the tetracoordinate $[PtI(PTA)_3I]^+$ followed by the appearance of $PtI_2(PTA)_3$, the data showed that *trans*-$PtI_2(PTA)_2$ was not formed. The latter derivate was soon thereafter described by the same group who reported the synthesis and crystal structure of the brightly yellow colored *trans*-$Pt(PTA)_2I_2$ (**97**) obtained by halogen exchange of Cl with I of *cis*-$PtCl_2(PTA)_2$ using excess NaI in water [73]. A similar SP geometry, with *trans*-disposition of the two phosphines, was ascertained by X-ray diffraction for the dicyano derivative *trans*-$Pt(CN)_2(PTA)_2$ which was serendipitously obtained as crystal platelets by studying the reaction of $K_2Pt(CN)_4$ with the gold complex $AuCl(PTA)_3$. The tricoordinate gold complex $AuCl(PTA)_2$ was also obtained (vide infra) [73].

In studies on a series of platinum(II) thiosalicylate–phosphines complexes, Pt(ts)PTA (**98**) (ts = thiosalicylate, $SC_6H_4COO^-$) was synthesized by ligand displacement from Pt(ts)(COD) with PTA in methanol [74]. The stability of **98**, which is highly water soluble, was measured using electrospray mass spectrometry (ESMS) which shows almost no fragmentation even at 200 V, in contrast to the PPh_3 derivative which fragments at 80 V.

4.6. Copper and gold-PTA complexes

Very little attention has been devoted to PTA coordination chemistry with copper or silver. In contrast, PTA was found to be an extremely important ligand in gold chemistry and this study was stimulated by the intention to prepare water-soluble phosphine–gold complexes which should show unusual reactivity patterns and self-aggregating properties. This latter feature, establishing short Au···Au interactions, provided an additional motivation to study these compounds as low energy luminescent materials (vide infra).

A single report by Dance and co-workers demonstrates using cyclotron resonance mass spectrometry (FTICR-MS) that PTA stabilizes in the gas phase monophosphine complexes of copper sulfides, $[Cu_xS_y(PTA)]^-$, which are generally considered unreactive [75]. Using laser ablation of Cu_2S, negatively charged anions combine more rapidly with PTA than PPh_3 because of the greater volatility of the former.

Currently there are no reports of isolated copper or silver complexes involving PTA [58].

The synthesis and characterization of gold-photoluminescent materials has sparked a revolution in gold chemistry and a whole field in this area has developed (for a general overview of gold luminescent materials see [76]). Gold–phosphine complexes represent an extremely important class of luminescent compounds [77] and with the advent of water-soluble ligands the possibility to prepare hydrophilic gold aggregates was carefully considered for application in photoluminescent devices (vide infra Section 8).

In 1995, Fackler began an in-depth investigation of the coordination chemistry of gold(I) with PTA aimed at evaluating the hydrophilicity and the photoluminescence properties of these complexes [78]. Scheme 17 summarizes some of the most important results in gold-PTA chemistry obtained by this group.

In a first paper, the dicoordinate, mono-substituted PTA-gold complex AuCl(PTA) (**99**) was synthesized by reacting the dimethylsulphide complex $AuCl(SMe_2)$ with PTA in chloroform [78]. The bromide AuBr(PTA) (**100**) and iodide AuI(PTA) (**101**) analogues of **99** were easily prepared by halogen exchange upon mixing **99** with either

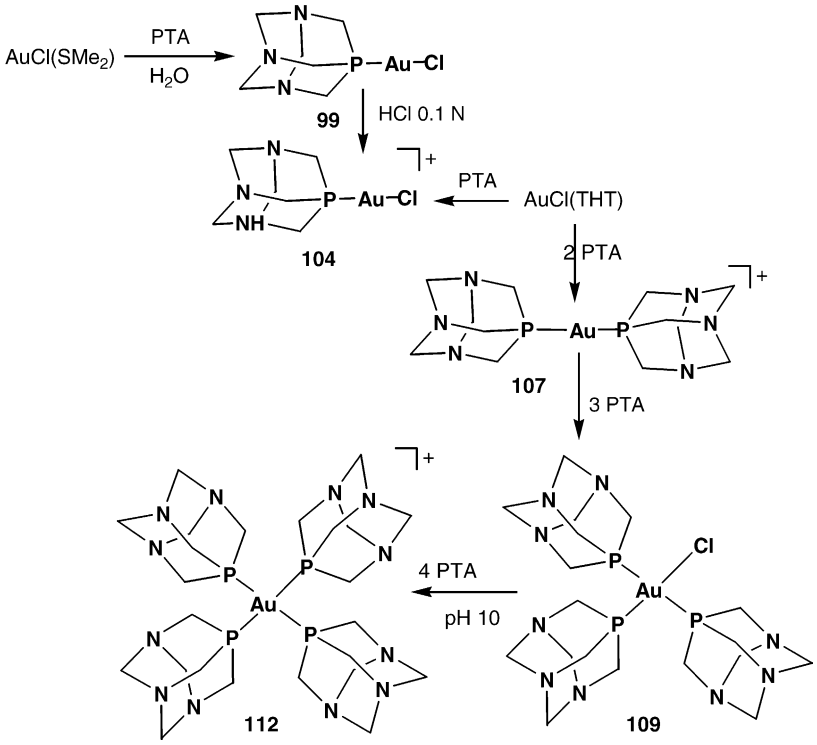

Scheme 17.

HBr in H_2O/acetone or KBr in dichloromethane/acetonitrile [78,79] or KI in refluxing acetone, respectively [78]. The methylgold complex Au(Me)(PTA) (**102**) was prepared through reaction of AuCl(PTA) with MeLi at 0 °C in Et_2O [78]. Reaction of **99** with MeOTf in CH_2Cl_2 at −35 °C results in the isolation of the PTA(Me) containing complex [AuCl{PTA(Me)}]OTf (**103**) in good yield (85%). The identity of **103** was determined from FAB-MS data. The solid-state thermal stability of Au(PTA)(Me) is significantly lower then that of the related halide complexes AuX(PTA) (X = Cl, Br, I), maybe in part due to lack of hydrogen bonding in the methylated complex.

The molecular structure of the chloride (**99**) and the bromide (**100**) derivatives containing MeCN solvated were determined by X-ray methods which disclosed the existence of dimeric aggregates in the solid-state through weak Au · · · Au interactions. A gold-gold separation of only 3.092 Å was determined in **99** while in the bromide complex it is 3.104 Å. These distances are among the shortest found in the wide family of tertiary phosphine gold(I)-halide complexes and have been ascribed to the very small cone angle exhibited by PTA [78,79]. Fig. 3 illustrates the crystal structure of the gold dimer originating from the "aurophilic" intercation in **99**.

More recently, an unsolvated fibrous form of **99**, obtained by crystallizing **99** from 1,2-dichloroethane/*n*-hexane solution, has been studied by X-ray diffractometry and instead of the dimeric aggregation, a polymeric helical chain of gold atoms featuring a longer [3.394(2) Å] Au · · · Au separation has been determined [80].

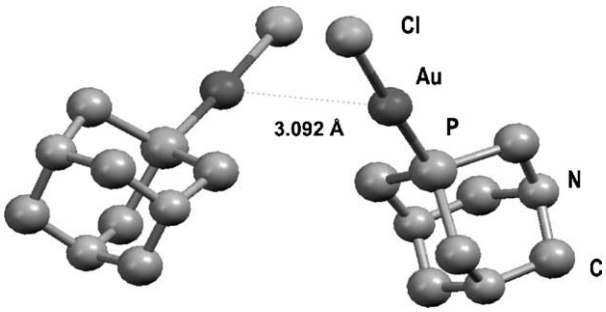

Fig. 3. Crystal structure of Au(PTA)Cl. Adapted from [79].

Compound **99** can be protonated using 0.1 M HCl giving [AuCl{PTA(H)}]Cl (**104**). Alternatively, the protonated complex may be prepared in MeOH/MeCN solvent by reacting PTA(H)Cl with AuCl(THT). Likewise, dissolving **100** in HBr 0.1 N affords the protonated bromide [AuBr{PTA(H)}]Br (**105**). In contrast, when the same protocol is applied to the iodide derivative **101** the diodoauride complex [AuI{PTA(H)}](AuI_2) (**106**) was obtained as light yellow crystals [79]. In the absence of HI in the solution, compound **106** slowly decomposes in solution releasing metallic gold. The structures of the protonated chloro- and iodo-derivatives were obtained by X-ray crystallography. The main structural pattern of **104** does not differ from **99**, apart a significant lengthening of the "aurophilic" interaction to 3.322 Å [79]. In contrast, the structure of **106** does not exhibit any dimeric pairing of the $[AuI\{PTA(H)\}]^+$ cation. Rather, it shows an Au · · · Au contact of only 2.920 Å

between the gold atom of the $[AuI\{PTA(H)\}]^+$ cation and the gold atom of the AuI_2^- anion. This distance is the shortest Au···Au separation found in Fackler's Au-PTA complexes to date. Remarkably, the Au···Au distance in **106** changes with the temperature slightly decreasing with lowering of the temperature up to 2.916 Å at 200 K [79].

Coordination gold(I) complexes featuring more than one PTA ligand are known and have been studied by Fackler and co-workers. Thus, the bis-substituted species $[Au(PTA)_2]Cl$ (**107**) can be prepared by reacting AuCl(THT) with two separate portions of PTA in MeCN [81]. The crystal structure of **107** has been determined showing a linear twofold coordination about gold [82]. The bis-PTA chloride **107** has been used to synthesize $[Au(PTA)_2][Au(CN)_2]$ (**108**) by reacting one equivalent of $KAu(CN)_2$ with $[Au(PTA)_2]Cl$ in water [80]. This compound crystallizes in long fibers which has implications with respect to its spectroscopic properties (vide infra Section 8). The geometry of **108** determined by X-ray analysis consists of linearly dicoordinated $[Au(PTA)_2]^+$ cations and $[Au(CN)_2]^-$ anions in a 1:1 ratio forming an alternating linear chain with a uniform Au···Au "aurophilic" interaction of 3.457 Å [80].

The four-coordinate Au(I) complex $AuCl(PTA)_3$ (**109**) was prepared by stirring together AuCl(THT) with three separate portions of PTA in a 1:2 MeCN/MeOH mixture [81]. In contrast to **107**, whose ^{31}P NMR spectrum in D_2O is sharp and slightly depends on pH changes in the range $3 < pH < 10$, the ^{31}P NMR spectra of $AuCl(PTA)_3$ is fluxional at room temperature and consists of two broad resonances even at −50 °C in CD_3CN/CD_3OD indicating a dynamic behavior exchanging the three PTA ligands [81].

Coordination of more than one alkylated PTA ligands to gold has been obtained. The complex $[AuI\{PTA(Et)\}_3]I_3$ (**111**) was synthesized by reacting three equivalents of [PTA(Et)]I with $AuCl(SMe_2)$ in aqueous dichloromethane biphasic mixture [83]. The X-ray analysis showed the gold atom coordinated to three PTA(Et) ligands in a distorted trigonal planar environment. The gold atom located on the threefold axis lies slightly above the trigonal plane weakly interacting with one iodide ion [$d_{Au\cdots I} = 2.9129(12)$ Å].

Fully substituted gold(I) complexes with either PTA or $[PTA(Me)]^+$ have been also described (Scheme 17) [84]. Then, the tetrakis-PTA complex $[Au(PTA)_4]Cl$ (**112**) was synthesized by the addition of four equivalents of PTA to $Au(Me_2S)Cl$ in an alkaline water/CH_2Cl_2 solution. The homoleptic $[Au\{PTA(Me)\}_4](PF_6)_5$ (**113**) was similarly prepared by reacting five equivalents of $[PTA(Me)]PF_6$ with $Au(SMe_2)Cl$ in H_2O/CH_2Cl_2.

A tris-protonated version of **112**, $[Au\{PTA(H)\}_3(PTA)](PF_6)_4$ (**114**) was obtained when four equivalents of [PTA(H)]Cl were added to a solution of Au(THT)Cl [84]. Furthermore, **112** can be obtained as hexafluorophosphate salt, $[Au(PTA)_4]PF_6$ (**115**), by reacting a single equivalent of $NaPF_6$ with $[Au\{PTA(H)\}_3(PTA)](PF_6)_4$ [84]. It is interesting to note that in **114** one proton is lost from one of the four protonated PTA ligands and attempts to obtain a fully protonated tetrakis-PTA(H) product have so far failed. In this mixed PTA/PTA(H) derivative a complete exchange of proton takes place between the four coordinated phosphines as witnessed by the single broad resonance appearing in the ^{31}P NMR spectra ($\delta = -59$ ppm). The X-ray crystal structures for the four-coordinate complexes **112**–**115** have been determined with the complex cation sharing a similar tetrahedral arrangement of PTA (**112** and **115**), PTA(H) (**114**) and PTA(Me) (**113**) ligands around the gold center. An extended three-dimensional $N^+H\cdots N$ hydrogen-bonding network, sometime supported by intermolecular H-bonding interactions with water solvate molecules, provides a robust scaffold for building up supramolecular assemblies of AuL_4 tetrahedra [84].

Treatment of $AuCl(SMe_2)$ with [PTA(Me)]I in CH_2Cl_2/H_2O with subsequent addition of KI led to formation of $[AuI\{PTA(Me)\}_3]I_3$ (**116**). Attempted removal of the iodide coordinated to the Au center of **116** with $NaPF_6$ and $NaBPh_4$ was unsuccessful. Then, metathesis of the three iodide counteranions occurred after reaction with $NaPF_6$ to give the salt $[AuI\{PTA(Me)\}_3](PF_6)_3$ (**117**) while the reaction with $NaBPh_4$ resulted in a transfer of the phenyl group to gold yielding the unexpected dicoordinate gold-phenyl salt $[AuPh\{PTA(Me)\}]BPh_4$ (**118**) [85]. A similar phenyl transfer reaction giving the mono-PTA complex AuPh(PTA) (**119**) takes place by reacting $AuCl(PTA)_3$ with $NaBPh_4$ in water. Crystals of **116**–**119** were obtained by slow evaporation of aqueous solution. And their structures determined by diffraction methods. The structure of **116** is similar to that of **111** with one iodide ion lying at 2.936(1) Å from the gold center. The two phenylated derivatives, **118** and **119**, show approximately linear coordinations about the gold atom [85].

A series of mono-substituted arylthiolate PTA-Au complexes of formula Au(SAr)PTA (**120**) (Ar = Ph, *o*-PhOMe, *m*-PhOMe, *o*-PhCl, *m*-PhCl, *p*-PhCl, 3,5-$PhCl_2$) were synthesized by Fackler et al. with the purpose of determining changes in lattice packing. By systematically varying the steric requirements of the aryl-thiolate group, the Au···Au distances of the "aurophilic" interaction changed and a correlation between the distance of the two gold atoms and the emission energy of the compound in the solid-state was proposed [86]. Complexes **120** were obtained by firstly deprotonating ArSH with KOH in MeOH and subsequent reaction with AuCl(PTA) in MeCN. The nature of thiolate group in **120** has little or no effect on the phosphorus chemical shift in the ^{31}P NMR spectrum (see Table 1), while it deeply affects the luminescence properties of the gold compounds.

4.7. Mercury-PTA complexes

A series of mercury(II)-PTA complexes of formula $[HgX_2(PTA)]$ (**121**) (X = Cl, Br, I, CN, SCN) were prepared by Alyea et al. by addition of mercury halides or pseudohalides to a hot PTA/MeOH solution in various ratios [22]. For these compounds, the solubility is greatly limited,

hence characterization was performed using IR and Raman methods and ^{31}P CP-MAS solid-state NMR spectroscopy. Use of mercury acetate or perchlorate resulted in deposition of elemental Hg. In the case of $Hg(NO_3)_2$, a mono-PTA adduct could not be isolated. Instead, depending on stoichiometry, either elemental Hg was obtained or, using a PTA/$Hg(NO_3)_2$ ratio of 1:2, $[Hg(NO_3)_2(PTA)_2]$ (**122**) was formed. Furthermore, NMR data showed the presence of tetrakis-substituted PTA complexes $[Hg(PTA)_4X_2]$ (**123**, X = Cl, Br, NO_3) as by-products. IR and NMR data of **122** suggest that the compound exists as a salt containing the cation $[Hg(PTA)_2]^+$. IR data indicate that all the bis-PTA compounds are highly symmetrical, containing C_{2h} symmetry and suggest a possible structure with bridging and terminal halides. Solid-state ^{31}P NMR spectroscopy showed that coupling constants with ^{199}Hg for these mercury-PTA complexes are smaller than those related complexes featuring Cy_3P or Bu_3P. An analysis of the $^1J_{HgP}$ indicates that increasing the number of PTA ligands about Hg decreases $^1J_{HgP}$ values (see Table 1) and allowed the authors to propose a linear correlation between ^{31}P chemical shift and $^1J_{HgP}$ [22].

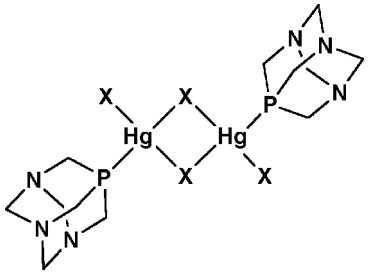

121 X = Cl, Br, I, CN, SCN

5. Single crystal X-ray diffraction data for transition metal complexes of PTA

The phosphaadamantane cage of PTA is a multifunctional ligand exhibiting four different potential coordination sites, one bridgehead phosphorus and three nitrogen atoms. In spite of this diversified bonding possibilities, all of the structurally determined transition metal complexes featuring PTA and its derivatives [PTA(H), PTA(Me)] contain the adamantane-like molecule coordinated to the metal through the phosphorus atom. While this behavior may be in part justified for those complexes involving second and third row transition metals, which have a more soft character, it remains apparently puzzling for metals, such as iron [39] and nickel [14b,57,58], belonging to the first transition period. The hard character of these metals, especially of iron(II), should have indeed favored *N*-coordination of PTA rather than the experimentally observed P-bonding of the cage molecule.

A comprehensive search of the Cambridge Database System performed in October 2003 indicates that 59 crystal structure determinations of transition metal complexes with PTA (and its derivatives) have been reported in the scientific literature. Although this number is still limited with respect to other traditional phosphines, which have been much more used as metal ligands, to allow us to draw explicit conclusions about the metal-PTA bonding properties, the available set of crystal data is representative enough for proposing some rationalization of the structural results. Tables 2 and 3 collect the crystallographic information available about transition metal complexes containing PTA and related ligands and also give some statistics. The compilation is based on a whole set of crystallographic determinations available in the literature (59 compounds).

The average distance between metal and PTA phosphorus donor atom is 2.297 Å, ranging from 2.145(3) Å in K[CpFe(CN)$_2$(PTA)] (**33**) [39] to 2.4976(15) Å in W(CO)$_5$(PTA) [26]. The M–P bond distance shows a small distribution around the average value and the observed differences in the bond length are mostly in agreement with the general behavior of the phosphorus-transition metal bond. Thus, the M–P bond lengths decrease as the metal increases the number of electrons in the valence shell within the same series, and increase moving from first to second and then to third series, as expected.

As a first general observation, P-coordination of the phosphaadamantane to a transition metal center causes only minor modifications with respect to the free ligand. In particular the P-CH_2 distance is rather similar in both free and coordinated PTA and only a short contraction of less than 0.05 Å is observed. This situation is in agreement with the pure σ-character of the bond. No other significant influence on the rest of the PTA molecule is observed by coordination of phosphorous to the metal, and the minor differences observed in a few cases are likely produced by packing effects.

An interesting aspect to be pointed out concerns the change of P–M bond length depending on whether or not the PTA nitrogen are protonated. In most cases, where both the $L_nM(PTA)_x$ and $L_nM\{PTA(H)\}_x^+$ species are available and have been studied by X-ray diffractometry, the M–P separation is increased by protonation of the PTA. A similar trend is observed in those compound containing in the ligand set both PTA and one or more protonated phosphines. For example, in $[RhCl\{PTA(H)\}_3(PTA)]Cl_3$ (**60**) the $Rh–P_{\{PTA(H)\}}^+$ distance involving the three PTA(H) ligands averages to 2.321(1) Å but the $Rh–P_{(PTA)}$ bond distance is 2.206(1) Å [23]. Although such variation (Δ_d = 0.115 Å) is crystallographically meaningful, it should be observed that in complex **60** the neutral PTA ligand is *trans* to the Cl atom while the three PTA(H) ligands occupy the three equatorial positions of the TBP about rhodium. Therefore, the *trans* effect of the chloride might account for the difference in the M–P bond length without invoking any effect associated with the PTA ligand protonation. Inspection of the M(PTA) complexes authenticated by X-ray crystallography

Table 2
M–P bond distance (Å) for PTA, PTA(H) and PTA(Me) metal complexes

Metal	Number of compounds	Number of data[a]	Unweighted sample mean (Å)	Range of sample data	Ligand
Au	**13**	16	2.301	2.221(2)–2.413(2)	PTA
Au	**1**	3	2.402	2.397(2)–2.405(3)	PTA(H)
Au	**4**	8	2.366	2.2274(3)–2.423(2)	PTA(Me)
Fe	**1**	1	2.145	–	PTA
Fe	**1**	1	2.128	–	PTA(H)
Ir	**2**	9	2.306	2.273(6)–2.3378(9)	PTA
Ir	**1**	4	2.313	2.2847(13)–2.3410(14)	PTA(H), $PTAH_2$
Mo	**1**	1	2.479	–	PTA
Ni	**3**	7	2.218	2.1853(13)–2.252(2)	PTA
Ni	**1**	1	2.133	–	PTA(H)
Pd	**3**	7	2.270	2.226(5)–2.338(2)	PTA
Pd	**2**	2	2.249	2.203(3)–2.2940(8)	PTA(H)
Pt	**2**	7	2.256	2.2229(13)–2.3214(11)	PTA
Pt	**2**	3	2.230	2.218(5)–2.254(3)	PTA(H)
Re	**3**	6	2.423	2.321(4)–2.4529(19)	PTA
Re	**1**	2	2.427	2.4254(13)–2.4287(13)	PTA(H)
Rh	**1**	1	2.206	-	PTA
Rh	**2**	5	2.269	2.187(2)–2.341(1)	PTA(H)
Rh	**3**	8	2.291	2.254(3)–2.318(2)	PTA(Me)
Ru	**5**	11	2.301	2.252(2)–2.388(2)	PTA
Ru	**2**	2	2.360	2.342(2)–2.379(1)	PTA(H)
Ru	**3**	5	2.302	2.228(2)–2.348(2)	PTA(Me)
W	**2**	2	2.458	2.418(3)–2.4976(15)	PTA

[a] The number of data may be different from the number of compounds because some PTA complexes, for which X-ray diffraction data are available, may contain more than one PTA ligand, thus contributing more than one time to the value of the number of data available for elaborating this statistic.

Table 3
Unweighted sample mean (Å) of the M–P distance as a function of transition metal series

Cr	Mn	Fe	Co	Ni	Cu	Zn	Ligand
		2.145		2.2184			PTA
		2.128		2.133			PTA(H)
							PTA(Me)
Mo	Tc	Ru	Rh	Pd	Ag	Cd	
2.479		2.3006	2.206	2.2700			PTA
		2.3605	2.2678	2.2485			PTA(H)
		2.3016	2.2907				PTA(Me)
W	Re	Os	Ir	Pt	Au	Hg	
2.458	2.4230		2.306	2.2559	2.3014		PTA
	2.4270		2.3135	2.2303	2.402		PTA(H)
					2.366		PTA(Me)

shows that more unambiguous examples are available to substantiate the M–P expansion following PTA protonation of the uncoordinated nitrogen donors. The tetrahedral gold(I) complex cation $[Au\{PTA(H)\}_3(PTA)]^{4+}$ exhibits an $Au–P_{(PTA)}$ separation of 2.397(2) Å but the averaged bond length $Au–P_{\{PTA(H)\}}{}^{+}$ is 2.408 Å [84]. These values should be compared with the tetrakis-PTA monocation $[Au(PTA)_4]^{+}$ which shows average $Au–P_{(PTA)}$ separations of only ca. 2.385 Å irrespective of the counteranion, Cl^{-} or $PF_6{}^{-}$ [84]. Such kind of generalization, should however be carefully considered as other factors may be relevant to dictate minor alterations of the metric parameters in the crystal. Without any doubt, for the case of PTA complexes these include the ability of the PTA ligand to form strong hydrogen bonds with solvated water molecules, a characteristic which is even amplified in protonated PTA(H) complexes which, in addition, regularly form strong intra- and intermolecular $NH^{+}\cdots N$ H-bonding interactions. Other factors, like the overall charge of the complex, the presence of co-crystallized molecules other than water, the nature of the counteranion, etc. can also play a significant role in governing the crystal packing of metal-PTA complexes. As a paradigmatic example stressing the subtle balance between cooperative effects for addressing the M–P distances in this class of compounds, we may emphasize that the two structurally related gold complexes $[AuCl(PTA)]\cdot 0.5H_2O$ (**99**) and $[AuCl\{PTA(H)\}]Cl\cdot MeCN$ (**104**) show no appreciable variation of the gold–phosphorus bond length with $Au–P_{(PTA)}$ in **99** [2.226(2) Å] almost identical to $Au–P_{\{PTA(H)\}}{}^{+}$ in **104** [2.221(2) Å] [80]. Likely, in this intriguing pair of compounds is the "aurophilic" interaction [$d_{(Au\cdots Au)}$ at 193 K = 3.092(1) Å in **99**; 3.304(1) Å in **104**. $\Delta_d = 0.212$ Å], building up a crystallographically defined dimer in the solid-state, mainly responsible for finely tuning all of the other structural parameters also including the Au–P bond distance.

6. Catalytic properties of PTA transition metal complexes

Homogeneous catalysis offers numerous advantages over related heterogeneous reactions, including higher activity

and selectivity, lower operating temperatures and pressures. Furthermore, numerous ways of controlling specific steric and electronic properties of the catalyst is possible using a wide variety of different ligands. However, short lifetime, high costs and toxicity are generally associated with homogeneous catalysts. The difficult regeneration of an homogeneous catalyst from its spent form makes catalyst recycling an important issue and product separation continues to be a great challenge. In order to reduce the environmental impact of organic solvents in industrial scale applications, water is the key choice for green catalysts as it is cheap, readily available and non-toxic [4]. Recent efforts have thus focused on the development of metal complexes with water-soluble ligands, in particular phosphines, including PTA [1].

Among the different PTA transition metal complexes described in Section 4, those of ruthenium and rhodium have attracted a lot of interest as potentially useful catalysts for a variety of processes in water or aqueous biphasic conditions. The most intriguing results in this area are summarized in this section which intends also to compare the effectiveness of PTA complexes with other hydrophilic transition metal catalysts. The advantages of using PTA-containing catalysts in aqueous and biphasic systems will be also highlighted and compared to conventional homogeneous processes. Limited descriptions of the catalytic properties of PTA derivatives have appeared in the literature whenever specific catalyzed processes, such as the catalytic hydrogenation of CO_2, have been reviewed [87].

The Ru-PTA complexes **35** and **36** were found to be suitable catalysts for the hydrogenation of various substituted benzaldehydes into alcohols and terminal aldehydes such as 1-hexanal [14,40]. Under biphasic aqueous-organic solvent conditions using sodium formate as the hydrogen source, $RuCl_2(PTA)_4$ accomplishes a 95.1% conversion of benzaldehyde into benzyl alcohol with a TOF of $22\,h^{-1}$ at 80 °C [40b]. However, the conversion was lower in cases where a substitutent was ortho with respect to the aldehyde group, i.e. conversion of 2-methoxybenzaldehyde was only 23.6%. For α,β-unsaturated aldehydes, hydrogenation catalysed by this kind of complexes is usually highly selective to the unsaturated alcohol [40b]. Conversion of saturated and unsaturated acyclic aldehydes using **35** with sodium formate also varied depending on the substrate, 87.6% for 2-butenal to 23.0% for 1-hexanal (Table 4). Long chain aldehydes such as 1-decenal failed to be hydrogenated in the presence of **35** [40b]. Kinetic studies of the hydrogenation of benzaldehyde (0.80 M in chlorobenzene) using **35** (0.03 mmol) with aqueous $NaHCO_2$ (5 M) as hydrogen source, showed the decay rate of benzaldehyde is exponential with a pseudo-first order rate of $1.01 \times 10^{-2}\,min^{-1}$ (80 °C). Deuterium labeling experiments were performed by Joó and co-workers to determine the source of hydrogen used by **35** in hydrogenation reactions, whether from water or sodium formate [40a]. Three benzaldehyde hydrogenation tests using **35** were carried out with the following conditions: (i) $D_2O/NaHCO_2$; (ii) $H_2O/NaDCO_2$; (iii) $D_2O/NaDCO_2$. [40b] MS analysis demonstrated that the level of deuterium incorporation in the benzyl alcohol was higher in experiment (ii), whereas 100% C_6H_4CDHOH was obtained, as expected, in experiment (iii). Therefore, the source of hydrogen was identified as the formate ion, with limited exchange with water occurring in the Ru hydride formed in situ (vide infra). Further studies on isotope exchange between D_2 and H_2O or H_2 and D_2O were also reported [88].

Table 4
Catalytic hydrogenation of aryl aldehydes to alcohols using $RuCl_2(PTA)_4$ (**35**) [40]

Substrate (mmol)	Conversion (%)
Benzaldehyde (4.92)	64.0
	7.1[a]
	0.41[b]
4-Methylbenzaldehyde (4.24)	23.6
4-Methoxybenzaldehyde (4.11)	26.7
4-Bromobenzaldehyde (1.35)	16.3
2-Hydroxybenzaldehyde (4.69)	0
1-Hexanal (4.16)	23.0
2-Butenal (6.04)	87.6
3-Phenyl-2-propenal (3.96)	21.2
1-Propanal (6.93)	81.6
1-Butanal (5.55)	72.8
1-Pentanal (4.70)	46.1
1-Hexanal (4.16)	23.0

Conditions: **35**, 0.0625 mmol, chlorobenzene 5 ml/H_2O 5 ml; 5 M $NaCO_2H$, 5 ml; 80 °C, 3 h.
[a] Under an atmosphere of CO.
[b] 10 equiv PTA added.

Catalyst recycling proved successful as no **35** was transferred into the organic phase in a series of experiments and the catalyst performed several hydrogenation cycles without loss of activity, although removal of Na_2CO_3, formed as a by-product of sodium formate, was required. If H_2 is used as the hydrogenation source, the limited solubility of the gas in H_2O is an issue, and pressures of over 400 psi are needed to obtain modest TOFs. For example, conversion of benzaldehyde using 1 atm of H_2 resulted in a 2.6% conversion whereas using 400 psi of H_2 increased the conversion to 45.9%. Furthermore, the catalytic reactions are inhibited by the presence of CO or excess PTA [40b].

In attempts to determine the hydrogenation mechanism involving $[RuCl_2(PTA)_4]$ (**35**), a ^1H and ^{13}C HPNMR study was conducted, where an aqueous solution of $NaHCO_3$ (1.6 mmol) $NaH^{13}CO_3$ (0.4 mmol) and a catalytic amount of **35** (5.4×10^{-3} mmol) was pressurized with H_2 [46]. Three species, the monohydride $RuHCl(PTA)_4$ (**47**), the hydrido(aquo) cation $[RuH(H_2O)(PTA)_4]^+$ (**124**) and the dihydride $RuH_2(PTA)_4$ (**48**), were observed. At pH 12.0, only **48** is observed by ^1H NMR as a typical multiplet resonance at −11.40 ppm. In acidic solutions (pH = 2.0), the monohydride **47** dominates, with the hydride signal giving a doublet of quartets at −8.31 ppm (see Table 1). In the presence of an excess of PTA, the new species $[RuH(PTA)_5]^+$ (**49**) was identified. The catalytic reaction does not require

the addition of amines, but can be promoted with inorganic bases such as NaOH or $CaCO_3$. High pressure ^1H and ^{13}C NMR measurements under different H_2 pressures show that the reaction rate is first order in H_2 pressure TOFs using **35** were measured at 0.24 h^{-1}, whereas the analogous $RuCl_2(TPPTS)_4$ achieved TOF values of 1.49 h^{-1}. Using sodium bicarbonate as the substrate improved conversion rates (TOF = 23 h^{-1}). From these studies, it appears that HCO_3^- is the substrate which is hydrogenated. The initiation time observed with **35** may be due to bicarbonate formation, as well as slow ligand exchange and formation of the hydride as the active catalytic species. An overall activation energy of 86 kJ mol^{-1} was calculated, higher than the 25 kJ mol^{-1} observed for the $RuCl(TPPTS)_3$ system. A proposed mechanism for the reduction of hydrogen carbonate to formate catalysed by **35** is shown in Scheme 18.

The authors have compared the efficiency of **35** for CO_2 and HCO_3^- reduction with that showed by other Ru(II) water-soluble complexes, namely $[RuCl_2(TPPTS)_3]$, $[RuCl_2(TPPMS)_3]$ and their Rh analogues, $[RhCl(TPPTS)_3]$, $[RhCl(TPPMS)_3]$, under mild conditions (60 bar CO_2, 30 bar H_2) [89,90]. The initial TOF increases linearly with H_2 pressure due to increased H_2 solubility in the water phase, i.e. the reaction appears to be first order with respect to $p(H_2)$. In the case of Rh(I) complexes, the presence of amines is required to achieve efficient hydrogenation (initial TOF 7260 h^{-1} at 81 °C under 40 atm total pressure CO_2/H_2 1:1) [89]. The use of Na_2CO_3 1 M instead of Me_2NH 0.5 M increased the overall TOF from 0.13 to 116 h^{-1} at 24 °C, by formation of $NaHCO_3$ which is more easily hydrogenated. $[RuCl_2(TPPTS)_2]_2$ catalyses the hydrogenation of CO_2 to formic acid (TOF 6 h^{-1}, 23 °C) again in the presence of amines. CO_2 has negative effect on the rate of hydrogenation of bicarbonate with $[RuCl_2(TPPTS)_2]_2$ as catalyst, whereas with **35** an increase of the rate is observed with increased CO_2 pressure. Comparison in the presence of $CaCO_3$ as a base showed TOFs of 26.6 h^{-1} with $[RuCl_2(TPPTS)_2]_2$ to 18.7 using $[RhCl(TPPTS)_3]$, to 2.5 h^{-1} with **35** [90].

Ruthenium(II) and rhodium(III) complexes of PTA(Me), namely *trans*-$RuI_4\{PTA(Me)\}_2$ (**39**), $[RuI_2\{PTA(Me)\}_3(H_2O)]I_3$ (**40**) and $[RhI_4\{PTA(Me)\}_2]I$ (**56**) are active catalysts for the hydrogenation of cinnamaldehyde and, in the case of **56**, hydroformylation of 1-hexene (TOF 138 h^{-1}, conversion 93%, linear/branched ratio 1.7) [41]. Whereas **39** and **40** are able to hydrogenate selectively the C=O bond, **56** gives selective reduction of the C=C double bond. Under biphasic conditions (water/toluene or chlorobenzene) with H_2 as the hydrogen source, average TOFs (h^{-1}) ranged

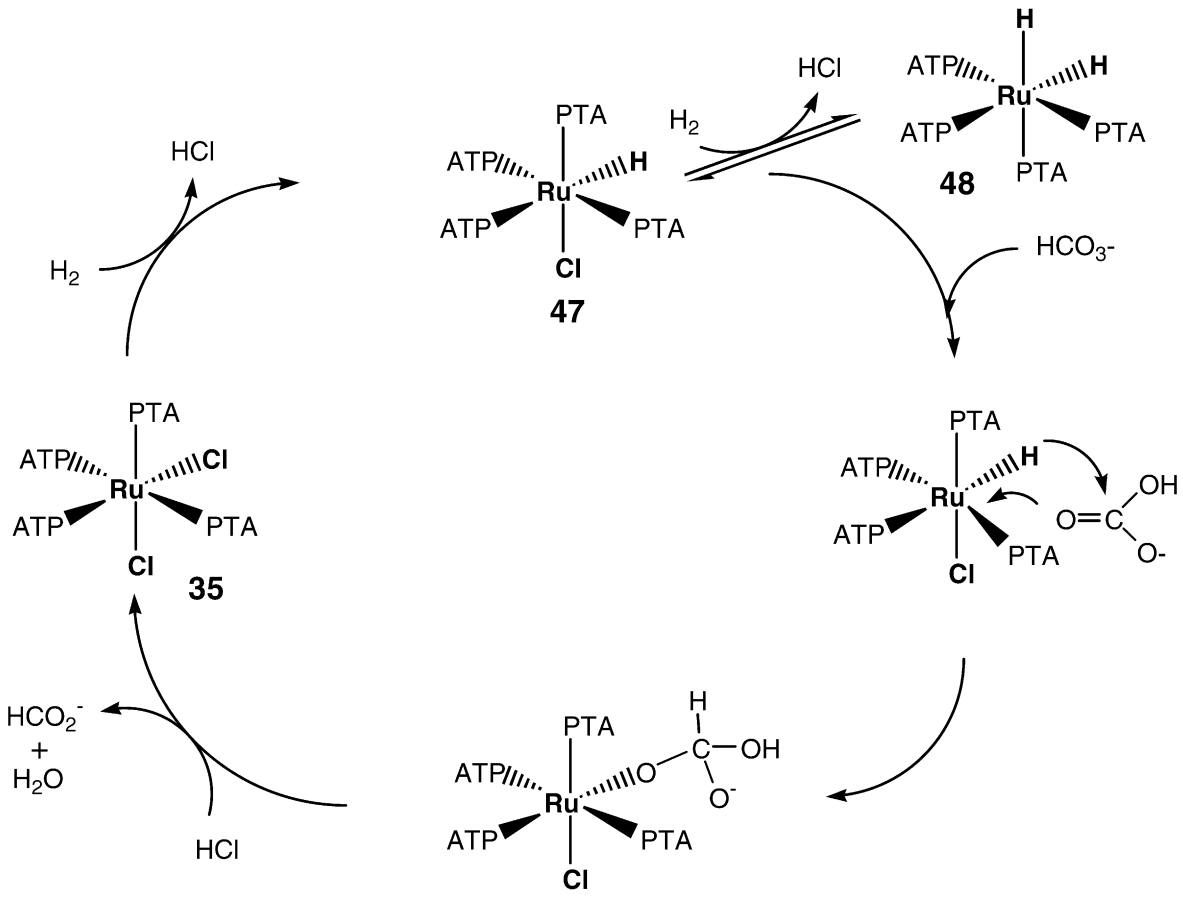

Scheme 18.

Table 5
Hydrogenation of cinnamaldehyde with catalysts **39**, **40** and **56** [41]

Conversion (%)	TOF (h^{-1})	Yield products (%)	Catalyst
89[a]	40	PhCH=CHCH$_2$OH (84), Ph(CH$_2$)$_3$OH (5)	**39**
4[b]	8	PhCH=CHCH$_2$OH (2.5), Ph(CH$_2$)$_2$CHO (1)	**39**
45[a]	183	PhCH=CHCH$_2$OH (36), Ph(CH$_2$)$_2$CHO (5), Ph(CH$_2$)$_3$OH (4)	**40**
2[b]	4	PhCH=CHCH$_2$OH (2)	**40**
95[a]	190	PhCH=CHCH$_2$OH (2.5), Ph(CH$_2$)$_2$CHO (84), Ph(CH$_2$)$_3$OH (8)	**56**
13[b]	25	Ph(CH$_2$)$_2$CHO (13)	**56**
17[c]	4	PhCH=CHCH$_2$OH (17)	**39**

[a] Toluene/water, $p(H_2) = 3.0$ MPa, [catalyst] 0.01 mmol, 333 K.
[b] Chlorobenzene/water, 5 M $NaCO_2H$, [catalyst] 0.01 mmol, 348 K.
[c] Toluene/water, $p(H_2) = 0.1$ MPa, [catalyst] 0.01 mmol, 293 K.

from 40 (**40**) to 183 (**39**) and 190 (**56**). Conversion of cinnamaldehyde using **56** was 95% with 84% selectivity to PhCH$_2$CH$_2$CHO, the best selectivity to PhCH=CHCH$_2$OH was achieved with **39** (84% yield at 89% conversion). Using sodium formate as the hydrogen source gave lower conversions (see Table 5). Recycling of the catalyst showed no loss of activity upon three cycles [41].

Hydrogenation of substituted arenes into completely saturated cyclohexanes can be accomplished by using the Dyson's arene-Ru complexes **41** and **42** as catalysts under biphasic conditions, see Table 6 [42a]. Tests showed that **41** is slightly more active than **42** and addition of elemental Hg (colloidal poison) did not influence the activity. The analogous [Ru(*p*-cymene)(TPPMS)Cl$_2$] complex has significantly higher catalytic activity than both **41** and **42**. In this case, the addition of Hg hinders the hydrogenation, hence Ru colloidal particles are likely to be the active catalytic species. Hydrogenation of chlorobenzene results in extremely poor TOFs. ^{31}P NMR and ESMS analysis, showing a peak m/z at 743, unexpectedly show that both **41** and **42** are converted into a tri-ruthenium cluster [Ru$_3$(*p*-cymene)$_3$(μ_3-Cl)]$^+$ (**125**) that does not contain any PTA, likely the resting state of the catalyst after few TONs. Arene hydrogenation catalyzed by **41** in ionic liquids such as [bmim]BF$_4$ (bmim = 1-butyl-3-methylimidazolium) was carried out by Dyson et al., showing a 50% increase was observed for the conversion of benzene if compared to catalytic tests run in water [91]. The advantage of using ionic liquids is lost if the solvent contains trace amounts of chloride, a common by-product from the synthesis of ionic liquids. Halides are detrimental to the catalytic conversion of arenes and should therefore be avoided (see Table 6). Recycling of the catalyst showed that over a series of five batch reactions the turnovers remain constant in [bmim][BF$_4$] and Cl-free [bmim][BF$_4$], decreasing slightly in water.

Table 6
Hydrogenation of various arenes using catalytic amounts of **41** and **42** [41,91]

Substrate	TOF (h^{-1})	Conditions	Catalyst
Benzene	170	H_2O	**41**
Benzene	140	[bmim]BF$_4$/Cl[a]	**41**
Benzene	137	[hmim]BF$_4$/Cl[a]	**41**
Benzene	141	[omim]BF$_4$/Cl[a]	**41**
Benzene	206	[bmim]BF$_4$	**41**
Benzene	54	CH_2Cl_2	**41**
Toluene	130	H_2O	**41**
Toluene	54	[bmim]BF$_4$/Cl[a]	**41**
Toluene	136	[bmim]BF$_4$	**41**
Ethylbenzene	122	H_2O	**41**
Ethylbenzene	53	[bmim]BF$_4$/Cl[a]	**41**
Ethylbenzene	145	[bmim]BF$_4$	**41**
Chlorobenzene	11	H_2O	**41**
Chlorobenzene	6	[bmim]BF$_4$/Cl[a]	**41**
Chlorobenzene	18	[bmim]BF$_4$	**41**
Benzene	150	H_2O	**42**
Toluene	129	H_2O	**42**
Ethylbenzene	72	H_2O	**42**

Conditions: $p(H_2)$ 60 atm, 90 °C, 1 h. Catalyst, 30 mg; solvent, 10 ml; substrate, 1 ml.
[a] Trace amounts. bmim = 1-butyl-3-methylimidazolium; hmin = 1-hexyl-3-methylimidazolium; omim = 1-octyl-3-methylimidazolium.

The catalytic hydrogenation of benzylidene acetone to 4-phenylbutan-2-one by **43** and **44** under H_2 pressure (450 psi) with a biphasic water/octane solvent mixture showed substrate conversion varying from 39.1% (3 h, 130 °C) to 99.7% (21 h, 130 °C), with high regioselectivity to C=C double bond reduction (Table 7) [44]. The presence of an excess of PTA was found to decrease conversion to 22.9% (13 h, 130 °C). Catalyst recycling for **43** and **44** under these conditions was found not be as effective as for other Ru-PTA systems as after the third cycle **43** showed loss in activity although accompanied by an increase in selectivity. Using high-pressure ^{31}P NMR, **43** was observed to react at 50 °C with H_2 (450 psi) in H_2O/THF-d_8 to form the mono-hydride species CpRuH(PTA)$_2$ (**51**) which remains stable upon heating to 80 °C. In contrast, **44** at 50 °C combines with H_2 to form a dihydride complex [Cp*RuH$_2$(PTA)$_2$]Cl (**53**) which converts to the mono-hydride [Cp*RuH(PTA)$_2$] **(52)** after heating to 80 °C. No evidence of PTA dissociation was observed during the reactions.

Water-soluble catalysts are finding use for non-traditional catalytic conversions. For example, the hydrogenation of phospholipid liposomes using the complex RhCl(PTA)$_3$ **54** was recently reported [50]. The fluidity of the various lipid membranes is determined by the proportion of sat-

Table 7
Hydrogenation of benzylidene acetone using **43** and **44**[a] [44]

Catalyst	Conversion (%) (h)[b]	A (%)[b]	B (%)[b]	C (%)[b]
43	39.1 (3)	34.7	2.0	2.4
43	52.7 (6)	43.6	3.8	5.3
43	78.5 (13)	60.0	13.6	4.9
43	99.7 (21)	74.8	21.9	3.0
43[c]	22.9 (13)	15.4	1.2	6.3
43[d]	26.3 (13)	23.7	1.6	1.0
44	24.3 (3)	19.7	1.2	3.4
44	32.1 (6)	26.3	1.2	4.6
44	38.7 (13)	32.5	1.4	4.8
44[d]	40.0 (13)	37.4	1.7	0.9

[a] Conditions: substrate, 1.8 mmol; catalyst, 9×10^{-3} mmol; *n*-octane, 30 ml; H_2O, 15 ml; 130 °C; $p(H_2)$, 450 psi; 1200 rpm.
[b] GC values based on pure samples.
[c] PTA, 18×10^{-3} mmol added.
[d] 80 °C: A = 4-phenylbutan-2-one; B = 4-phenyl-butan-2-ol; C = 4-phenyl-but-3-en-2-ol.

urated and unsaturated fatty acid residues carried by the lipid molecules. A controlled and specific modification of the membranes without undesired side reactions can be achieved by catalytic hydrogenation. Thus, the target is the hydrogenation of the C=C double bonds in the unsaturated acyl chains within the lipid bilayer. Previous methods have proven too harsh in terms of H_2 pressures (up to 12 bar) to achieve meaningful conversions at physiological temperature ranges. Furthermore, catalysts such as $[RhCl(TPPMS)_3]$ and $[RuCl_2(TPPMS)_2]$ were hardly removable from the membranes due to negative charge on the ligands. Complex **54** was tested under mild conditions (37 °C, 1 bar H_2) for the hydrogenation of the unsaturated fraction in soybean lecithin and dioleoylphosphatidylcholine (DOPC). The proportion of linolenic (18:3) and linoleic (18:2) acids decreased and after 40 min, no linolenic acid was present. An overall conversion of 10–20% was achieved in a short period of time. The highest conversion rate was achieved at pH 4.70, suggesting that the hydrogenation of lipid dispersion is catalyzed by hydrido species such as $RhH_2Cl(PTA)_3$ or $RhH(PTA)_4$, in analogy with the hydrogenation of simple olefins, also verified by H/D exchange experiments monitored by FT-IR.

The complex Rh(acac)(CO)(PTA) (**61**) was tested for catalytic hydrogenation of alkenes and allyl alcohol [52]. Under biphasic conditions (water/substrate), under H_2 pressure, initial TOF values ranged from 26 h^{-1} for hydrogenation of allyl alcohol into *n*-propanol (selectivity 90%) to 143 h^{-1} for the hydrogenation of 1-hexene. These experiments suggest that C=C bond in the case of allyl alcohol is strongly coordinated to Rh slowing down transfer of the hydrido ligand to the substrate. In this study, the activity of **61** was compared to other [Rh(acac)(CO)L] derivatives with hydrophilic phosphines (L = cyep, TPPTS). It was observed that although all complexes were active catalysts for alkene and allyl alcohol hydrogenations, **61** shows initial TOFs for conversion of 1-hexene sensibly lower than for the TPPTS system (260 h^{-1}) but higher than for cyep (96 h^{-1}), reflecting the relative stability of the hydrido complexes. In all cases, hydrogenation of allyl alcohol resulted in partial isomerization to propanal. When the hydrogenation of allyl alcohol was carried out in D_2O the incorporation of deuterium was observed at the alpha position in the case of *n*-propanal part of which was acetalized as $CH_3CHDCH(OD)_2$, see Scheme 19. Hydroformylation of 1-hexene in the presence of **61** gave low TOF and scarce selectivity (l/b ratio 2.5) (Table 8).

Complexes $[RhI(CO)\{PTA(Me)\}_2]I_2$ **57** and $[RhI(CO)\{PTA(Me)\}_3]I_3{\cdot}4H_2O$ **58** were tested for alkene hydroformylation, alkene and olefin hydrogenation under biphasic or aqueous phase conditions [51]. For the hydroformylation of 1-hexene, l/b ratio was found to be ca. 1 in the presence of **57**, with a significant amount of isomerization products. Although reaction rates are fast, the activity of **57** and **58** are about two times lower than the corresponding TPPTS analogues. The use of **58** together with an excess of ligand did not improve selectivity although both conversion (from 70 to 91%) and TOF (from 117 to 150 h^{-1}) increased. The presence of an excess of PTA(Me) favored hydrocarboxylation and hydrogenation (under H_2/CO) as side reactions.

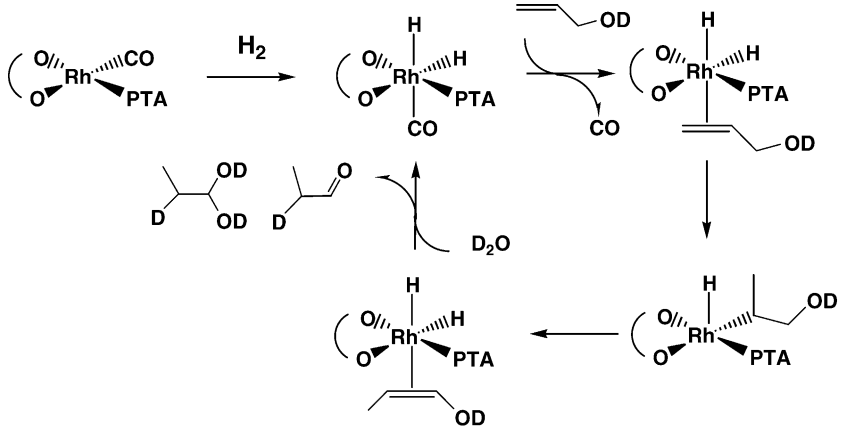

Scheme 19.

Table 8
Hydrogenation and hydroformylation of alkenes and allyl alcohol in the presence of **61** [52]

Substrate	Yield products (%)	Initial TOF (h^{-1})
1-Hexene[a]	*n*-Hexane (100)	143
Cyclohexene[a]	Cyclohexane (100)	92
Allyl alcohol[a,c]	*n*-Propanol (90) *n*-Propanal (10)	26
1-Hexene[b]	*n*-Heptanal (34.1) 1-Heptanal (13.6) 2-Hexene (11.0) 3-Hexene (6.2)	61[d]

[a] Substrate 0.02 mol; catalyst 10^{-5} mol; 15 ml H_2O; $p(H_2)$ 0.1 MPa; 30 °C.
[b] Substrate 0.02 mol; catalyst 10^{-5} mol; 15 ml H_2O; $p(H_2) = p(CO)$ 3.0 MPa; 60 °C, 18 h.
[c] One phase system.
[d] Average TOF.

As both **57** and **58** are active catalysts for water gas shift reaction (WGSR), hydroformylation of 1-hexene proceeds also under a H_2/CO_2 mixture due to CO_2 reduction to CO, albeit the rate of the reaction is five times slower. Complexes **57** and **58** catalyze the hydrogenation of aldehydes, in contrast to Rh-PTA complexes [40b]. The hydrogenation of unsaturated carboxylic acids such as maleic and fumaric acid was also carried out, interestingly the rate was found to be significantly higher for the latter, see Table 9. The mechanism of hydrogenation of these substrates in buffered water solutions covering a wide pH range ($2 < pH < 11$) was studied in the presence of $[RhCl(TPPMS)_3]$ and *trans*-$[RhCl(CO)(TPPMS)_2]$. The effect of pH on the rate of hydrogenation of maleic and fumaric acid catalyzed by $[RhCl(TPPMS)_3]$ in the $2 < pH < 7$ range could be described by considering solely the changes in the ionization state of these substrates [92].

Another Rh-PTA hydrogenation catalyst is the mixed PTA/PTA(H) $[RhCl\{PTA(H)\}(PTA)_2]Cl$ complex **59**. Its performance on the conversion of *trans*-cinnamaldehyde under biphasic conditions using sodium formate as the hydrogen source demonstrates very high selectivity for C=C double bonds [23]. From the catalytic experiments, the primary product was shown to be hydrocinnamaldehyde (93.3%) with 3.0% cinnamyl alcohol and phenyl propanol (3.1%). Furthermore, decabornylation of the aldehyde, typical of similar Wilkinson-type catalysts, was not observed.

Table 9
Biphasic hydroformylation and hydrogenation tests with **57** and **58** [51]

Substrate	Yield product distribution (%)	Average TOF (h^{-1})	Conversion (%)	Catalyst
1-Hexene[a]	*n*-$C_6H_{13}CHO$ (29) $C_4H_9CH(CH_3)CHO$ (25) $CH_3CH{=}CHC_3H_7$ (10) $CH_3CH_2CH{=}CHC_2H_5$ (6)	117	70	**57**
1-Hexene[a] + 6 equiv PTA(Me)	*n*-$C_6H_{13}CHO$ (39) $C_4H_9CH(CH_3)CHO$ (25) *n*-$C_6H_{13}COOH$ (14) $C_4H_9CH(CH_3)COOH$ (13)	150	91	**58**
n-C_3H_7CHO[b]	*n*-BuOH (6) *n*-PrCH=C(Et)CHO (6) $BuEtCHCH_2OH$ (2) $EtC(n\text{-}PrCHOH)_2CHO$ (77) *n*-PrCOO(*n*-Bu) (1)	109	98	**57**
n-C_4H_9CHO[b]	*n*-$C_5H_{11}OH$ (80) *n*-BuCH=C(*n*-Pr)CHO (3) Other (14)	108	97	**58**
n-$C_5H_{11}CHO$[b]	*n*-$C_6H_{13}OH$ (84) *n*-$C_5H_{11}CH{=}C(n\text{-}Bu)CHO$ (6) *n*-$C_6H_{13}CH(n\text{-}Bu)CH_2OH$ (2) Other (8)	108	97	**58**
n-$C_6H_{13}CHO$[b]	*n*-$C_7H_{15}OH$ (78) *n*-$C_6H_{13}CH{=}C(n\text{-}C_5H_{11})CHO$ (12) *n*-$C_7H_{15}CH(n\text{-}C_5H_{11})CHO$ (2) Other (3)	109	95	**58**
Maleic acid[c]	$HO_2C(CH_2)_2CO_2H$	110[d]	>99	**58**
Fumaric acid[c]	$HO_2C(CH_2)_2CO_2H$	210[d]	>99	**58**
$CH_2{=}CHCH_2OH$[c]	C_3H_7OH	160[d]	>99	**58**

[a] Substrate 30 mmol; catalyst 0.01 mmol; H_2O 15 ml; $p(CO) = p(H_2)$ 3.0 MPa; 353 K.
[b] Substrate 20 mmol; catalyst 0.01 mmol; H_2O 15 ml; $p(H_2)$ 8.0 MPa; 353 K.
[c] Substrate 10 mmol; catalyst 0.01 mmol; H_2O 15 ml; $p(H_2)$ 0.1 MPa; 293 K.
[d] Initial TOF.

Table 10
Allylbenzene hydrogenation using **59** [23][a]

Yield products (%)			Time (h)	Reducing agent
Propyl benzene (50.6)	*cis*-Propenylbenzene (2.0)	*trans*-Propenylbenzene (44.5)	1.75	H_2[b]
Propyl benzene (3.7)	*cis*-Propenylbenzene (4.3)	*trans*-Propenylbenzene (7.7)	3	H_2[c]
Propyl benzene (11.6)	*cis*-Propenylbenzene (5.2)	*trans*-Propenylbenzene (66.1)	3	HCO_2Na[d]
Propyl benzene (3.0)	*cis*-Propenylbenzene (3.6)	*trans*-Propenylbenzene (60.8)	8	HCO_2Na[e]

[a] **59**, 0.082 mmol; allylbenzene, 5.0 mmol, H_2O, 50 °C.
[b] 0.08 M Na_3PO_4 buffer.
[c] 0.08 M HCl.
[d] HCO_2Na 5 M, 5 ml.
[e] HCO_2Na 5M, 5 ml; 25 °C.

The catalytic activity decreased upon addition of cyclooctatetraene and elemental Hg, indicating that heterogeneous "unperceived" metal colloids are produced during the reactions. The hydrogenation tests showed a linear correlation between reaction rate and concentration of **59**, with a mixed reaction order in substrate (0.5) reaching saturation at aldehyde concentration values greater than 3 M. Increases in sodium formate concentration also influenced reactions rates, but leveled around 4 M. Addition of excess PTA inhibits catalysis. Complex **59** is also a transfer hydrogenation catalyst for allylbenzene which proceeds accompanied by extensive isomerization to *cis*- and *trans*-propenylbenzene, in fact, the main reaction at room temperature replacement of sodium formate with H_2 leads to faster reactions and decreased isomerization (see Table 10). Mechanistic studies on hydrogenation catalyzed by **59** were carried out. Complex **59** was dissolved in water in the presence of an excess of sodium formate at room temperature and analyzed by ^{1}H and ^{31}P NMR spectroscopy. The two broad signals in the ^{1}H NMR spectrum corresponding to **59** disappeared, and the resulting spectrum showed formation of PTA(O). ^{31}P NMR confirmed the presence of PTA(O) together with a rhodium compound with four phosphines, whose signals were not attributed due to extensive broadening, probably indicating fast exchange processes in solution. Attempts to observe the presence of intermediate hydride complexes by ^{31}P HP-NMR under 1000 psi of H_2 in the presence of **59** failed. Catalyst recycling for **59** was not successful as the activity greatly diminished after the fourth cycle.

The use of transition metal-PTA complexes other than rhodium and ruthenium as catalysts has received much less attention and only scattered data refer to their inactivity or low efficiency in some catalytic processes. The only significant exception is represented by the $Pd(PTA)_4$ complex **83**, which was shown, under non-optimized conditions, to oligomerize 1,3-butadiene into various dienes under biphasic water/substrate conditions [$Pd(PTA)_4$ 0.03 mol/L, autoclave, 80 °C, 20 h], whereas the analogous $Ni(PTA)_4$ under identical conditions was found to be inactive, possibly due to low thermal stability [56b]. Complex **83** gives complete conversion and preferentially the octadienyl ethers (87%) with small amounts of alcohols (7%) and rearrangement products (8%). This product distribution resembles that found in telomerization of 1,3-butadiene in water emulsion. In contrast, using $Pd(P(CH_2OH)_3)_4$ as the catalyst, linear dimerization is the main reaction as for $Pd(PPh_3)_4$ in single phase THF/water mixture. Catalyst recycling with **83** is extremely low, leaching of the metal into the organic layer is significant (63%).

7. Medicinal applications of PTA complexes

Water-soluble monodentate and polydentate phosphines complexes are playing an important role in studies on chemical diagnostic and therapy. Indeed, following their adaptable capacity to coordinate metals ions and their radioisotopes, such complexes allow for the preparation of new water-soluble radiopharmaceutical compounds. The strong metal-phosphorus bond make the complexes highly stable even under less favorable conditions as those encountered in vivo; however, only a few studies have been so far carried out to explore their biological activity. Among the few known examples, it is worth mentioning the antitumoral activity exhibited by copper(I), silver(I) and gold(I) complexes containing diphosphines such as 1,2-diphenylphosphinoethane (dppe) [93] and the recent account by Sadler and co-workers describing the biological activity of a family of platinum complexes stabilized by the aminodiphosphine PNP [94]. Bidentate water-soluble phosphines are superior complexating agents for ^{99m}Tc with which they form complexes stable in both biological liquids and targeted tissues. Recent examples of such kind of radiopharmaceutical complexes include the commercial drugs ^{99m}Tc-fosfim® and ^{99m}Tc-furifosfim® which have been successfully used for myocardial perfusions. [95] Moreover, copper(I) complexes with bidentate phosphines have been employed to develop a new family of short/middle lived-PET (positron emission tomography) imaging and therapy agents containing copper radioisotopes, due to their simple synthesis and to their proclivity to form bio-conjugate compounds [96].

With the only exception of Pt(ts)PTA (**98**), whose cytotoxicity against P388 leukemia cells, bacteria and fungi was briefly compared with other thiosalicylate platinum deriva-

Table 11
Effects of compounds **43** and **44** on tumor cell proliferation [45]

μM	$CpRuCl(PTA)_2$ (**43**)			$Cp^*RuCl(PTA)_2$ (**44**)		
	24 h	48 h	72 h	24 h	48 h	72 h
0	100 ± 12.8	100 ± 14.7	100 ± 21.0	100 ± 12.8	100 ± 14.7	100 ± 21.0
1	95.1 ± 9.20	91.9 ± 2.50	90.6 ± 7.65	88.2 ± 0.20	91.9 ± 3.40	95.8 ± 2.20
3	97.2 ± 5.90	90.2 ± 7.90	84.9 ± 3.10	83.7 ± 2.00	92.5 ± 4.00	93.6 ± 1.60
10	96.5 ± 7.11	85.9 ± 10.3	81.4 ± 6.30	81.1 ± 3.20	64.4 ± 8.10*	92.0 ± 0.30
30	87.6 ± 5.80	87.5 ± 7.40	88.4 ± 1.40	88.1 ± 3.20	76.6 ± 3.30	86.8 ± 1.10
100	93.3 ± 5.11	83.6 ± 6.10	85.4 ± 6.90	77.8 ± 3.63	37.4 ± 5.60**	53.5 ± 16.9

Murine adenocarcinoma TS/A cells, sown 24 h before, were treated with the compounds at 1/100 μM concentrations for 24, 48 or 72 h in complete medium supplemented with 5% fetal calf serum. Cell viability was evaluated at the end of each treatment by the MTT assay [98]. The reported data were the mean of three different experiments and each value was expressed as percentage of optical density of treated cells vs. controls (%T/C) ± S.E. calculated on the average of four separate wells per experiment. Statistical analysis: ANOVA and Dunnett post-test.

* $P < 0.05$.

** $P < 0.01$, vs. controls.

tives [74][3] all research to date relating the biological properties of PTA compounds have been focused on ruthenium. PTA confers high solubility to the complexes and ruthenium is the metal of choice because its low toxicity due to its ability to mimic iron in binding serum proteins such as transferrin and albumin. These two proteins are able to solubilize and transport iron, therefore reducing its toxicity. Cancer cells require high amounts of iron for their metabolism, and increase the number of transferrin receptors on their surface, hence sequestering high amounts of iron-rich transferrin. Ruthenium can bind to transferrin which can therefore be delivered to the cell [97]. As cancer cells have a higher number of transferrin receptors compared to the healthy cells, ruthenium is properly targeted to cancer cells.

The water-soluble ruthenium PTA complex [$RuCl_2$(*p*-cymene)(PTA)] complex **(41)** has shown a marked DNA damage strongly dependent from the pH of the diseased cells [42b,43]. The acid–base properties of the PTA ligand are hence crucial for the biological activity of (**41**). At physiological pH, neutral **41** can diffuse through lipid membranes and move freely into the cells. In some diseased tissue the pH is reduced; in this environment PTA is likely to be protonated and this in turn traps the protonated version of **41** in the cell. In addition, tests using agarose gel electrophoresis show that the Dyson's complex is non-damaging to DNA substrates (95% supercoiled and 5% open circular), whereas the protonated analogue appears to change the structure of DNA. Therefore, in tumor cells, which generally have more acidic environments due higher metabolic activity, DNA might be selectively damaged by **41** whereas healthy cells remain practically unaffected.

From complex **41** a whole new class of compounds with formula [RuX_n(arene)$(PTA)_n$] (X = Br, I, SCN; n = 1, 2), have been developed and their biological activity was tested [42b]. The complexes interact with proteins and DNA in vitro causing apoptosis (programmed cell death) in human cancer cell lines. Complex **41** showed activity against SK-N-SH neuroblastoma cells inducing apoptosis in nanomolar concentrations. The cell line was derived from human metastasis of a neuroblastoma.

The two cyclopentadienyl water-soluble ruthenium complexes **43** and **44** were tested on the proliferation of TS/A murine adenocarcinoma tumor cells (Table 11) [44]. Compound **43** is devoid of antiproliferative effects at any tested concentration and at any time of tumor cell exposure. Interestingly, the substitution of H (**43**) with Me (**44**) on the cyclopentadienyl moiety confers to this compound the capability to inhibit tumor cell proliferation. This activity is present starting from 10 μM concentration and is maximal (−62.6% versus controls) after 48 h treatment. A longer time of tumor cell exposure of 72 h did not increase such antiproliferative effects. Studies are in progress to evaluate the antimetastatic activity of these and related complexes.

8. Photoluminescent properties of PTA complexes

Currently a large number of gold compounds show the phenomenon of photoluminescence in both solution and solid-state and new applications involving these complexes are increasingly being sought. A wide variety of gold–phosphine complexes have been synthesized in an effort to clarify the relationship between spectroscopic and structural properties (the photoluminescence of gold–phosphine complexes was firstly described in [$AuCl(PPh_3)_3$] in 1970, see [99]). The theory and the general aspects of photoluminescence in gold compounds have been thoroughly reviewed [76,77] and the nature of photoluminescent gold compounds has been the subject of intense research [76].

The phenomenon results from the relaxation (emission) of an excited triplet state ($^3A_1$) back to the ground state, through a symmetry allowed but overlap forbidden $^1E_1 \rightarrow$

[3] In spite of its high hydrophilicity, the antitumor activity of **98** versus P388 leukemia cells was modest (IC_{50} 49,680 ng ml^{-1}) with respect to Pt(ts)(PPh_3) (IC_{50} 671 ng ml^{-1}) which shows the highest activity among the thiosalicylate platinum derivatives investigated in this study [74].

$^1A_1$ transition. A typical luminescence spectrum is characterized by a large Stokes shift between the excitation and emission wavelengths, involving decay through phosphorescence with largely distorted excited state compared to the ground state [79]. The HOMO–LUMO gap of the luminescent Au compound determines the position of both excitation and emission bands, which, in turn, is strongly influenced by the intermolecular distance between two gold centers, resulting into "aurophilic" interactions. Primarily, the steric and electronic nature of the ligands in the Au complex control the strength of the "aurophilic bond". Importantly, the small steric profile of PTA favors possible Au···Au interactions. Changes in unit cell volumes and lattice enthalpy also affect "aurophilic" Au···Au contacts, thus photoluminescence is often temperature dependent.

Recent interest in PTA as a ligand for the preparation of photoluminescent gold complexes is due to several factors including solubility in water and the small cone angle of the phosphine ligand that allows the occurrence of short gold–gold separations in the solid-state. Furthermore PTA does not have any π-system hence no low-energy interligand transition should be considered in the emission and excitation spectra.[4] The first photoluminescent complexes featuring PTA, reported by Fackler et al., were di-coordinated linear species of the type AuX(PTA) [X = Cl (**99**) or Br (**100**)] and [AuCl{PTA(H)}]Cl (**104**). All compounds feature strong temperature-dependent emissions (Table 12), but only in the solid-state and not in dilute MeOH solutions or frozen MeOH glass matrix. Both **99** and **104** have a single strong emission at low temperature which dramatically decreases in intensity (50%) and blue-shifts (400 cm^{-1} **99**, 700 cm^{-1} **104**) when measured at room temperature [78]. The effect of protonation of **100** causes a red shift of about 2000 cm^{-1} at 78 K. However, the absorption spectra of **100** and **104** are nearly identical with two bands at 228 and 242 nm [78]. A comparison of AuCl(PTA) with other phosphine containing Au-halide complexes shows that those with Me_3P and Et_3P are blue-shifted by 1400 cm^{-1}. This suggests that these ligands have a stronger π-contribution to the LUMO, resulting in increased stability, than is apparent for PTA which is a stronger σ-donor. MO calculations, at the Extended Huckel (EH) level, suggest that the HOMO of AuCl(PTA) (σ_u) is destabilized when two monomer units are combined together through Au···Au interactions. This result is consistent with the lack of photoluminenscence in solution where solvation disrupts the weak "aurophilic" interaction. Additional calculations on **104** show that protonated PTA has a lower contribution to the HOMO with significantly less σ-donation resulting in the red shifting of the photoluminescence [78]. Furthermore, the increased positive charge in the PTA(H) complex caused by protonation at one nitrogen site contributes to greater electrostatic repulsion and hence weaker Au···Au interactions. This would explain the differences in emission spectra when Au compounds featuring PTA are protonated forming $[Au\{PTA(H)\}]^+$ species [78].

Detailed studies of AuBr(PTA) (**100**) show, at excitations of 320 nm or less, a low-energy emission (LE) (647 nm, 78 K) with a blue-shift (320 cm^{-1}) occurring at room temperature (Table 12). This band is quenched if the excitation wavelength is set at 340 nm [79]. A high energy band (HE) (450 nm, 78 K) is also present with notable vibronic components. The intensity of the HE band has a strong correlation with the excitation wavelength [79]. The emission spectrum of the protonated version of **100**, [AuBr{PTA(H)}]Br (**105**) shows an unsymmetrical emission band blue-shifted (1600 cm^{-1}) with respect to **100** [79], with similar emission behavior to **104**. The iodo-substituted AuI(PTA) (**101**) displays similar behavior to AuBr(PTA) having an emission spectrum with both a high- and low-energy band (Table 12). Unlike AuCl(PTA), the emission bands of both **100** and **101** are relatively unaffected by changes in temperature [79]. For both **100** and **101**, the LE and HE are directly excited and are uncoupled with respect to each other. Protonation of **101** leads to the formation of $[AuI\{PTA(H)\}][AuI_2]$ (**106**) which displays intense but broad, red luminescence at 655 nm (298 K). Whereas the position of the band remains unchanged with different temperatures, it was observed to broaden at higher temperature. As mentioned in chapter 4, where the gold-PTA complexes have been reviewed, unlike the other PTA-Au halide complexes, the "aurophilic" interaction in **106** occurs between the metal centers in AuI(PTA) cation and AuI_2 anion and not between distinct monomeric AuX(PTA) units. Comparison of the AuX(PTA) series (X = Cl, Br and I) show that the LE band blue-shifts with increasing "softness" of the halide. A detailed study on the mixed Au species $[Au(PTA)_2][Au(CN_2)]$ (**108**) shows strong thermochromic luminescence [80], with primary Au···Au interaction occurring through the $Au(PTA)_2$ and $Au(CN)_2$ units. The high energy emission (425 nm, 77 K) is dominant only at excitation wavelengths lower than 365 nm and the intensity of this band decreases rapidly with excitations greater than 365 nm. The LE is dominant when the emission wavelength is around 500 nm. The LE band is also more dominant (by 23 times) over the HE band at room temperature [80]. Interestingly, neither single crystals of **108** nor crystals ground to a fine powder show luminescence [80]. The authors suggest that luminescence may result from defects in short-range order and localized surface deformations within the crystal lattice [80]. Similarly, when AuCl(PTA) is crystallized as fibers, an emission at 580 nm at 78 K is observed. Scanning electron microscopy of **99** and **108** demonstrates conductor capability along the chain axis, the latter complex having weaker conducting properties [80]. Interestingly, $[Au(PTA)_2]^+$ without the accompanying AuI_2 or $Au(CN)_2$ anions is not luminescent [83].

The dicoordinate arylgold complex AuPh(PTA) (**119**) is reported to have an extremely weak blue emission (473 nm,

[4] A solution of PTA in water does not show any band above 210 nm in its UV-Vis spectrum.

Table 12
Comparison of photoluminescence properties and Au···Au distances in gold-PTA complexes

Compound	$\lambda_{(emission)}$ (nm)	$\lambda_{(excitation)}$ (nm)	Temperature (K)	Au···Au distance (Å)	State	Reference
AuCl(PTA) (**99**)	674	290	78	3.092	Powder	[78]
	643	290	298		Powder	[79]
	580		77		Fibers	[80]
[AuCl{PTA(H)}]Cl (**104**)	596	290	78	3.322	Powder	[78]
	582	290	298		Powder	[79]
AuBr(PTA) (**100**)	674	320	78	3.107	Powder	[79]
	633	320	298		Powder	
[AuBr{PTA(H)}]Br (**105**)	580	295	78	–	Powder	[79]
	580	295	298		Powder	
AuI(PTA) (**101**)	617	295	78	–	Powder	[79]
	614	295	298		Powder	
[AuI{PTA(H)}]AuI_2 (**106**)	655	330	78	2.920	Powder	[79]
	652	330	298		Powder	
[AuCl$(PTA)_3$] (**109**)	517	320	77	7.181	Powder	[81]
	533	320	298		Powder	
	547	320	298		Aqueous	
[AuI{PTA(Me)}]I_3 (**116**)	598		140	4.581	Powder	[85]
	686		140		Powder	
AuPh(PTA) (**119**)	473	330	77	3.774	Powder	[85]
[Au$(PTA)_2$][Au$(CN)_2$] (**108**)	425 (HE)	<365	78	3.457	Powder	[80]
	500 (LE)	380	78		Powder	
Au(SPh)(PTA) (**120**)	596		77	5.243	Powder	[86]
Au{S(*o*-OMePh)}(PTA)	589		77	–	Powder	[86]
Au{S(*m*-OMePh)}(PTA)	685		77	3.263, 3.341	Powder	[86]
Au{S(*o*-ClPh)}(PTA)	540		77	–	Powder	[86]
Au{S(*m*-ClPh)}(PTA)	702		77	3.078	Powder	[86]
Au{S(*p*-ClPh)}(PTA)	698		77	–	Powder	[86]
Au{S(3,5-Cl_2Ph)}(PTA)	485		77	3.047	Powder	[86]
Au{S(^{i}Pr)}(PTA)	669		77	–	Powder	[86]

77 K), which probably arise from transitions originating from the phenyl group [85]. A series of different thiolate PTA gold complexes (**120**) were examined and all compounds exhibited broad and indistinctive luminescence at low temperature (77 K) in the solid-state with a wide variation in emission maxima (485–702 nm) [86]. Excitation maxima span from 358 to 362 nm, but only Au(SAr)PTA complexes with Ar = Ph(*m*-OMe), Ph(*m*-Cl) or Ph(*p*-Cl) show luminescence at room temperature [86]. The effect of aryl substitution has a strong correlation with emission wavelength. For complex series **120**, the presence of ligand-metal charge-transfer is associated with sulfur–gold interactions. Although no correlation exists between the Au···Au distances and emission energy in these complexes, a relationship can be envisaged for the emission maxima. This is likely to arise from the $6p_z$ orbitals of Au which are split into $p\sigma^*$ and $p\sigma$ MOs by the interaction of two Au monomers [86]. The $p\sigma$ MO is lower in energy and a MLCT (metal-ligand charge transfer) occurs between the metal-based $p\sigma$ and a $p\pi$ orbital situated on the coordinated thiolate group. Differences between the various substituted thiolate groups are attributed to steric effects. Importantly, the authors stress that emission maxima alone are not a reliable measure of Au···Au distances [86].

Three-coordinate Au gold complexes are well known for featuring strong photoluminescent properties. However, contrasting with the di-coordinated Au-PTA complexes, they are devoid of Au···Au interactions. Complex **109** is the first compound to display photoluminescence both in the solid-state (3.2 μs at 77 K) and in water (0.53 μs at 77 K) [100]. The emission band is broad and unsymmetrical in the solid-state (517 nm at 77 K, 533 nm at 298 K) and in aqueous solution (547 nm) differing only by 17 nm. In the excitation spectra, two bands (295, 321 nm at 298 K) are blue-shifted (279, 308 nm at 77 K) upon a decrease in temperature. In water solution, the photoluminescence is quenched by the addition of excess of PTA which forms the non-luminescent tetrakis species $[Au(PTA)_4Au]^+$ [81]. Furthermore, quenching of the photoluminescence of **109** follows the addition of different species like SCN^-, $[Fe(CN)_6]^{4-}$, O_2 or NO_3^-. In aqueous solution, luminescence is observed to be pH dependent [100]. At neutral pH, an emission is present at 547 nm. At pHs lower than 3, photoluminescence is quenched as most probably the protonated PTA(H) species is not photo-

luminescent. Increasing the pH above 3 also increases the intensity of the emission with a maximum obtained at a pH of 10. Further increment of pH beyond 10 leads to decomposition forming elemental gold and PTA(O) [81]. A comparison of $[Au(PTA)_2]^+$ ($D_{\infty h}$ symmetry) and $[Au(PTA)_3]^+$ (C_{3v} symmetry), using EH calculations, shows that the nature of the HOMO consists of a σ-type phosphorus based orbital in $[Au(PTA)_2]^+$ and π-type in $[Au(PTA)_3]^+$. Thus, the HOMO is considerably destabilized in the three-coordinate species relative to the linear di-coordinated complex and consequently, the HOMO–LUMO gap is 1.2 eV smaller in $[Au(PTA)_3]^+$ than in $[Au(PTA)_2]^+$ which corresponds to a red shift in the emission spectra, the emission being σ-based ligand charge transfer rather than being metal centered [81].

The tetrakis-iodo-substituted Au complex $[AuI\{PTA(Me)\}_3]I_3$ (**116**) is luminescent only in the solid-state where it displays two separate temperature dependent photoluminescent bands [85]. The low temperature (77 K) emission occurs at 598 nm and decreases in intensity with increasing temperature. The second emission (686 nm) is only observable above 140 K. The emission is thought to be MLCT-based.

9. Latest developments

At the time of writing this review, a couple of relevant contributions to PTA chemistry and applications in catalysis were submitted for publication. The reactions of $[(\eta^6\text{-}C_6H_6)RuCl_2]_2$ and $[(\eta^6\text{-}p\text{-cymene})RuCl_2]_2$ with hydrogen in the presence of the water-soluble phosphines TPPTS and PTA afforded as the main species $[(\eta^6\text{-}C_6H_6)RuH(TPPTS)_2]$, $[(\eta^6\text{-}C_6H_6)RuH(PTA)_2]$, $[(\eta^6\text{-}p\text{-cymene})RuH(TPPTS)_2]$ and $[(\eta^6\text{-}p\text{-cymene})RuH(PTA)_2]$. This latter complex was also formed in the reaction of $[(\eta^6\text{-}p\text{-cymene})RuCl_2(PTA)]$ and hydrogen with a redistribution of PTA. In addition, prolonged hydrogenation at elevated temperatures and in the presence of excess of PTA led to the formation of the arene-free $[RuH(PTA)_4Cl]$, $[RuH(PTA)_4(H_2O)]$, $[RuH_2(PTA)_4]$ and $[RuH(PTA)_5]$ complexes. Ru-hydrides, such as $[(\eta^6\text{-arene})RuH(L)_2]$ (L = TPPTS, PTA) catalyzed the hydrogenation of bicarbonate to formate in aqueous solutions at $p(H_2) = 100$ bar, 50–70 °C [101].

Acylation of 1,3,5-triaza-7-phosphaadamantane (PTA) and its oxide with acetic anhydride afforded the 3,7-diacetyl-1,3,5-triaza-7-phosphaadamantane (DAPTA) and its oxide, which have been fully characterized both in solution and in the solid-state. These compounds were found to be soluble in most common organic solvents, in addition to possessing extremely large molar solubilities in water. In order to assess the metal to phosphorus binding characteristics of DAPTA, several groups 10 and 6 complexes were prepared and their M–P bond distances were shown to be quite similar with those of their PTA analogs [102].

Acknowledgements

Thanks are due to EC through COST D17, D29 Chemistry Actions (WGs D17-003/00 and D29-0009/03) and RTN "HYDROCHEM" (HPRN-CT-2002-00176) for promoting this scientific activity and for a postdoctoral grant (to A.D.P.).

References

[1] (a) N. Pinault, D.W. Bruce, Coord. Chem. Rev. 241 (2003) 1, and refs therein;
(b) G. Verspui, G. Papadogianakis, R.A. Sheldon, Chem. Commun. (1998) 401;
(c) G. Verspui, J. Feiken, G. Papadogianakis, R.A. Sheldon, J. Mol. Catal. A 146 (1999) 299;
(d) W.A. Hermann, C.W. Kohlpainter, H. Bahrmann, W. Konkol, J. Mol. Catal. 73 (1992) 191;
(e) W.A. Hermann, C.W. Kohlpainter, in: M. Y. Darensbourg (Ed.), Inorg. Synth. 32 (1998) 8;
(f) H. Ding, B.B. Bunn, B.E. Hanson, in: M.Y. Darensbourg (Ed.), Inorg. Synth. 32 (1998) 29;
(g) S. Ahrland, J. Chatt, N.R. Davies, A.A. Williams, J. Chem. Soc. (1958) 264;
(h) Z. Tóth, F. Joó, M.T. Beck, Inorg. Chim. Acta 42 (1980) 153;
(i) A.F. Borowski, D.J. Cole-Hamilton, G. Wilkinson, New J. Chem. 2 (1978) 137;
(j) F. Joó, J. Kovács, A. Kathó, A.C. Bényei, T. Decuir, D.J. Darensbourg, in: M.Y. Darensbourg (Ed.), Inorg. Synth. 32 (1998);
(k) C. Bianchini, P. Frediani, V. Sernau, Organometallics 14 (1995) 5458;
(l) C. Bianchini, A. Meli, V. Patinec, V. Sernau, F. Vizza, J. Am. Chem. Soc. 119 (1997) 4945.
[2] J.G. Verkade, Coord. Chem. Rev. 137 (1994) 233.
[3] D.J. Daigle, A.B. Pepperman Jr., S.L. Vail, J. Heterocycl. Chem. 11 (1974) 407.
[4] (a) B. Cornils, W.A. Herrmann (Eds.), Aqueous Phase Organometallic Catalysis, Wiley-VCH, Weinheim, 1998;
(b) I.T. Horváth, F. Joó (Eds.), Aqueous Organometallic Chemistry and Catalysis, NATO ASI Series 3/5, Kluwer Academic Publishers, Dordrecht, 1995;
(c) F. Joó, Aqueous Organometallic Catalysis, Kluwer Academic Publishers, Dordrecht, 2001.
[5] D.J. Daigle, in: M.Y. Darensbourg (Ed.), Inorg. Synth. 32 (1998) 40.
[6] J. Navech, R. Kraemer, J.-P. Majoral, Tetrahedron Lett. 21 (1980) 1449.
[7] M. Benhammou, R. Kraemer, H. Germa, J.-P. Majoral, J. Navech, Phosphorus Sulfur 14 (1982) 105.
[8] D.J. Daigle, A.B. Pepperman Jr., G. Boudreaux, J. Heterocycl. Chem. 11 (1974) 1055.
[9] D.J. Darensbourg, J.C. Yarbrough, S.J. Lewis, Organometallics 22 (2003) 2050.
[10] (a) V.I. Siele, J. Heterocycl. Chem. 14 (1977) 337;
(b) D.J. Daigle, A.B. Pepperman Jr., J. Heterocycl. Chem. 12 (1975) 579.
[11] M.M. Abu-Omar, J.H. Espenson, J. Am. Chem. Soc. 117 (1995) 272.
[12] J.R. Delerno, R.J. Majeste, L.M. Trefonas, J. Heterocycl. Chem. 13 (1976) 757.
[13] A.H. Cowley, M. Lattman, P.M. Stricklen, J.G. Verkade, Inorg. Chem. 21 (1982) 543.
[14] (a) D.J. Darensbourg, T.J. Decuir, J.H. Reibenspies, in: I.T. Horváth, F. Joó (Eds.), Aqueous Organometallic Chemistry and Catalysis,

Kluwer Academic Publishers, Dordrecht, 1995, pp. 61–80;
(b) D.J. Darensbourg, J.B. Robertson, D.L. Larkins, J.H. Reibenspies, Inorg. Chem. 38 (1999) 2473;
(c) K.J. Fisher, E.C. Alyea, N. Shahnazarian, Phosphorus Sulfur 48 (1990) 37.
[15] J.M. Forward, R.J. Staples, C.W. Liu, J.P. Fackler, Acta Cryst. C 53 (1997) 195.
[16] E. Fluck, J.E. Förster, J. Weidlein, E. Hädicke, Z. Naturforsch. 32 (1977) 499.
[17] J.M. Forward, R.J. Staples, J.P. Fackler Jr., Z. Kristallogr. 211 (1996) 129.
[18] (a) E. Fluck, H.J. Weissgraber, Chem.-Ztg. 101 (1977) 204;
(b) B. Assmann, K. Angermaier, H. Schmidbaur, J. Chem. Soc. Chem. Commun. (1994) 941;
(c) B. Assmann, K. Angermaier, M. Paul, J. Riede, H. Schmidbaur, Chem. Ber. 128 (1995) 891.
[19] D.J. Daigle, G.J. Boudreaux, S.L. Vail, J. Chem. Eng. Data 21 (1976) 240.
[20] A.W. Frank, D.J. Daigle, Phosphorus Sulfur 10 (1981) 255.
[21] C.A. McAuliffe, in: G. Wilkinson, R.D. Gillard, J.A. McCleverty (Eds.), Comprehensive Coordination Chemistry, vol. 2, Pergamon Press, New York, 1987, Chapter 14, pp. 1016–1017.
[22] E.C. Alyea, K.J. Fisher, S. Johnson, Can. J. Chem. 67 (1989) 1319.
[23] D.J. Darensbourg, N.W. Stafford, F. Joó, J.H. Reibenspies, J. Organomet. Chem. 488 (1995) 99.
[24] R.E. Marsh, M. Kapon, S. Hu, F.H. Herbstein, Acta Cryst. B58 (2002) 62.
[25] V. Galasso, J. Mol. Struct. (Theochem.) 336 (1995) 47.
[26] M.Y. Darensbourg, D. Daigle, Inorg. Chem. 5 (1975) 1217.
[27] E.C. Alyea, K.J. Fisher, S. Foo, B. Philip, Polyhedron 12 (1993) 489.
[28] J.R. DeLerno, L.M. Trefonas, D.J. Darensbourg, R.J. Majeste, Inorg. Chem. 15 (1976) 816.
[29] D.J. Darensbourg, R.L. Kump, Inorg. Chem. 9 (1978) 2680.
[30] E.C. Alyea, G. Ferguson, S. Kannan, Polyhedron 16 (1997) 3533.
[31] K.J. Asali, H.H. Awad, J.F. Kimbrough, B.C. Lang, J.M. Watts, G.R. Dobson, Organometallics 10 (1991) 1822.
[32] D.R. Tyler, in: I.T. Horvath, F. Joó (Eds.), Aqueous Organometallic Chemistry and Catalysis, Kluwer Academic Publishers, Dordrecht, 1995, pp. 47–60.
[33] F. Shafiq, D.J. Szalda, C. Creutz, R.M. Bullock, Organometallics 19 (2000) 824.
[34] B.E. Schultz, R. Hille, R.H. Holm, J. Am. Chem. Soc. 117 (1995) 827.
[35] D.E. Berning, K.V. Katti, P.R. Singh, C. Higgenbotham, V.S. Reddy, W.A. Volker, Nucl. Med. Biol. 23 (1996) 617.
[36] R. Schibli, K.V. Katti, W.A. Volkert, C.L. Barnes, Inorg. Chem. 37 (1998) 5306.
[37] X. Shan, A. Ellern, J.H. Espenson, Angew. Chem. Int. Ed. Engl. 41 (2002) 3807.
[38] J. Long, R. Holm, W. Sanderson, S.-B. Yu, Z. Zheng, United States Patent 98/5,804,161 (1998).
[39] D.J. Darensbourg, A.L. Phelps, M.J. Adams, J.C. Yarbrough, J. Organomet. Chem. 666 (2003) 49.
[40] (a) D.J. Darensbourg, F. Joó, M. Kannisto, A. Katho, J.H. Reibenspies, D.J. Daigle, Inorg. Chem. 33 (1994) 200;
(b) D.J. Darensbourg, F. Joó, M. Kannisto, A. Katho, J.H. Reibenspies, Organometallics 11 (1992) 1990.
[41] P. Smolenski, F.P. Pruchnik, Z. Ciunik, T. Lis, Inorg. Chem. 42 (2003) 3318.
[42] (a) P.J. Dyson, D.J. Ellis, G. Laurenczy, Adv. Synth. Catal. 345 (2003) 211;
(b) C.S. Allardyce, P.J. Dyson, D.J. Ellis, S.L. Heath, Chem. Commun. (2001) 1396.
[43] P. Dyson, International Patent WO 02/40491 A1 (2002).
[44] D.N. Akbayeva, L. Gonsalvi, W. Oberhauser, M. Peruzzini, F. Vizza, P. Brüggeller, A. Romerosa, G. Sava, A. Bergamo, Chem. Commun. (2003) 264.
[45] D.J. Darensbourg, F.A. Beckford, J.H. Reibenspies, J. Cluster Sci. 11 (2000) 95.
[46] G. Laurenczy, F. Joó, L. Nadasdi, Inorg. Chem. 39 (2000) 5083.
[47] A.C. Benyei, in: I.T. Horváth, F. Joó (Eds.), Aqueous Organometallic Chemistry and Catalysis, Kluwer Academic Publishers, Dordrecht, 1995, pp. 159–171.
[48] A.D. Phillips, L. Gonsalvi, M. Peruzzini, unpublished results.
[49] A.D. Phillips, L. Gonsalvi, A. Lledos, O. Maresca, M. Peruzzini, unpublished results.
[50] L. Nadasdi, F. Joó, Inorg. Chim. Acta 293 (1999) 218.
[51] (a) F.P. Pruchnik, P. Smolenski, E. Galdecka, Z. Galdecki, New J. Chem. 22 (1998) 1395;
(b) F.P. Pruchnik, P. Smolenski, Appl. Organometal. Chem. 13 (1999) 829.
[52] F.P. Pruchnik, P. Smolenski, K. Wajda-Hermanowicz, J. Organomet. Chem. 570 (1998) 63.
[53] F.P. Pruchnik, P. Smolenski, E. Galdecka, Z.S. Galdecki, Inorg. Chim. Acta 293 (1999) 110.
[54] (a) D.A. Krogstad, J.A. Halfen, T.J. Terry, V.G. Young Jr., Inorg. Chem. 40 (2001) 463;
(b) J. Kovacs, T.D. Todd, J.H. Reibenspies, F. Joó, D.J. Darensbourg, Organometallics 19 (2000) 3963.
[55] (a) G. Papadogianakis, L. Maat, R.A. Sheldon, J. Chem. Soc. Chem. Commun. (1994) 2659;
(b) W.A. Herrmann, J. Kellner, H. Riepl J. Organomet. Chem. 389 (1990) 103.
[56] (a) J. Cermak, M. Kvicalova, V. Blechta, Collect. Czech. Chem. Commun. 62 (1997) 355;
(b) J. Cermak, M. Kvicalova, V. Blechta, Abst. ISHC-10, Princeton, NJ, 1996 (abstract B54).
[57] E.C. Alyea, G. Ferguson, S. Kannan, Polyhedron 17 (1998) 2727.
[58] C. Lidrissi, A. Romerosa, M. Saoud, M. Serrano, L. Gonsalvi, M. Peruzzini, unpublished results.
[59] D.J. Darensbourg, T.J. Decuir, N.W. Stafford, J.B. Robertson, J.D. Draper, J.H. Reibenspies, A. Kathó, F. Joó, Inorg. Chem. 36 (1997) 4218.
[60] C.A. Tolman, Chem. Rev. 77 (1977) 313.
[61] D.J. Darensbourg, C.G. Ortiz, J.C. Yarbrough, Inorg. Chem. 42 (2003) 6915.
[62] E.C. Alyea, G. Ferguson, S. Kannan, Chem. Commun. (1998) 345.
[63] A.M.M. Meij, S. Otto, A. Roodt, Acta Cryst. 58E (2002) M644.
[64] E.C. Alyea, G. Ferguson, S. Kannan, Polyhedron 17 (1998) 2231.
[65] D.M. Saysell, G.J. Lamprecht, J. Darkwa, A.G. Sykes, Inorg. Chem. 35 (1996) 5531.
[66] D.M. Saysell, C.D. Borman, C.H. Kwak, A.G. Sykes, Inorg. Chem. 35 (1996) 173.
[67] S. Otto, A. Roodt, W. Purcell, Inorg. Chem. Commun. 1 (1998) 415.
[68] K.J. Fisher, I.G. Dance, G.D. Willett, R. Zhang, E.C. Alyea, Eur. J. Mass Spectrom. 6 (2000) 23.
[69] M.M. Muir, J.A. Muir, E.C. Alyea, K.J. Fisher, J. Cryst. Spect. Res. 23 (1993) 745.
[70] E.T. Papish, M.P. Magee, J.R. Norton, in: M. Peruzzini, R. Poli (Eds.), Recent Advances in Hydride Chemistry, Elsevier, The Netherlands, 2001 (Chapter 2) and references therein.
[71] S. Otto, A. Roodt, Inorg. Chem. Commun. 4 (2001) 49.
[72] S. Otto, A. Roodt, Acta Crystallogr. C: Cryst. Struct. Commun. 57 (2001) 540.
[73] Z. Assefa, B.G. McBurnett, R.J. Staples, J.P. Fackler, Acta Cryst. 51C (1995) 1742.
[74] L.J. McCaffrey, W. Henderson, B.K. Nicholson, J.E. Mackay, M.B. Dinger, J. Chem. Soc., Dalton Trans. (1997) 2577.
[75] K. Fisher, I. Dance, G. Willett, Polyhedron 16 (1997) 2731.

[76] (a) D.M. Roundhill, Photochemistry and Photophysics of Metal Complexes, Plenum Press, New York, 1984;
(b) D.M. Roundhill, J.P. Fackler, Optoelectronic Properties of Inorganic Compounds, Plenum Press, New York, 1999.
[77] (a) K.P. Hall, D.M. Mingos, Prog. Inorg. Chem. 32 (1984) 237;
(b) P.G. Jones, Gold Bull. 14 (1981) 102;
(c) P.G. Jones, Gold Bull. 19 (1986) 46;
(d) R. Uson, A. Laguna, Coord. Chem. Rev. 70 (1986) 1;
(e) K. Angermaier, E. Zeller, H. Schmidbaur, J. Organomet. Chem. 472 (1994) 371;
(f) M.A.-O. Rawashdeh, M.A. Omary, H.H. Patterson, J.P. Fackler Jr., J. Am. Chem. Soc. 123 (2001) 11237.
[78] Z. Assefa, B.G. McBurnett, R.J. Staples, J.P. Fackler, B. Assmann, K. Angermaier, H. Schmidbaur, Inorg. Chem. 34 (1995) 75.
[79] Z. Assefa, B.G. McBurnett, R.J. Staples, J.P. Fackler, P. John, Inorg. Chem. 34 (1995) 4965.
[80] Z. Assefa, M.A. Omary, B.G. McBurnett, A.A. Mohamed, H.H. Patterson, R.J. Staples, J.P. Fackler, Inorg. Chem. 41 (2002) 6274.
[81] Z. Assefa, J.M. Forward, T.A. Grant, R.J. Staples, B.E. Hanson, A.A. Mohamed, J.P. Fackler, Inorg. Chim. Acta 352 (2003) 31.
[82] Z. Assefa, R.J. Staples, J.P. Fackler, Acta Crystallogr. C 52 (1996) 305.
[83] J.M. Forward, R.J. Staples, C.W. Liu, J.P. Fackler, Acta Cryst. C 53 (1997) 195.
[84] J.M. Forward, Z. Assefa, R.J. Staples, J.P. Fackler Jr., Inorg. Chem. 35 (1996) 16.
[85] J.M. Forward, J.P. Fackler Jr., R.J. Staples, Organometallics 14 (1995) 4194.
[86] J.M. Forward, D. Bohmann, J.P. Fackler, R.J. Staples, Inorg. Chem. 34 (1995) 6330.
[87] P.G. Jessop, T. Ikariya, R. Noyori, Chem. Rev. 95 (1995) 259.
[88] (a) G. Kovacs, L. Nadasdi, G. Laurenczy, F. Joó, Green Chem. 5 (2003) 213;
(b) G. Kovács, L. Nádasdi, F. Joó, G. Laurenczy, C. R. Acad. Sci. Paris, Serie IIc: Chem. 3 (2000) 601.
[89] G. Laurenczy, F. Joó, L. Nadasdi, High Pressure Res. 18 (2000) 251.
[90] F. Joó, G. Laurenczy, P. Karady, J. Elek, L. Nadasdi, R. Roulet, Appl. Organomet. Chem. 14 (2000) 857.
[91] P.J. Dyson, D.J. Ellis, W. Henderson, G. Laurenczy, Adv. Synth. Catal. 345 (2003) 216.
[92] F. Joó, J. Kovacs, A.C. Benyei, L. Nadasdi, G. Laurenczy, Chem. Eur. J. 7 (2001) 193.
[93] S.J. Berners-Price, P.J. Sadler, Struct. Bonding 70 (1988) 27.
[94] (a) A. Habtemarian, J.A. Parkinson, N. Margiotta, T.W. Hambley, S. Parson, P.J. Sadler, J. Chem. Soc., Dalton Trans. (2001) 362;
(b) N. Margiotta, A. Habtemarian, P.J. Sadler, Angew. Chem. Int. Ed. Engl. 11 (1997) 1185;
(c) A. Habtemarian, P.J. Sadler, Chem. Commun. (1996) 1785.
[95] S. Jurrison, J.D. Lydon, Chem. Rev. 99 (1999) 2205.
[96] J.S. Lewis, J. Zweit, J.L.J. Dearling, B.C. Rooney, P.J. Blower, Chem. Commun. (1996) 1093.
[97] F. Kratz, M. Hartmann, B.K. Keppler, L. Messori, J. Biol. Chem. 269 (1994) 2581.
[98] T. Mosmann, J. Immunol. Methods 65 (1983) 55.
[99] Z.J. Dori, J. Chem. Soc. Chem. Commun. (1970) 1124.
[100] J.M. Forward, Z. Assefa, J.P. Fackler Jr., J. Am. Chem. Soc. 117 (1995) 9103.
[101] H. Horváth, G. Laurenczy, A. Kathó, J. Organomet. Chem. 689 (2004) 1034.
[102] D.J. Darensbourg, C.G. Ortiz, J.W. Kamplain, Organometallics 23 (2004) 1747.